Addis Ababa University
Addis Ababa Institute of Technology (AAiT)
School of Electrical and Computer Engineering

DYNAMIC MODELING AND TECHNO-ECONOMIC ANALYSIS OF PV-WIND-FUEL CELL HYBRID POWER SYSTEM: THE CASE STUDY OF NIFASSO

A thesis Submitted to Addis Ababa Institute of Technology, School of Graduate Studies, Addis Ababa University

In Partial Fulfillment of the Requirement for the Degree of
Masters of Science in Electrical Engineering (Electrical Power Engineering)

By
Mikias Hailu Kebede

Under the Supervision of
Dr. Getachew Bekele Beyene

Addis Ababa, Ethiopia
July 2014

Addis Ababa University
Addis Ababa Institute of Technology (AAiT)
School of Electrical and Computer Engineering

DYNAMIC MODELING AND TECHNO-ECONOMIC ANALYSIS OF PV-WIND-FUEL CELL HYBRID POWER SYSTEM: THE CASE STUDY OF NIFASSO

By
Mikias Hailu Kebede

Approval by Board of Examiners:

Professor Kwon Ho Yeol Dean of School of Electrical and Computer Engineering	____________________ Signature	____________________ Date
Dr. Getachew Bekele Advisor	____________________ Signature	____________________ Date
Dr. Mengesha Mamo Internal Examiner	____________________ Signature	____________________ Date
Professor N.P. Singh External Examiner	____________________ Signature	____________________ Date

Declaration

I, the undersigned, declare that this thesis is my original work, has not been presented for a degree in this or other universities, all sources of materials used for this thesis work have been fully acknowledged.

Name: Mikias Hailu

Signature: _____________

Place: Addis Ababa Institute of Technology (AAiT), Addis Ababa University, Addis Ababa, Ethiopia.

Date: _________________

This thesis has been submitted for examination with my approval as a university advisor.

Advisor: - Dr. Getachew Bekele

Signature: _________________

Date: _____________________

Dedication

...to

All people who are positive thinkers.

and

...to the following Schools and Universities

Shewarobit Primary School, Shewarobit Secondary School, Debresina Preparatory School, Arbaminch University and Addis Ababa Institute of Technology.

Acknowledgements

Simply, words just *"thank you!"* respecting and heartfelt believe are not enough for **God** and **Virgin Mary**. But, all human beings have nothing to be given for them except the mentioned once. Therefore, as I have nothing to be given for them, let me use this opportunity to say *"Thank you! As you have kept my life starting from my childhood up to now, please follow me, lead in front and stand in my right and left for the rest of my life."*

I will take this chance to thank my advisor, **Dr. Getachew Bekele**, for his indispensable guidance of this thesis work from the early title selection up to the motivation, follow up and proof reading during the progress of the work.

I would like to thank my family and friends for keeping me in prayer and for their help. In particular, I would like to thank **Ato Hailu Kebede**, **W/ro Yiketetu Shewandagn**, **Ato Wondimagegn Hailu,** and **W/t Alemitu G/tsadik**.

Ato Fikireselam, who works in the EEPCo-UEAP (**U**niversal **E**lectricity **A**ccess **P**rogram) office, needs to be acknowledged for the materials and ideas he gave to me which were very important in the design and cost estimation of grid extension.

Finally, I would like to thank all doctors and professors who taught me in the successful accomplishment of my study. Hence, (in alphabetical order), **Dr.-Ing. Fikadu Shewarega** *(who taught me Power System Operation and Control),* **Dr. Frehiwot Woldehanna** *(who taught me Renewable Energy Technologies),* **Dr. Getachew Bekele** *(my advisor-who taught me "Energy Conservation" and "Distributed Generation"),* **Dr.-Ing. Getachew Biru** *(who taught me "High Voltage Engineering" and "Electrical Power Quality"),* **Dr. Mengesha Mamo** *(who taught me Applied Power Electronics),* **Dr.-Ing. Mohammed Abdo** *(Who taught me Analytical and Computational Methods),* **Professor N.P. Singh** *(Who taught me "Power System Analysis" and "Power Distribution Engineering") and* **Professor Woldeghiorgis Woldemariam** *(Who taught me Power System Planning and Management)* need to be acknowledged for their respective knowledge transfer.

Mikias Hailu Kebede

Abstract

Due to ever increasing energy consumption, rising public awareness of environmental protection and steady progress in distributed generation, alternative (i.e., renewable and fuel cell based) distributed generation (DG) systems have attracted increased interest. Wind and photovoltaic (PV) based power generation are two of the most promising renewable energy technologies. Fuel cell (FC) systems also show great potential in DG applications of the future due to their fast technological development and the merits they have, such as high efficiency, zero or low emissions (of pollutant gases) and flexible modular structure.

In this thesis work, the techno-economic feasibility study (using HOMER) of emission free hybrid power system of solar, wind and fuel cell power source unit for a given rural village (Nifasso) that can meet the electricity demand in a sustainable manner has been studied. The main power for the hybrid system comes from the solar and wind energy while the fuel cell and rechargeable batteries are used as a secondary and primary energy back up units respectively.

The modeling and control of a hybrid PV-Wind-FC DG system is also addressed. Dynamic models for the major system components, namely, wind energy conversion system (WECS), PV energy conversion system (PVECS), fuel cell, electrolyzer, inverter, battery, hydrogen storage tank and an overall power flow controller unit are developed. Then, a simulation model for the proposed hybrid power system has been developed using MATLAB/Simulink environment. This is done by creating a subsystem and masked block sets of the major dynamic component models and then cascading (assembling) in to a single aggregate model.

The overall power management strategy for coordinating and/or controlling power flows among the different energy sources is also presented in the thesis. Simulations have been carried out to verify the system dynamic performance using a practical load profile and weather data. The result show that the overall power management strategy is effective and the load demand is balanced successfully.

To make the thesis work complete, a grid extension from the closest substation has been designed. Cost of the grid extension is estimated based on the data obtained from EEPCo-UEAP office. This is done in order to compare the cost of the designed hybrid RES power system against the cost of grid extension. The result shows that breakeven grid extension distance to be 25.1 km which indicates that grid extension is preferable.

Key Words: *PV-Wind-Fuel Cell Hybrid Power System; Dynamic Modeling; Techno-Economic Analysis; Load Profile; Grid Extension; Overall Power Flow Control.*

Table of Contents

List of Figures

List of Tables

Nomenclatures

A	Area	(m^2)
a	Ideal factor of the diode	
AAAC	All aluminum alloy conductor	
AC	Alternating current	
AFC	Alkaline fuel cell	
A_{rot}	Area swept by the rotor blades exposed to the wind	(m^2)
BC	Battery capacity	(Ah)
c	Scale parameter of Weibull distribution	(m/s)
c	The speed of light	(m/s)
CC	Cyclic charging dispatch strategy	
CFL	Compact fluorescent lamp	
CO_2	The concentration of oxygen	($mol.cm^{-3}$)
COE	Cost of energy	($/kWh)
C_p	The power coefficient of wind turbines	
DC	Direct current	
DF	Distortion Factor	
DG	Distributed generation	
E	The ideal equilibrium potential	(V)
E_0	Standard cell potential	(V)
$e_b(t)$	Energy delivered to the load and/or stored energy	(Wh)
$e_{b\text{-}init}(t)$	Initial energy of the battery	(Wh)
EEPCo	Ethiopian electric power corporation	
Eg	The band-gap energy	(eV)
E_{Nernst}	The thermodynamic potential of the cell in open circuit	(V)
E_o	The reversible standard potential for a cell reaction	(V)
F	Faraday's constant	
FC	Fuel cell	
g	The gravitational constant	(m/s^2)
h	The Planck constant	
HOMER	Hybrid optimization model for electric renewable	
HPS	Hybrid power system	
h_r	Rotor height	(m)
I	The load current	(A)
$I_{rated,\ source}$	Rated source current	(A)
I_o	Reverse saturation current of the diode	(A)
$i_b(t)$	Current output of the battery to the load	(A)
I_D	The diode current	(A)
i_{FC}	The fuel cell current	(A)
I_L	Current produced by the cell	(A)
i_o	The exchange current density	
IRENA	International renewable energy agency	
I_{RS}	The cell's reverse saturation current	(A)
I_{sh}	Current through the shunt resistance	(A)

k	A constant known as shape factor of Weibull distribution	
KE	Kinetic energy	(J)
K_I	The cells short-circuit current temperature coefficient	
l	The cell thickness	
LF	Load following dispatch strategy	
m	Mass of air	(kg)
M	The hydriding substance	
MCFC	Molten carbonate fuel cell	
mfr	The mass flow rate of air	(kg/s)
MH_2	Molar mass of hydrogen	(kg $kmol^{-1}$)
MV	Medium voltage	
n	The number of electrons participating in the reaction	
N	The number of photons	
NASA	National aeronautics and space administration	
NH_2	Hydrogen moles per second delivered to the storage tank	(kmol s^{-1})
NPC	Net present cost	($)
NREL	National renewable energy laboratory	
P	Pressure	(Pa)
PAFC	Phosphoric acid fuel cell	
P_b	Pressure of tank	(Pa)
$P_b(t)$	Battery power delivered to the load	(W)
P_{bi}	Initial pressure of the storage tank	(Pa)
PEMFC	Proton exchange membrane fuel cell	
PH_2	The partial pressures of hydrogen	(Pa)
Po	Standard sea level atmospheric pressure	(Pa)
PO_2	The partial pressures of oxygen	(Pa)
PSIM	Power electronics simulator	
PV	Photovoltaic	
P_w	Power in the wind	(W)
$P_{wind}(t)$	Output power of wind turbine	(W)
q	Charge on an electron	(C)
Q_d	Ampere hour discharge	(Ah)
R	Universal (Rydberg) gas constant	(J/ (kmolK))
R_{cell}	The overall cell resistance	(Ω)
RES	Renewable energy source	
R_i	Internal resistance of the battery bank	(Ω)
R_{ohm}	Conductor resistance	(Ω)
R_S	Series resistance	(Ω)
R_{SH}	Shunt resistance	(Ω)
SOC	State of charge	
SOFC	Solid oxide fuel cell	
SWERA	Solar and wind energy resource assessment	
T	The absolute temperature	(K)
t_{charge}	Charging time of the battery	(hr)
T_b	Operating temperature	(K)
t_C	The center time	

THD	Total harmonic distortion	
T_{Ref}	The cell's reference temperature	
U_{dc}	DC voltage at the DC-bus connection	(V)
UEAP	Universal electricity access program	
U_o	Internal voltage of the battery bank	(V)
v	Wind speed	(m/s)
V	Output voltage of PV cell	(V)
v	Upstream wind velocities at the entrance of rotor blades	(m/s)
V_{act}	Activation polarization	(V)
V_b	Volume of the tank	(m^3)
V_{conc}	Concentration polarization	(V)
v_o	Downstream wind velocities at the exit of rotor blades	(m/s)
V_{oc}	Open circuit voltage	(V)
V_{ohm}	Resistive or ohmic polarization	(V)
w_r	Rotor width	(m)
z	Compressibility factor (typical value is 1)	
α	The electron transfer coefficient	
λ	The solar insolation	(kW/m^2)
λ_{max}	The maximal radiation intensity at a given time	
λ_p	The wavelength of light	(m)
ρ	Air density	(kg/m^3)
ρ_M	The specific resistance of the membrane	
σ	The standard deviation of Gaussian function	

CHAPTER ONE

1. INTRODUCTION

1.1 Motivation and Statement of the Problem

Most people in the rural villages use kerosene for lamp, diesel for water pumping and flour mills, fire wood for cooking and dry cells for radio and tape recorders. Desertification of the land is getting worse and worse due to deforestation and backward agricultural practices.

As figure 1-1 shows, the community that live in the rural villages are suffering from lack of electricity. Therefore, women are forced to do their day to day domestic activities such as cooking, using fuel wood which leads to a rapid growth of deforestation; they travel long distances to fetch water; they also use kerosene lamp at night. Additionally, due to lack of access to electricity, the communities in the rural villages are not able to benefit from social services such as clinics and schools sufficiently.

Figure 1-1Lack of electricity accesses and its consequences in rural villages

Therefore, village electrification is a vital step for improving the socio-economic conditions of rural areas and crucial for the country's overall development. The villages' welfare is one of the main aims of the rural electrification program. Enormous benefits can be achieved in irrigation, food preservation, crop processing, agriculture and rural small-scale industries. It creates employment opportunities for the villages' youth and promotes a better standard of life. Hence, availability of electricity reduces poverty and helps economic development by enhancing the health, education, water supply (for drinking and irrigation) needs of the rural population.

The author's secondary motivation so as to conduct this study comes from the fact that most research works in AAiT (**A**ddis **A**baba **I**nstitute of **T**echnology) which have been conducted till now on the hybrid systems are merely feasibility studies. Hence, it is the author's secondary motivation, to present a study which is somehow a complete work taken as a good reference that comprises of feasibility study, dynamic modeling and grid extension comparison. Hence, it will be well known (in the future) that the understanding of a hybrid system is beyond a mere feasibility studies.

1.2 Objective of the Thesis

1.3.1 Main Objective

The main objective of this thesis is to do techno-economic analysis and feasibility study of a hybrid electric power supply system consisting of PV-Wind-Fuel Cell power source that can meet a given load and constraints for rural village electrification at Nifasso (Latitude of 9.98 (9°58'40"N) and Longitude of 39.83 (39°50'3"E) [46]).

1.3.2 Specific Objectives

- Solar and wind potential study
- Community load estimation
- Optimization of PV/Wind/Fuel Cell hybrid power system and sensitivity analysis
- Dynamic modeling of the selected optimal hybrid power system
- Grid extension design and cost comparisons against the designed hybrid RES power system

1.3 Methodology

Step by step procedures have been followed during the progress of this thesis to accomplish the task successfully. The followed method includes the followings:

- **Data collection:** The data required such as solar radiation, wind speed, altitude, longitude, latitude, atmospheric pressure and air temperature of the study area were obtained from NASA and SWERA. Then, after comparison of the two, the NASAs data was used as an input for further feasibility study. Because, the data obtained from SWERA are somehow underestimated. Besides this, the software itself (HOMER) recommends the data values of NASA.

- **Community load estimation:** The primary and deferrable electric loads for the households, schools and clinics of the community were estimated by considering the equipments that might exist in the rural village of Ethiopia. For this purpose **Microsoft-Excel** software tool has been used.

- **Study of techno-economic feasibility of the hybrid system:** Optimization and sensitivity analysis of the hybrid system were studied using **HOMER** software tool using the collected data and loads estimated. Then, the optimal hybrid system was selected.

- **Developing the dynamic model of the selected optimal hybrid power system:** To study the 24 hour dynamic response of the hybrid system, a simulation has been run using power balance equation. For modeling purpose a Math Works Inc. software **MATLAB/Simulink** has been used.

- **Grid extension design, cost estimation and comparisons with the hybrid RES power system:** In order to study breakeven grid extension distance (the distance at which the cost of standalone system and grid extension equates), first a grid extension from the closest substation (Shewarobit) has been designed and cost comparisons was done to see whether the proposed hybrid system is a cost effective solution or not.

- **Simulation observation and drawing conclusion:** Finally, all the simulation results which are in line with the objective were recorded, interpreted and conclusions and recommendations are made based on the results obtained from techno-economic analysis, dynamic modeling and grid extension comparisons point of views.

1.5 Literature Review

In this section previous works which are directly or indirectly related to the idea of this thesis work are examined. Works reviewed in this section are generally categorized in to three as: a recently published journal papers, M.Sc. thesis and Ph.D. thesis. Even though this work is benefited from ample related materials, due to space limitation, only some selected materials from each category are reviewed. The rest are listed in the reference section and mentioned within the text.

A work entitled as *"A Stand-Alone Mobile House using PV/Wind/Fuel Cell Hybrid Power System"* has been developed by a group of authors and got published in the 3rd world congress of young scientists on hydrogen energy systems [16]. In the work it is anticipated that the presented mobile house can produce sufficient power to cover the peak load. Photovoltaic and wind energy are used as primary sources and a fuel cell as backup power for the system. The power budgeting of the system is designed based on the local data of solar radiation and wind availability.

Mahalakshmi M. and Latha S. presented *"Modeling, Simulation and Sizing of Photovoltaic/Wind/Fuel Cell Hybrid Generation System"* in International Journal of Engineering Science and Technology (IJEST) [30]. In the work the simulation results of the PV/Wind /Fuel Cell hybrid system are presented in graph showing the effectiveness of the proposed system model. Also, hardware implementation of microcontroller based MPPT for solar-PV is depicted in the paper.

Another work which uses the hybridization of PV/FC energy system also has been developed [1]. The work assumes as if the main power for the hybrid system comes from the photovoltaic (PV) panels, while the fuel cell (FC) and secondary batteries are used as a backup units. In the work HOMER (Hybrid Optimization Model for Electric

Renewable) is used as optimization software. In this system the authors specified one sensitivity variable with two values; which are the intercept coefficient in FC and the marginal fuel consumption of the FC. And the result shows that the Net Present Cost (NPC) and the Cost of Energy (COE) have increased due to the rise in fuel consumption in the FC. But, the work refrains from carrying out the issue of dynamic modeling.

The paper indicated in [55] entitled as "*Power Management of a Stand-Alone Wind/Photovoltaic/Fuel Cell Energy System"* has been published by Wang C. and Hashem M. in the journal of IEEE Transactions on Energy Conversion. In this work, wind and PV are the primary power sources of the system, and FC–Electrolyzer combination is used as a backup and a long-term storage system. Moreover, an overall power management strategy is designed for the proposed system to manage power flows among the different energy sources and the storage unit in the system. The system performance under different scenarios has also been verified by carrying out simulation studies using a practical load demand profile and weather data.

The work indicated in [17] entitled as *"Simulation of Dynamic Response of Small Wind-Photovoltaic-Fuel Cell Hybrid Energy System"* has been contributed by Esmaeili S. and Shafiee M. The work describes dynamic modeling and simulation results of a small PV-Wind-FC hybrid energy system. The hybrid system consists of a 500 W wind turbine, a photovoltaic, a proton exchange membrane fuel cell (PEMFC), ultracapacitors, an electrolyzer, controllers and a power converter that simulated using MATLAB Solver. Dynamics of fuel cell component such as double layer capacitance are also taken into account. In this work, dynamic responses of the system for a step change in the electrical load and wind speed are also presented.

In the International Journal of Engineering Research & Technology (IJERT) there is another work which is the hybridization of PV and FC entitled as *"Optimization and Modeling of PV/ FC/Battery Hybrid Power Plant for Standalone Application"* [13]. In the work, a hybrid power generation system suitable for remote area for agricultural application is proposed and studied using HOMER software. The load has a peak value of 13kW with a 2.2 % day-to-day and hour-to-hour variation. To satisfy this load demand, a hybrid PV/FC/Battery /Electrolyzer system with 80 kW PV and10 kW FC has been suggested with a COE of 0.431 $/kWh.

M.Sc. thesis entitled as "*A Wind Power-Fuel Cell Hybrid System Study*" has been developed by Sobotka K. in the University of Iceland [45]. A model was developed to determine the key technical parameters influencing the operation of a wind energy system with hydrogen storage. The model incorporates the simulation results of a 600 kW wind energy system with a 100 kW proton exchange membrane fuel cell (PEMFC) and an electrolyzer.

A Ph.D. dissertation in the Montana State University entitled as *"Modeling and Control of Hybrid Wind/Photovoltaic/Fuel Cell Distributed Generation Systems"* has been developed [54]. In this work what is new is that the DG's impacts on the existing power system are also investigated in the dissertation. Analytical methods for finding optimal sites to deploy DG sources in power systems are presented and verified with simulation studies.

"Modeling and Simulation of a Photovoltaic-Fuel Cell Hybrid System" has also been developed in Candidacy for the Degree of Doctor in Engineering (Dr.-Ing.) [2]. What makes this work different from the other studies in this area is that the model library, ISET Alternative Power Library (ISET-APL), designed by the Institute of Solar Energy supply Technology (ISET) is used for the simulation of the hybrid system. Besides this, the physical, analytical and/or empirical equations of each component in the hybrid system are programmed and implemented separately by C^{++} language rather than MATLAB/Simulink and/or MATLAB Solver.

Even though this work took some ideas and methods from the above mentioned works in the literature reviewed, it has some unique future. In the first place, in the above mentioned once, nothing of them are carried out comparison of their hybrid system with grid extension. Hence this work can be taken as complete as we compared it from other works that has been studied so far. In the second place, the dynamic model of this thesis presents every detailed model without approximating and rounding the systems algebraic equation which are used to model any sub system or masked blokes. For instance, in the

PV sub system modeling, most journal papers and dissertations simplify their model by ignoring the saturation and reverse saturation current to be zero. But in this work the effect of saturation and reverse saturation currents are taken in to account. Hence the work contains too complex but more accurate model.

1.5 Over View of the Study Area: Nifasso

1.5.1 Site Maps, Geographical Location and Demography

The closer look of the study area, for which the hybrid system is studied, from the Google earth satellite map is shown in figure 1-2. In the map, the school and church are identified and circled.

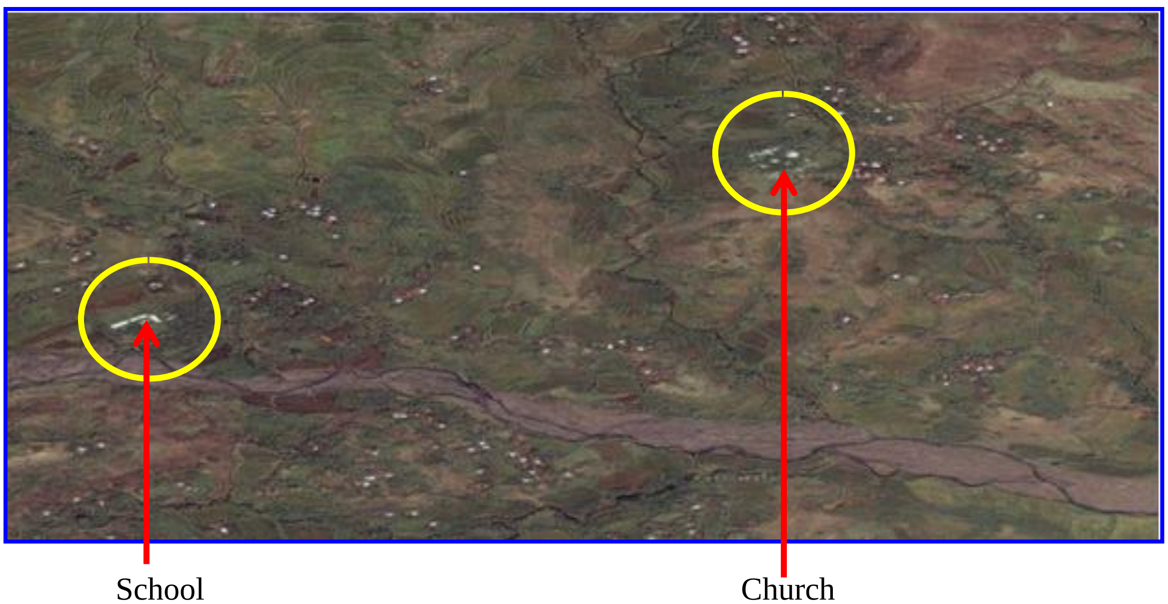

Figure 1-2 Closer looks of the study area: Nifasso [21]

The geographical location of the study area is at Latitude of 9.98 (9°58'40"N) and Longitude of 39.83 (39°50'3"E) with elevation above sea level 1770m [46].

Regarding the demography, the report of Kewot district rural development office shows that there are 289 households with an estimated population of 1059 (631 Male and 428 Female), one primary school (Grade 1 - 8), one small health post (Clinic) and one church (St. Michael).

1.5.2 Wind and Solar Resources

Two renewable data sources have been investigated for the wind, solar, atmospheric pressure and air temperature data of the study area. Table 1-1 shows the data which are obtained from the mentioned sources.

As it can be seen clearly in the Table 1-1, both the solar radiation data and wind speed data of NASA are higher than SWERA (a reader is advised to take a note that the wind speed data of SWERA given in Table 1-1 is at 50 m where as that of NASA is at 10 m above the surface of the earth). And in this study the data values of NASA have been used for the further feasibility study and dynamic modeling of the hybrid system as it is also well discussed in the methodology.

Table 1-1 Wind, radiation, pressure and temperature data of the study area

Month	Daily Solar Radiation		Wind Speed		Atmospheric Pressure	Air Temperature
	kWh/m²/d		*m/s*		*kPa*	*°C*
	NASA	SWERA	NASA @10m	SWERA @50m	NASA	NASA
January	5.97	3.27	3.60	4.32	82.6	18.6
February	6.33	3.43	3.30	4.21	82.5	20.3
March	6.30	2.95	3.10	3.94	82.4	22.2
April	6.21	3.63	3.00	3.64	82.4	22.3
May	6.27	3.20	2.80	3.60	82.4	22.7
June	5.61	1.89	3.10	3.93	82.4	20.6
July	5.06	2.20	3.00	3.76	82.4	19.1
August	5.09	2.58	2.70	3.41	82.4	19.0
September	5.71	3.06	2.50	3.10	82.4	19.6
October	6.22	3.77	2.80	3.39	82.5	19.7
November	6.13	3.69	3.00	3.74	82.6	18.9
December	5.95	2.94	3.20	3.98	82.6	18.1
Average	5.90	3.05	3.00	3.75	82.5	20.1

1.6 Organization of the Thesis

Chapter one is the introductory part of the thesis work. Topics which are covered under this chapter are: motivation and statement of the problem, objective of the study, review of related works and overview of the study area.

Chapter two covers the basic theoretical concepts of PV-Wind-Fuel Cell hybrid power system. Basic theory related with PV energy conversion system (PVECS), wind energy conversion system (WECS), fuel cell, electrolyzer, hydrogen storage tank and rechargeable battery are well explained.

Chapter three presents the techno-economic feasibility study of the hybrid micropower system using HOMER software tool. Hence, detail of load estimation, HOMER model of the hybrid system, resource inputs to the software and additional specification inputs to the software are included.

Chapter four is about the MATLAB/Simulink modeling approaches of the optimum PV-Wind-Fuel Cell hybrid power system. Hence, detailed subsystem and masked model of each component: PV, wind turbine, fuel cell, electrolyzer, hydrogen storage tank, battery, inverter and an overall control unit are discussed.

Chapter five is dedicated to deal with the design of grid extension and comparison against the designed hybrid RES (Renewable Energy Source) power system. Grid extension design issues, MV line construction assembly structural drawings and detailed cost estimation are carefully addressed in the chapter.

Chapter six deals with the results obtained from techno-economic analysis, dynamic modeling and grid extension comparisons. Moreover, brief discussions of the results are also included.

Chapter seven contains short concluding remarks and recommendations are made based on the research basic findings.

CHAPTER TWO

2. PV-WIND-FUEL CELL HYBRID POWER SYSTEM: BASIC THEORY

2.1 The Overall Concept

In this work, a hybrid system based on hydrogen technology is considered which needs a hydrogen producing unit (Electrolyzer), a hydrogen storing unit (Storage Tanks), and a hydrogen utilizing unit (PEM Fuel Cell). However, the system is based on intermittent energy sources and is likely to experience large minutely, hourly, and daily fluctuations in energy input. Thus, it should be emphasized that the main purpose of the hydrogen storage system is to store energy over a long period of time (hour to hour and season to season). Other small short-term energy storage such as a battery must also be included to supply power during transient load conditions. In addition, a control system is required to monitor and guide the operation of the components of the system.

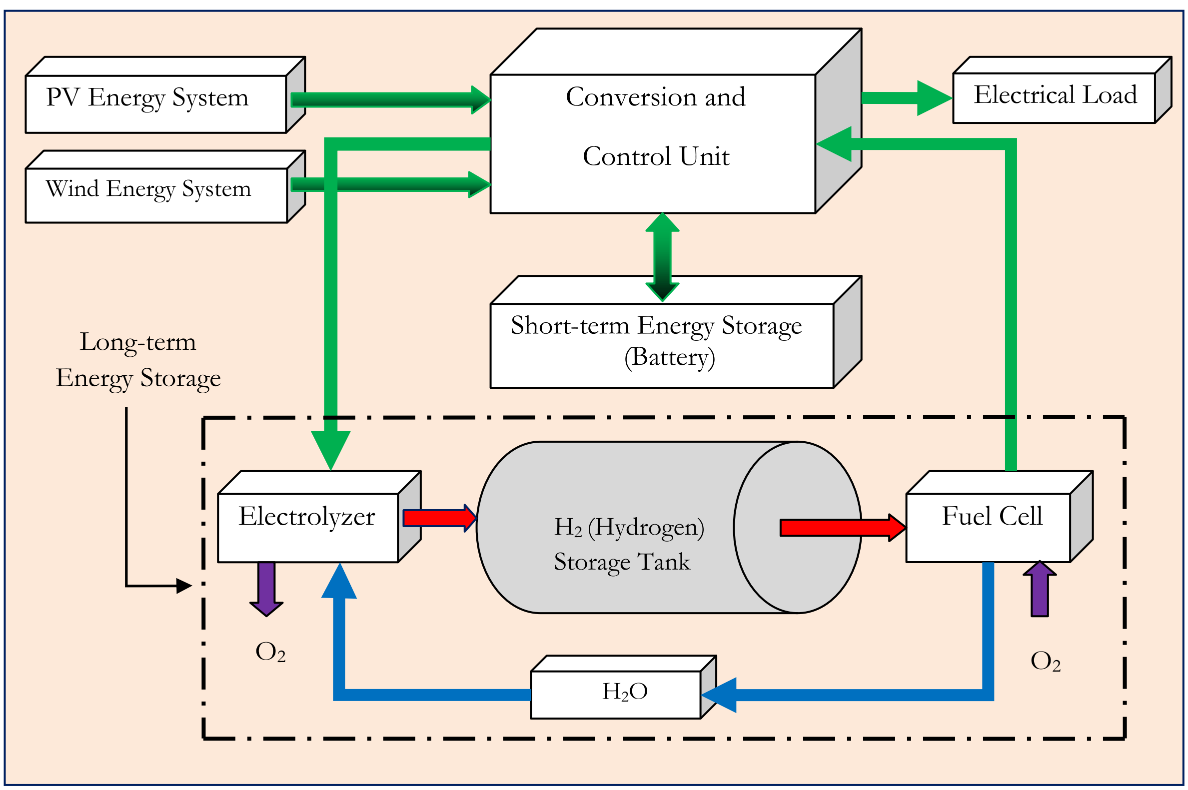

Figure 2-1 Concept of PV/Wind/Fuel Cell hybrid power system [2]

2.2 Solar Energy Conversion System (SECS)

2.2.1 The Sun

The sun, the source of solar radiation, is a sphere of intensely hot gaseous matter with a diameter of about 1.39×10^9 m, a total mass of 1.99×10^{30} kg and on the average 1.50×10^{11} m away from the earth. An atomic reaction taking place in the inner active part of the sun makes the outer surface to have a temperature of 5800K [14]. Solar radiation in the form of radio magnetic wave emanates from this surface and propagates spherically in space. Some part of the radiation reaches the earth surface after atmospheric effect (reflection, refraction, absorption, scattering etc.). Such radiation is called diffused radiation. There is also some part of radiation that reaches the earth's surface without such atmospheric effect which is called direct radiation [3], [14], [40].

2.2.2 Energy from the Sun

Energy from the sun can be used in three ways. Hence, when we are talking about solar energy, it is important to distinguish between these three types as stated in [19].

- **Passive heat:** This is heat that we receive from the sun naturally. This can be taken in to account in the design of buildings so that less additional heating is required.
- **Solar thermal:** Where we use the sun's heat to provide hot water for homes or swimming pools (also heating systems).
- **Photovoltaic energy (PV):** Uses energy from the sun to create electricity to run appliances and lighting. A photovoltaic system requires only daylight - not direct sunlight - to generate electricity. And this is the concern of this thesis.

2.2.3 Photovoltaics

In short, Photovoltaic means (photo = light; voltaic = produces voltage) or PV systems convert light energy from the sun directly into DC electricity using semiconductor technology (figure 2-2 clarifies this fact).

The physics of PV cell is very similar to the classical p-n junction diode. Solar cells consist of two types of materials, often p-type silicon and n-type silicon. Light of certain wavelength is able to ionize the atoms in the silicon and the internal field produced by the junction separates some of the positive charge (“holes”) from the negative charge (electrons) within the photovoltaic device.

These charge carriers (electron-ion pairs or electron-hole pairs in a solid semiconducting material) in the junction region create a potential gradient, get accelerated under the electric field and circulate as the current through an external circuit [3], [14], [40], [51].

The holes are swept into the positive or p-layer and the electrons are swept in to the negative or n-layer. Although these opposite charges are attracted to each other, most of them can only recombined by passing through an external circuit outside the material because of the internal potential energy barrier. Hence, if a circuit is made as is shown in the figure 2-2 below, power can be produced from the cell under illumination, since the free electrons have to pass through the load to recombine with the holes [48].

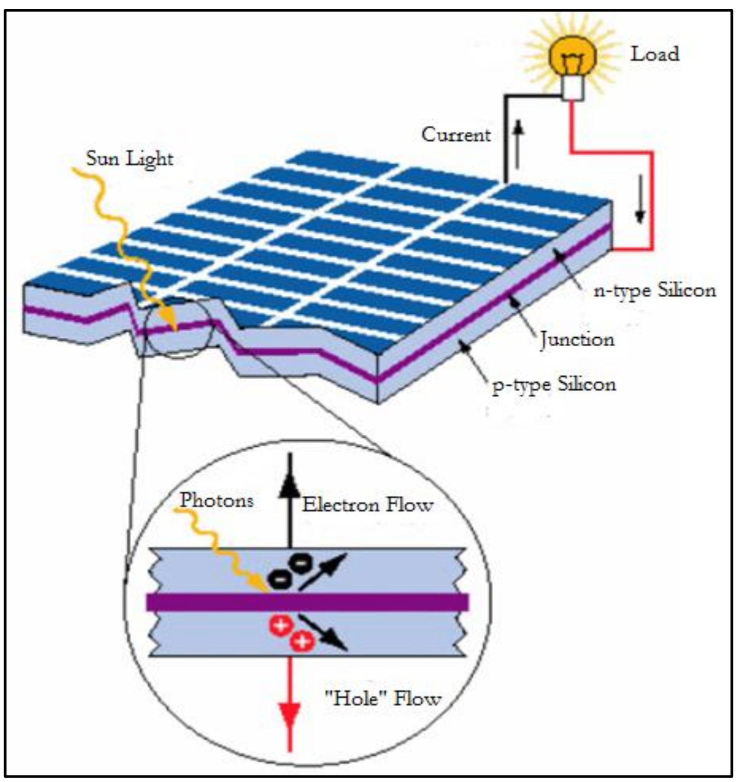

Figure 2-2 Photovoltaic effect in a solar cell [48]

2.2.4 Energy in the Photon

The intensity of light energy determines the amount of electricity generated. In other words, the conversion of energy relies on the quantum nature of light, whereby we perceive light as a flux of particles - photons - which carry the energy, E_{ph}, as given by eq. (2-1) [10].

$$E_{ph}(\lambda) = \frac{hc}{\lambda_p} \tag{2-1}$$

Where: h = the Planck constant,

c = the speed of light (m/s), and

λ_p= the wavelength of light (m).

On a clear day, approximately 4.4 x 10^{17} photons strike a square centimeter of the earth's surface every second. Those photons with energy in surplus of the band gap energy of the semiconductor material being used can be converted into electricity by the solar cell. An estimate of the current that can be generated by a solar cell is given by eq. (2-2). Ignoring losses in the cell, and assuming each photon produces one electron charge, for an electron charge of 1.6 x 10^{-19}coulomb, and 4.4 x 10^{17} photons striking a square centimeter of cell area, the current density is approximately 70mA/cm^2 [10].

$$I_L = qNA \tag{2-2}$$

Where: N = the number of photons,

A = the area exposed to light, and

q = charge in coulomb

The maximum voltage, V, that a solar cell can generate is equal to the band gap of the semiconductor in use and is expressed in electron volts. Hence, the maximum voltage is given by eq. (2-3) [10].

$$V = \frac{Eg}{q} \tag{2-3}$$

2.2.5 Model of PV Cell

A typical model or equivalent circuit for a PV cell is given in figure 2-3. For practical operation, solar cells are usually assembled into modules consisting of several cells or an array consisting of several modules.

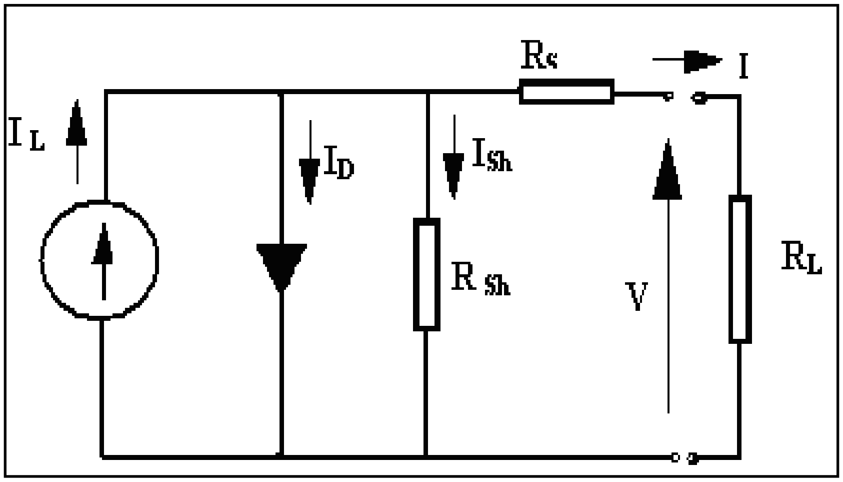

Figure 2-3 The one diode model of a solar cell [10]

The output-terminal current I is equal to the light-generated current I_L, less the diode-current I_D and the shunt-leakage current I_{SH}. The series resistance R_S represents the internal resistance to the current flow, and depends on the p-n junction depth and the impurities. The shunt resistance R_{SH} is inversely related with leakage current to the ground. In an ideal PV cell, $R_S = 0$ (no series loss), and $R_{SH} = \infty$ (no leakage to ground). In a typical high quality one square inch silicon cell, R_S = 0.05 to 0.10 ohm and R_{SH} = 200 to 300 ohm [3], [10], [40], [51].

The current at the output terminal is given by:

$$I = I_L - I_D - I_{SH} \tag{2-4}$$

$$I = I_L - I_O \left[\exp\left(\frac{q(V + IR_S)}{aKT} \right) - 1 \right] - \frac{V + IR_s}{R_{SH}} \tag{2-5}$$

Where: I = the load current (A)

I_D = the diode current (A)

I_L = current produced by the cell (A)

I_{SH} = current through the shunt resistance (A)

I_O = reverse saturation current of the diode (A)

q = charge on an electron (C)

V = output voltage (V)

K = Boltzmann's constant

T = working temperature of the cell (K)

a = the diode quality/curve fitting factor

2.2.6 Pros and Cons of PV System

PV technology has numerous advantages listed below as stated in [10].

- The energy resource is free, renewable, and everlasting everywhere it counter balances greenhouse gas and pollutant emissions.
- It produces energy during the day time when demand peaks, which is when power is typically most expensive to produce.
- After the initial setup, the facilities can operate with diminutive maintenance.
- Operating costs are extremely low compared to other power technologies.
- It is highly reliable and generates electricity at the actual point of use.
- PV systems are easily expandable, allowing for initial set-up even with a small budget and the addition of more modules in the future, when convenient.

With regard to the application of PV in a country such as Ethiopia and more generally in the developing world, where there is abundant sunlight, a large rural population and where there is no proper infrastructure or resources to develop an electrical grid, it should be a very attractive option.

Considering the case of Ethiopia, solar energy is available almost everywhere across the country than other renewable resources, such as hydro and/or wind. Where wind and hydro are available, they too are good sources of energy, but only selected areas have good wind and hydro power potential is not evenly distributed either. The impact that water storage for hydropower may have on the already meager availability of arable land is also a concern that needs to be addressed before embarking on the process of harnessing this resource [10].

2.2.7 Cells Modules and Arrays

PV cells are the fundamental building blocks of PV systems. The power generated by a PV cell is only not enough to power small devices such as electronic calculators. Each silicon solar cell produces about 0.5 volts.

To meet higher loads the PV cells must be connected in series and/or in parallel depending on the magnitude of the voltage and current required. Typically, 36 to 48 cells are connected in series to form a module which is capable of producing enough voltage to charge 12 volt batteries and run pumps and/or motors [10].

Modules are the basic building blocks of systems. For more voltage or current modules are connected in series or in parallel respectively to form a panel and then panels can be assembled into a group to form a complete PV array. Figure 2-4 shows the schematic configuration of cells, modules and arrays.

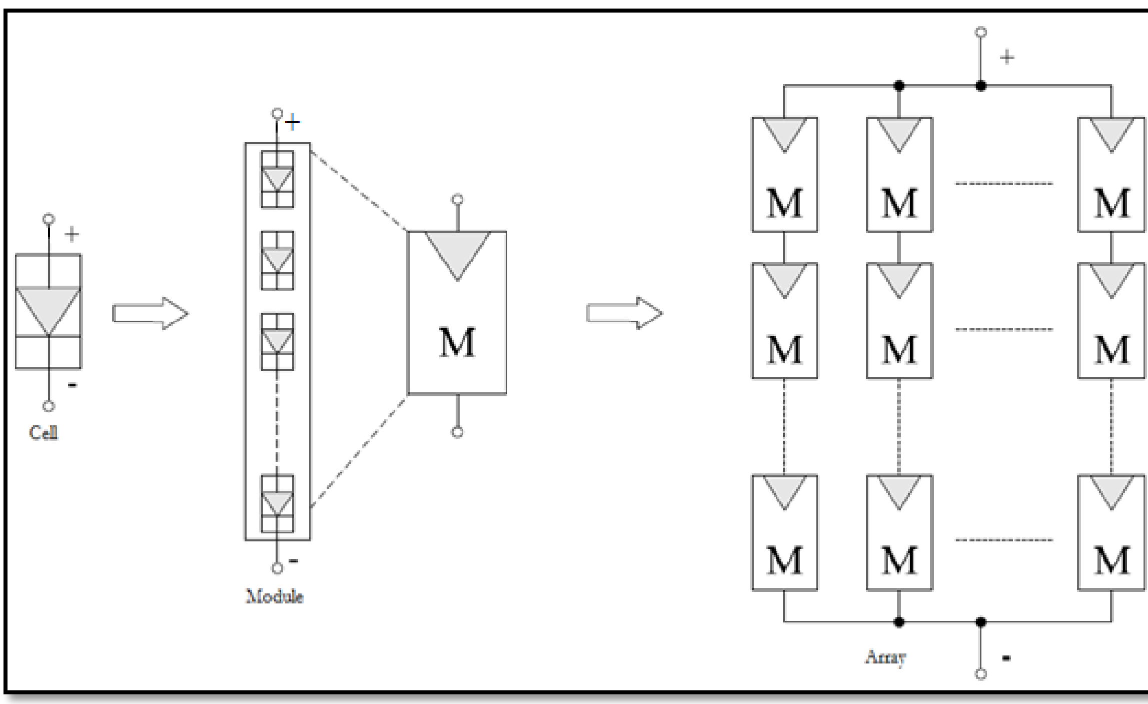

Figure 2-4 PV cell, module and array [54]

2.3 Wind Energy Conversion System (WECS)

Figure 2-5 Wind park (farm) [21]

2.3.1 The Wind

Wind is a form of solar energy. Winds are caused by the uneven heating of the atmosphere by the sun, the irregularities of the earth's surface, and rotation of the earth. Wind flow patterns are modified by the earth's terrain, bodies of water, and vegetative cover.

2.3.2 Wind Turbines

Wind turbines, like aircraft propeller blades, turn in the moving air and power an electric generator that supplies an electric current. Simply stated, a wind turbine is the opposite of a fan. Instead of using electricity to make wind, like a fan, wind turbines use wind to make electricity. The wind turns the blades, which spin a shaft, which connects to a generator and makes electricity.

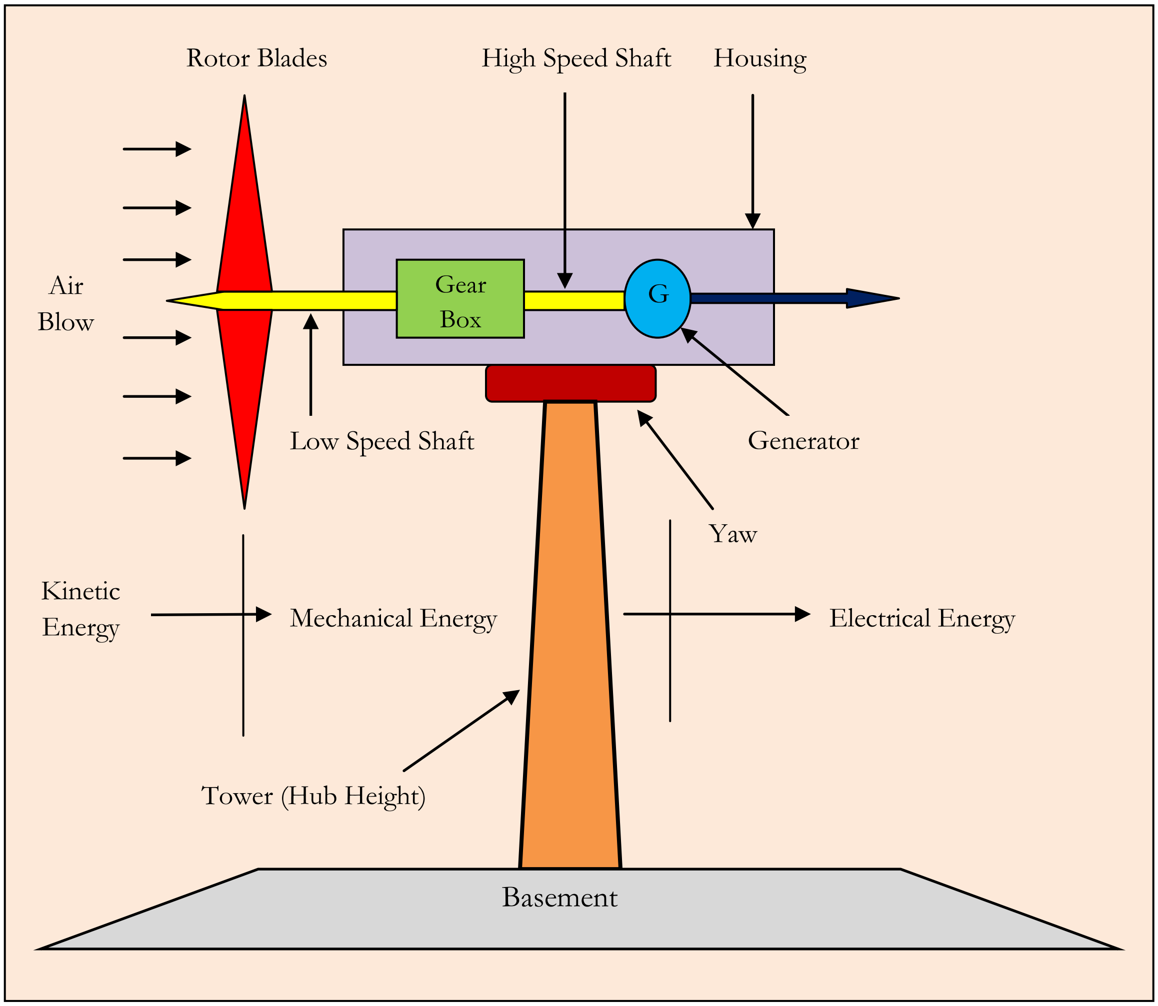

Figure 2-6 Block diagram of a typical WECS redrawn from [54]

2.3.3 Description of Wind Turbine Parts

The main principal components of a typical wind turbine as stated in [48] are:

- **Hub:** Hub is the connection point for the rotor blades and the low speed shaft.
- **Gear box:** Gears connect the low-speed shaft to the high-speed shaft and increase the rotational speeds from about 30 to 60 rotations per minute (rpm) to about 1200 to 1500 rpm, the rotational speed required by most generators to produce electricity.
- **Generator:** The generator is connected to the high-speed shaft and is the component of the system that converts the rotational mechanical energy of the high speed shaft into an electrical output.

- **Tower (Hub Height):** The tower is used to support the housing and rotor blades and typically made of rolled, tubular steel, and built and shipped in sections because of its size and weight. Common tubular towers incorporate a ladder within the hollow structure to provide maintenance access.
- **Nacelle:** The rotor attaches to the nacelle, which sits at the top of the tower and includes the gear box, low-speed and high-speed shafts, generator, controller, and brake. A cover protects the components inside the nacelle. Some nacelles are large enough for a technician to stand inside while working.
- **Brake:** A disc brake which can be applied mechanically, electrically, or hydraulically to stop the rotor in emergencies.
- **Controller:** The controller starts up the machine at wind speeds of about 3.5 to 7.2 meters per sec (m/s) and shuts off the machine at about 30 m/s.
- **High-speed shaft:** Drives the generator.
- **Low-speed shaft:** The rotor turns the low-speed shaft at about 30 to 60 rpm.
- **Pitch:** Blades are turned, or pitched, out of the wind to keep the rotor from turning in winds that are too high or too low to produce electricity.
- **Rotor:** The blades and the hub together are called the rotor.
- **Yaw drive:** The yaw drive is used to keep the rotor facing into the wind as the wind direction changes.
- **Yaw motor:** Powers the yaw drive.
- **Electronic equipment:** Such as controllers, electrical cables, ground support equipment and interconnection equipment.

2.3.4 How Wind Power is Generated?

The terms “wind energy” or “wind power” describe the process by which the wind is used to generate mechanical power or electricity. Wind turbine captures the wind’s kinetic energy in the rotor consisting of two or more blades. The gear box transforms the slower rotational speeds of the wind turbine to higher rotational speeds on the electrical generator side. Electrical generator will generate electricity when its shaft is driven by the wind turbine, whose output is maintained as per specifications, by employing suitable control and supervising techniques. In addition to monitoring the output, these control systems also include protection equipment to protect the overall system [34], [28].

2.3.5 Advantages and Disadvantages of Wind Power Generation

Some major advantages of using wind turbines to generate power are:

- Environmentally friendly
- Produce no pollution
- No traditional fuel required
- Requires relatively little maintenance
- Long life time (up to 30 years)

Disadvantages:

- Interference with radio/TV signals if located inappropriately
- The wind doesn't blow all the time at required speed
- High initial cost

2.3.6 Energy in the Wind

Now consider again figure 2-7 which is the rotor part of the whole wind turbine indicated in figure 2-6.

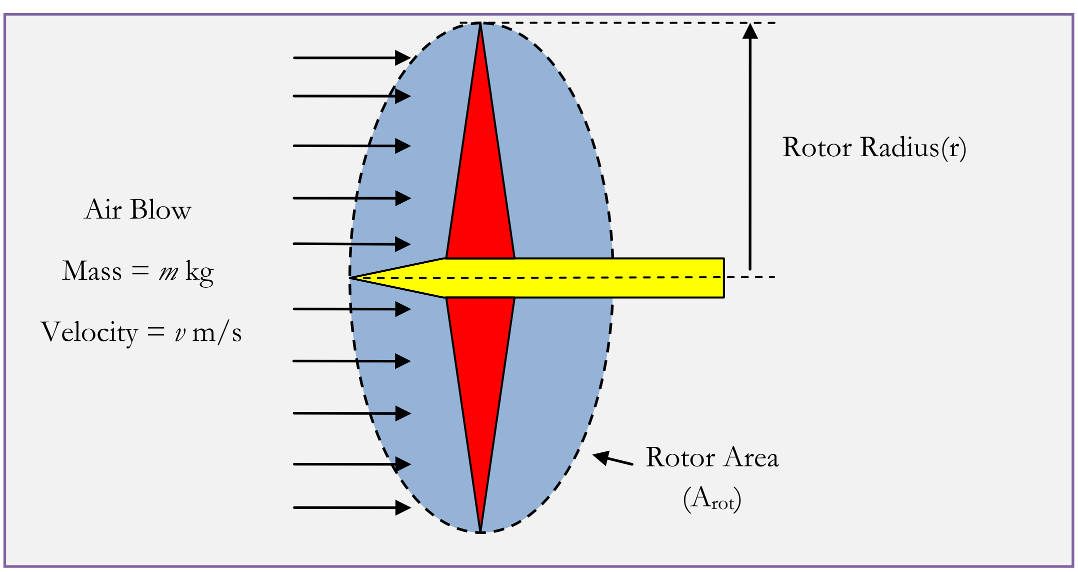

Figure 2-7 Turbine rotor area and radius

Air of mass *"m"* moving with speed "*v*" has a kinetic energy given by [28], [34]:

$$KE = \frac{1}{2} m v^2 [J] \tag{2-6}$$

Hence, the power per unit mass flow would be:

$$P = \frac{d}{dm}(KE) = \frac{1}{2}\frac{dm}{dt} v^2, and \ \frac{d}{dm}(m) = 1 \times \frac{dm}{dt} \tag{2-7}$$

Therefore,

$$\frac{dm}{dt} = \frac{d}{dt}(\rho V) = \frac{d}{dt}(\rho A h) = \rho A \frac{dh}{dt} = \rho A v \tag{2-8}$$

This is the mass (m) of air passing through a given area A_{rot} at speed *v* during a time period *t*. When we substituting this value in eq. (2-7), it gives:

$$P = \frac{1}{2}\frac{dm}{dt} v^2 = \frac{1}{2}(\rho A_{rot} v) v^2 = \frac{1}{2}\rho A_{rot} v^3 \tag{2-9}$$

Where: P = Mechanical power in moving air, W

ρ = Air density, kg/m^3

A_{rot} = Area swept by the rotor blades exposed to the wind, m^2

v = Wind speed, m/s

The swept area, A_{rot}, depends on the dimensions of the rotor. For a horizontal axis turbine of rotor radius r (as shown in Figure 2-7), the swept area can be given by [28], [34]:

$$A_{rot} = \pi r^2 [m^2] \tag{2-10}$$

For a vertical axis turbine of maximum rotor width w_r and rotor height h_r, the swept area can be approximated by [28], [34]:

$$A_{rot} = \frac{2}{3} w_r h_r [m^2] \tag{2-11}$$

The air density, ρ, depends on pressure and temperature. It can be expressed as [28], [34]:

$$\rho = \frac{P}{RT}[kg/m^3] \tag{2-12}$$

Where, P = the air pressure,

T = the absolute temperature and

R = universal gas constant.

For the available temperature data:

$$\rho = \frac{P_0}{RT}\exp\left(-\frac{gz}{RT}\right)[kg/m^3] \tag{2-13}$$

Where *Po* is standard sea level atmospheric pressure (101,325 Pa), g is the gravitational constant (9.8 m/s^2); and z is the region's elevation (m) [10].

If pressure and temperature data is not available, the correlation formula in eq. (2-14) may be used for estimating the air density [10].

$$\rho = 1.225 - \left(1.194 \times 10^{-4}\right) \times z[kg/m^3] \tag{2-14}$$

2.3.7 Power Extracted from the Wind

The actual power extracted by the rotor blades from wind is the difference between the upstream and the downstream wind powers. The extracted power by the blades is, therefore, less than the above value in eq. (2-9) as some power is left in the downstream air which continues to move at reduced speed. The actual mechanical power extracted by the rotor blades is [28], [34]:

$$P_w = \frac{1}{2} m_{fr}(v^2 - v_o^2)[W] \tag{2-15}$$

Where v and v_o are the upstream and downstream wind velocities at the entrance and exit of rotor blades respectively and the mass flow rate of air, m_{fr}, is given as a function of the average speed [28].

$$\textit{Mass flow rate, } m_{fr} = \rho A_{rot}\frac{v + v_0}{2}[kg/s] \tag{2-16}$$

With some algebraic manipulation, the power extracted by the rotor blades can be expressed as a fraction of upstream wind power as follows in eq. (2-17) [34], [39], [43].

$$P = \frac{1}{2}\rho A_{rot} v^3 C_p [W] \tag{2-17}$$

Where C_p is the fraction of upstream wind power captured by the rotor blades, also called as power coefficient of the rotor, expressed as [28]:

$$C_p = \frac{\left(1+\frac{v_o}{v}\right)\left(1-\left(\frac{v_o}{v}\right)^2\right)}{2} \tag{2-18}$$

The power coefficient of the rotor or the rotor efficiency, *Cp*, depends on v_o/v ratio and its maximum value is 0.59.

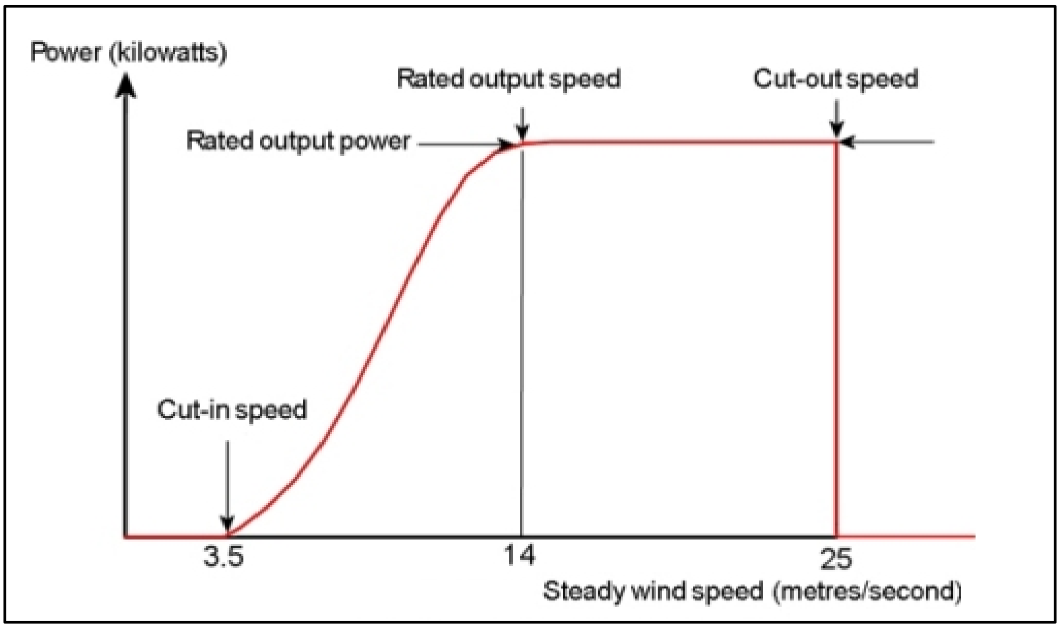

Figure 2-8 Typical wind turbine power output with steady wind speed [28]

From the characteristic curve in figure 2-8, there are three important points at which much attention is paid for the speeds and the corresponding turbine output powers for every wind turbine. These are the cut-in speed, rated output speed and cut-out speed. The important terms characterizing the turbine power-speed characteristics (Figure 2-8) are described below.

Cut-in speed: The speed at which the turbine first starts to rotate is called the cut-in speed and is typically between 3 and 4 m/s.

Rated output wind speed: Depending on the type of turbines, the wind turbine reaches a point where its capability of generating the maximum output power limit is attained at some speed. This limit to the generator output is called the rated power output and the wind speed at which it is reached is called the rated output wind speed.

Cut-out speed: As the speed increases above the rated output wind speed, the forces on the turbine structure continue to rise and, at some point, there is a risk of damage to the rotor. As a result, a braking system is employed to bring the rotor to a standstill. This is called the cut-out speed and is usually around 25 m/s.

2.4 Fuel Cell

2.4.1 Fuel Cells in General

Fuel cells are electrochemical devices that convert the chemical energy of a fuel (Hydrogen) directly to usable energy - electricity and heat - without combustion. This is quite different from most electric generating devices (e.g., steam turbines, gas turbines, and reciprocating engines) which first convert the chemical energy of a fuel to thermal energy, then to mechanical energy, and, finally, to electricity. In the last decade, fuel cells have emerged as one of the most promising technologies to meet the nation's energy needs for the 21st century. They produce electricity at efficiencies of 40 to 60% with negligible harmful emissions, and operate so quietly that they can be used in residential neighborhoods. Fuel cells are particularly well suited to the distributed power generation market because of these characteristics as well as their scalability, high efficiency, and modularity [12].

2.4.2 Principles of Operation

Figure 2-9 presents the basic components of a fuel cell, which include a positive electrode (anode), a negative electrode (cathode), and an electrolyte. Fuel is supplied to the anode, while oxidant is supplied to the cathode. Fuel is electrochemically oxidized on the anode surface, and oxidant is electrochemically reduced on the cathode surface. Ions created by the electrochemical reactions flow between the anode and cathode through the electrolyte. Electrons produced at the anode flow through an external load to the cathode, completing an electric circuit [12].

A typical fuel cell requires both gaseous fuel and oxidants. Hydrogen is the preferred fuel because of its high reactivity, which minimizes the need for expensive catalysts. Oxygen is the preferred oxidant because of its availability in the atmosphere. As indicated in figure 2-9, the electrolyte serves as an ion conductor [12].

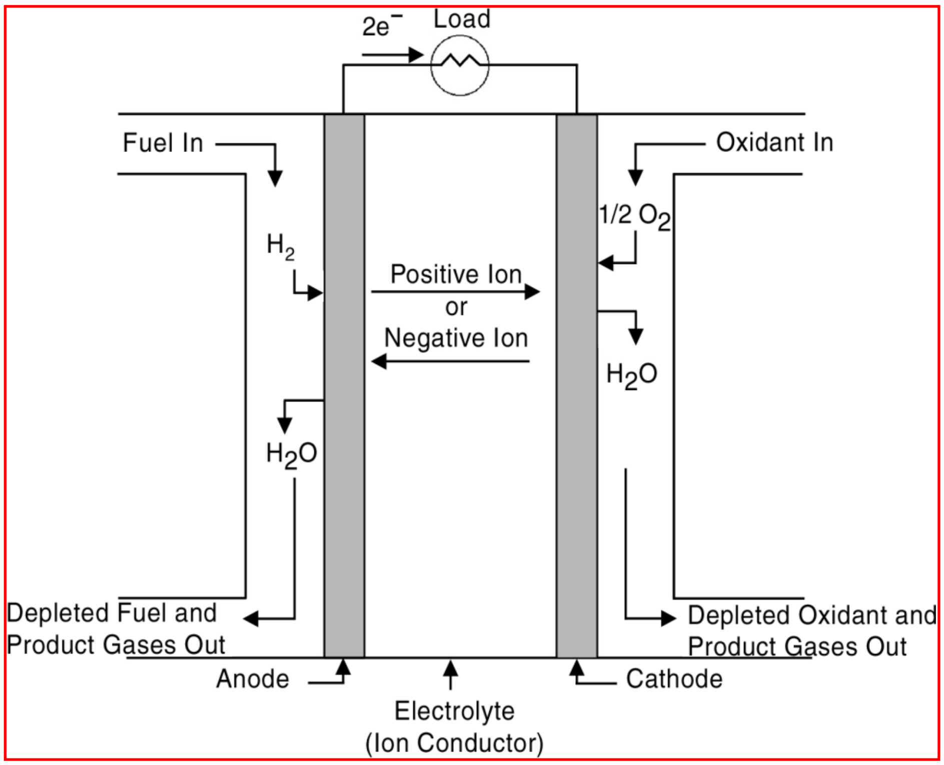

Figure 2-9 Fuel cell diagram [12]

The anodic half reaction; cathodic half reaction and the overall reaction takes place in the typical fuel cell can be generalized by the set of reactions indicated in eq. (2-19), eq. (2-20) and eq. (2-21) as well explained in [12].

Anodic half reaction: $H_2 \Rightarrow 2H^+ + 2e^-$ (2-19)

Cathodic half reaction: $\frac{1}{2} O_2 + 2H^+ + 2e^- \Rightarrow H_2O$ (2-20)

The overall reaction: $H_2 + \frac{1}{2} O_2 \Rightarrow H_2O$ (2-21)

2.4.3 Fuel Cell Stack

A single fuel cell is only capable of producing about 1 volt, so typical fuel cell designs link together many individual cells to form a stack that produces a more useful voltage. A fuel cell stack can be configured with many groups of cells in series and parallel connections to further tailor the voltage, current, and power produced [12].

2.4.4 Fuel Cell Types and their Field of Application

Fuel cell types are listed in Table 2-1 according to the order of operating temperature. Probable fields of application for the different fuel cell types are given in Table 2-2.

Table 2-1 Overview of the fuel cell Technologies [22]

Fuel Cell Type	Electrolyte	Temperature [°c]	Efficiency [%]
PEMFC	Polymer	80	60-65
AFC	Potassium Hydroxide, KOH	100	60-70
PAFC	Concentrated Phosphoric acid, H_3PO_4	200	40-45
MCFC	Molten Carbonate melts, Li_2CO_3	650	53-57
SOFC	Yittrium-stabilized Zirkondioxide, ZrO_2	1000	55-65

Table 2-2 Overview of the fuel cell applications [57]

FC Type	Fields of Application
PEMFC	- Stationary applications for domestic power and heat production - Stationary applications for dedicated power and heat production - Mobile applications for buses and service vehicles - Mobile applications for railroad systems
AFC	- Space and special military applications
PAFC	- Stationary applications for dedicated power and heat production - Mobile applications
MCFC	- Stationary applications for combined power and vapor production - Stationary applications for utility use
SOFC	- Stationary applications for domestic heat and power production - Stationary applications for commercial heat and power production - Stationary applications for utility use

2.4.5 Advantages and Disadvantages of Fuel Cells

The major and most important advantages of fuel cells and fuel cell plants as stated in [20] and [23] are:

- It combines at relatively high efficiency with a very low and/or zero level of environmental emission.
- It operates at a constant temperature, and the heat from the electrochemical reaction is available for co-generation applications.
- Direct conversion of chemical to electrical energy.
- Zero or very low noise except for occasional vibrations.

The major disadvantages are:

- Relatively high costs compared to conventional power sources.
- Decreasing electrical efficiency as a function of the operating life time.
- Special treatment of fuel (H_2) is necessary.
- Noble materials are needed for membranes and electrodes, e.g., platinum is one of the most effective catalysts.

2.5 Electrolyzer

2.5.1 What is an Electrolyzer?

An electrolyzer converts electricity into chemical energy which produces hydrogen. Hydrogen can be produced from water electrolysis in several ways such as alkaline, acidic, and solar photo production. Alkaline and acidic water electrolyzers are two of the most hydrogen producing electrolyzers and they are commercially available today. Alkaline water electrolyzer will be the main topic of interest in this thesis and its operating principle is discussed in the next section.

2.5.2 Principle of Operation

The decomposition of water into hydrogen and oxygen can be achieved by passing a DC electric current between two electrodes separated by a KOH electrolyte with good ionic conductivity. Water is a very poor ionic conductor and for this reason a conductive electrolyte must be used, so that the reaction can proceed at a technically acceptable cell voltage.

The half-cell reactions and the overall reaction are [2]:

Anodic half reaction: $2OH^{-} \Rightarrow \frac{1}{2}\, O_2 + H_2O + 2e^{-}$ (2-22)

Cathodic half reaction: $2H_2O + 2e^{-} \Rightarrow H_2 + 2OH^{-}$ (2-23)

The overall reaction: $H_2O \Rightarrow H_2 + \frac{1}{2}\, O_2$ (2-24)

2.6 Hydrogen Storage Tank

Hydrogen is characterized by a low density under normal conditions, so that its storage is difficult compared with liquid fuels. It can be stored in many basic configurations such as: (1) pressurized (compressed) hydrogen gas in tanks or in underground reservoirs; or (2) liquid hydrogen in tiny micro spheres; or (3) Metal hydride compounds, i.e., H_2 is stored in a metal or an alloy. The various storage types have different characteristics. The selection of a specific storage type depends on these characteristics, and mainly on energy density and cost of each type [2].

2.6.1 Compressed Gaseous Hydrogen Storage

Compressed gaseous hydrogen can be stored in pressure tanks at ambient temperature. The most common materials used for hydrogen tanks are steel and aluminum. From all storage technologies, the compressed gaseous hydrogen has the longest history and cheapest price. This storage type is suitable for electrolyzers, which can produce hydrogen at high pressures [2].

2.6.2 Liquid Hydrogen Storage

Liquid hydrogen has been used as a fuel in space technology for several years. The hydrogen liquefies to a colorless liquid at –253°C and thus the storage tanks require sophisticated insulation techniques. Liquid hydrogen is stored in standing or lying tanks of 3-75m³ under a pressure of 12bar [33]. The energy needed to liquefy the hydrogen is about 20 to 30% of the energy content of hydrogen. This is one of the largest problems concerning the use of liquid hydrogen. However, this loss of energy is quite compensated with high energy density of liquid hydrogen. This type of storage has fast refueling (125 liter tank of liquid hydrogen can be refueled within only 3 minutes) [7].

2.6.3 Metal Hydrides Storage

A special way of hydrogen storage is done by using metal hydride. Metal hydride is a metal or an alloy, which is able to bind the hydrogen chemically. This metal or alloy can store multiple hundreds of its capacity of hydrogen. When a hydride is formed with a metal or an alloy, heat is generated, i.e., the process is exothermic. Conversely, in order to release hydrogen from a metal hydride, heat must be supplied, i.e., the process is endothermic. These processes can be represented by the chemical reactions indicated in eq. (2-25) and eq. (2-26) as stated in [52].

Charging or Absorption process: $M + xH_2 \Rightarrow MH_{2x}$ (2-25)

Discharging or Desorption process: $MH_{2x} \Rightarrow M + xH_2$ (2-26)

Where M represents the hydriding substance, a metal or an alloy, MH is the metal hydride; x is ratio of the number of hydrogen atoms to the number of hydriding substance atoms.

2.7 Rechargeable Battery

Figure 2-10 Rechargeable lead-acid battery [21]

Battery is an electrochemical device which uses electrochemical reactions to store electricity in the form of potential chemical energy. The energy storing batteries used with HPSs are rechargeable in a sense that they can charge when there is enough supply from the RESs and discharge when there is larger load demand than there is supply. They are sometimes also called as secondary batteries. The charging time for the battery bank as formulated in [29] is:

$$t_{charge} = \frac{BC}{I_{rated,source}} (hr) \tag{2-27}$$

Where, t_{charge} = charging time of the battery (hr)

BC = Battery Capacity (Ah)

$I_{rated, source}$ = rated source current (A)

Rechargeable batteries have standard electric potential which is the potential difference between the cathode and anode. A simplified equivalent circuit of a battery when it is in steady state is given in [28] and is shown in figure 2-11 working as a voltage source with an internal resistance.

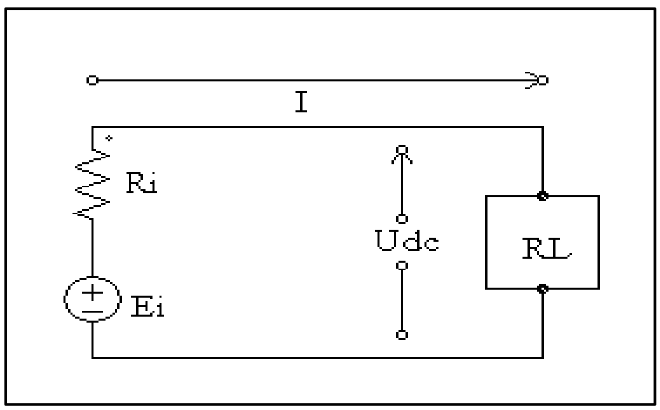

Figure 2-11 Simplified equivalent circuit of a battery [28]

Assuming that the open circuit voltage and resistance when the battery was fully charged are E_0 and R_0, then the open circuit voltage and internal resistance at any time when battery is discharging can be given as [34]:

$$E_i = E_0 - K_1 Q_d \tag{2-28}$$

$$R_i = R_0 - K_2 Q_d \tag{2-29}$$

The open circuit voltage decreases and the internal resistance increases with the Ah discharge, Q_d. The constants K_1 and K_2 can be found from curve-fitting test data [34].

Figure 2-12 shows simple circuit model of the simplified electric circuit with the conducting resistance, R_{ohm}, included.

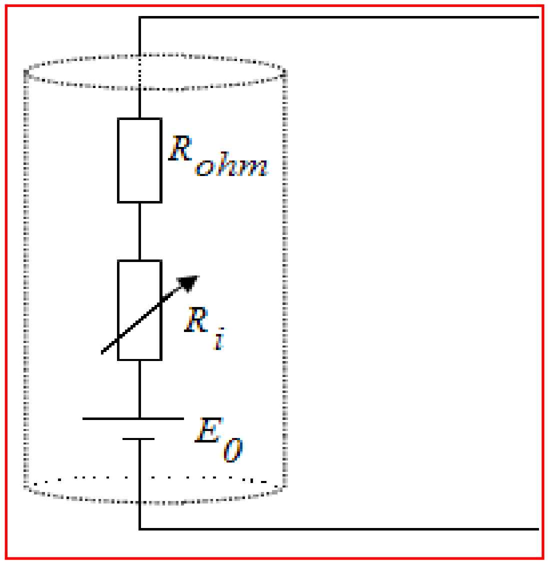

Figure 2-12 General electric circuit models for a rechargeable battery [28].

The simple electric circuit model shown in figure 2-12 includes an internal resistance, R_i conductor resistance, R_{ohm} and a standard cell potential E_o. Applying the maximum power transfer theory, the peak power, delivered from the battery in the above model is [34]:

$$P_{peak,stored} = \frac{E_o^{2}}{4(R_i + R_{ohm})} \tag{2-30}$$

The energy storage is dependent on the amount of active material in the battery cell. Thus, for an active material of mass, m (in gram) and a cell volume, V (in liters), the specific power (in W/g) and peak power density (in W/l) can be determined from the peak power [6].

$$P_{peak,specifuc} = \frac{P_{peak,stored}}{m} \tag{2-31}$$

$$P_{peak,density} = \frac{P_{peak,stored}}{V} \tag{2-32}$$

2.7.1 Battery Characteristics

Battery Capacity: This is a measure of how much energy the battery can store. The three main ratings to specify the capacity of a battery are [29]:

- *Ampere-hour (Ah)*: the current at which a battery can discharge at a constant rate over a fixed interval of time.
- *Reserve capacity*: the length of time (in minutes) that a battery can produce a specified level of discharge.
- *kWh capacity*: a measure of energy required to fully charge a depleted battery. A depleted battery is not usually a fully discharged battery.

Battery Voltage: The battery voltage is that of a fully charged battery. It depends up on the number of cells and voltage per cell.

Energy Density/Specific Energy: Energy density is a measure of how much energy can be extracted from a battery per unit of battery weight or volume.

Power Density/Specific Power: Power density is a measure of how much power can be extracted from a battery per unit of battery weight or volume.

Autonomy: This variable is defined by the ratio of restorable energy capacity to maximum power discharge. It refers to the maximum amount of time the system can continuously release energy [29].

$$a = \frac{E_{restore}}{P_{discharge}} \tag{2-33}$$

Durability (Cycling Capacity): The number of times the energy storage can release the energy level it was designed for after each recharge is referred to as durability or cycling capacity. It is expressed in number of cycles, N_{cycles}.

Self-Discharge: This refers to the portion of energy which was initially stored and dissipated in a given non-use period of time [29].

CHAPTER THREE

3. TECHNO-ECONOMIC FEASIBILITY STUDY OF THE HYBRID POWER SYSTEM

3.1 Load Estimation

Deciding on the load is one of the most important steps in the design of a hybrid system. Primary load, which must be met immediately, and deferrable load, which must be met within a certain time, are both considered in this thesis.

Electric load in the rural villages of Ethiopia can be assumed to be composed of lighting radio and television, water pumps, health post and primary schools load [10]. The work indicated in [48] considered only lighting, radio and television as a community load. Other studies in AAiT cited in the reference as [11] & [47] assumes additional electricity demand for cooking and for flour mills to the load together with the load considered in [10]. In this thesis work barbers, shops and church loads are incorporated additionally.

The daily power demand and energy need for the community of 289 households are estimated by considering basic domestic appliances such as television (70W), CFL of 11W and 15W for lighting, radio/tape (5W), VCD/DVD player (15W), refrigerator (70W), "electric mitad" (2.5kW), cell phone (2.5W) and stove (1.5kW). The graph in figure 3-1 shows the one day load trend curve of the households.

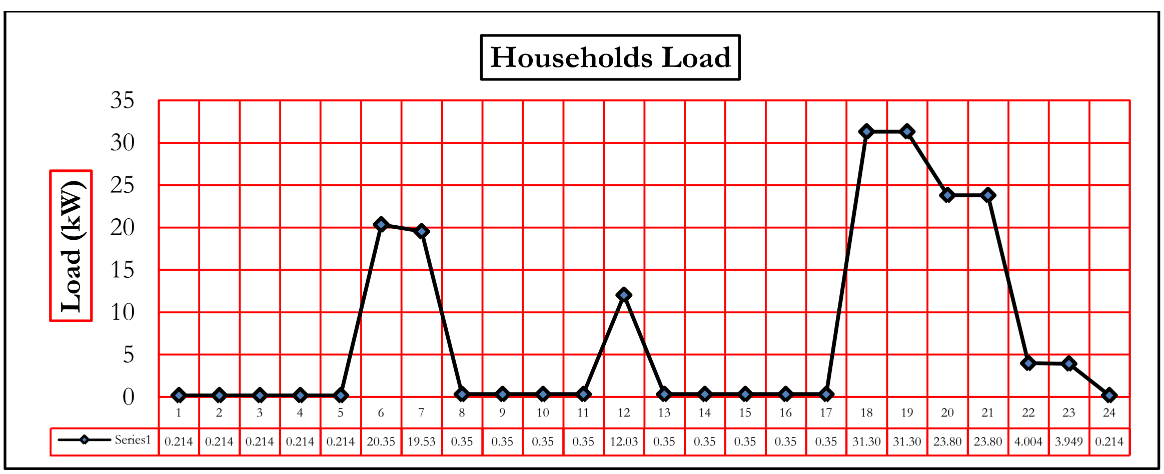

Figure 3-1 The 24 hour load profile of households

The primary school consists of 8 classrooms, director office, teacher's staff, toilet, and guard house. Each classroom is assumed to be installed with four 15W CFLs (Compact Fluorescent Lamps); one 15W CFL is suggested for the teacher's staff; one 15W CFL is assumed for director office; two 11W CFLs are allowed for the toilet; one 11W CFL for the guard house and additional 4 CFLs (of 15W) for external lighting are also considered. Evening classes are conducted from 18:00 to 21:00.

Additionally, four computers (LCD desktop type of 200W) one in the director office and three in the teachers staff; one printer (360W), one photocopy machine (1000W), tape/radio (5W), one GSM wireless telephone (2W) and two ceiling fan (80W each) one in the director office and one in the teachers staff are proposed.

Accordingly, the final synthesized load profile for the school in a typical day looks like as indicated by figure 3-2 below.

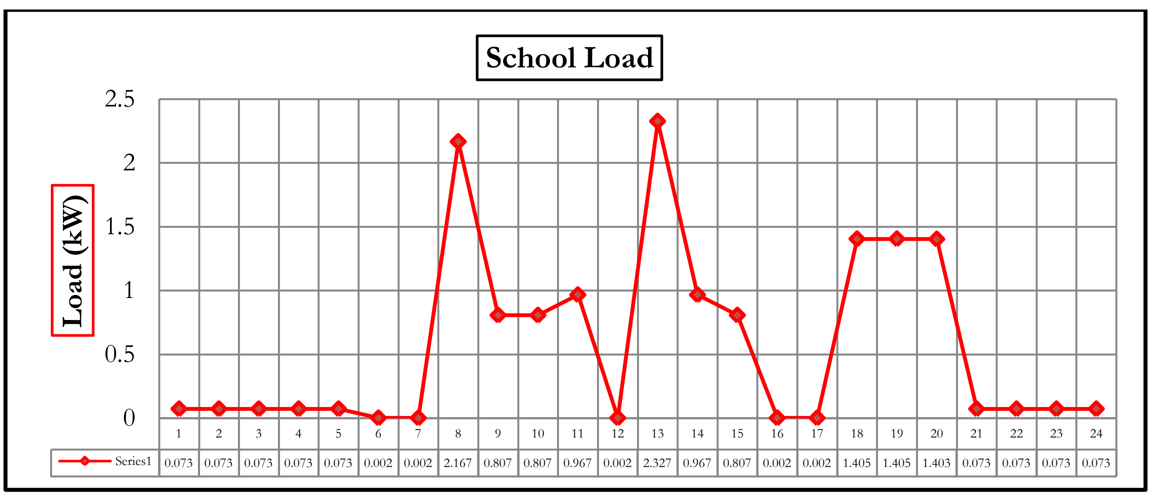

Figure 3-2 The 24 hour load profile of a primary school

For the health centers, having 3 rooms, 15W CFL per room, one 15W CFL for external lighting, one 11W for the toilet and one 11W CFL for guard house are considered.

When we come to the appliances used, it is based on the typical category I rural health clinic presented in [53]. Accordingly, basic small health post clinical equipment's such as vaccine refrigerator (134W), a 15W capacity microscope, a 135W capacity centrifuge, 2kW water heater, 400W incubator, a 75 W television, GSM wireless telephone (2W) and three ceiling fan (each of 80W in each room) are suggested. The final 24 hour daily load profile curve was obtained as indicated by figure 3-3.

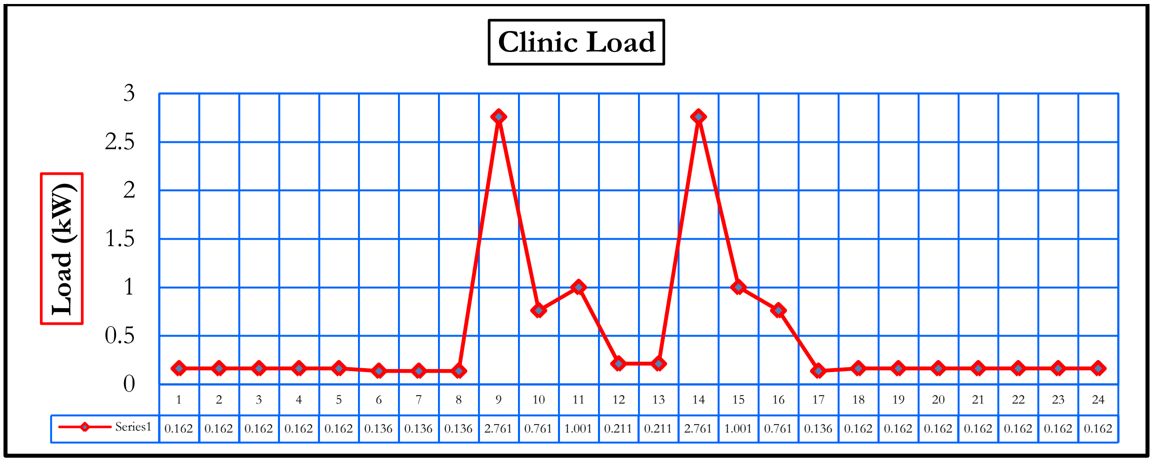

Figure 3-3 The 24 hour load profile of a health post

For the community two flour milling machines of 12.5 kW capacity each working from 9:00 to 12:00 and 14:00 to 18:00 with four 15W CFL for internal lighting (from 18:00 to 20:00) and two 15W CFL for external lighting (from 18:00 to 6:00) are assumed. Figure 3-4 shows the daily power consumption of the flour milling machines.

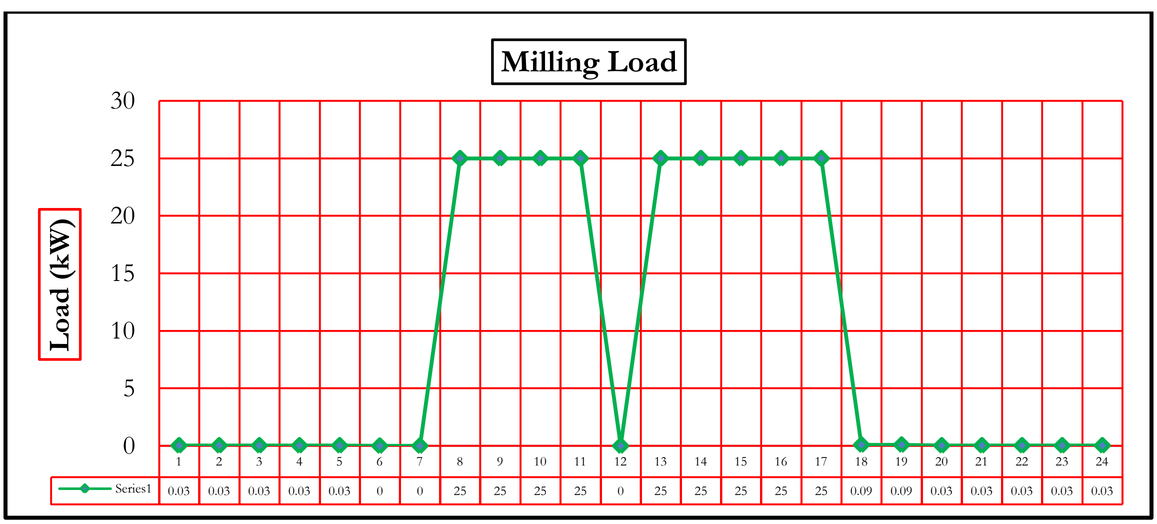

Figure 3-4 The 24 hour load profile of flour milling machines

For the church six 15W CFL in the internal lighting, one 15W CFL in the "Bethlehem", one 15W in the office, four 11W CFL in the "meeting hall", four 15W CFL for the external lighting and one 11W for the guard house are assumed. Besides these, a GSM wireless telephone of 2W is proposed. Figure 3-5 shows the one day power consumption profile of the loads considered.

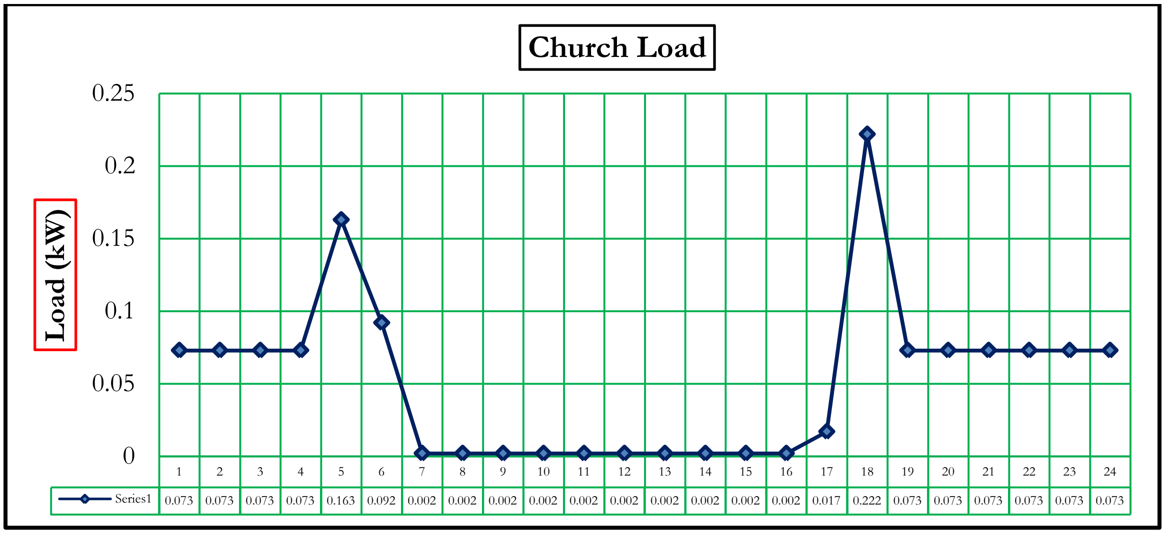

Figure 3-5 The 24 hour load profile of a church

There are a total of three shops assumed and each shops are expected to have a radio/tape of 5W and 15W CFL. The CFL is supposed to operate from 18:00-21:00. The daily profile can be recognized from figure 3-6.

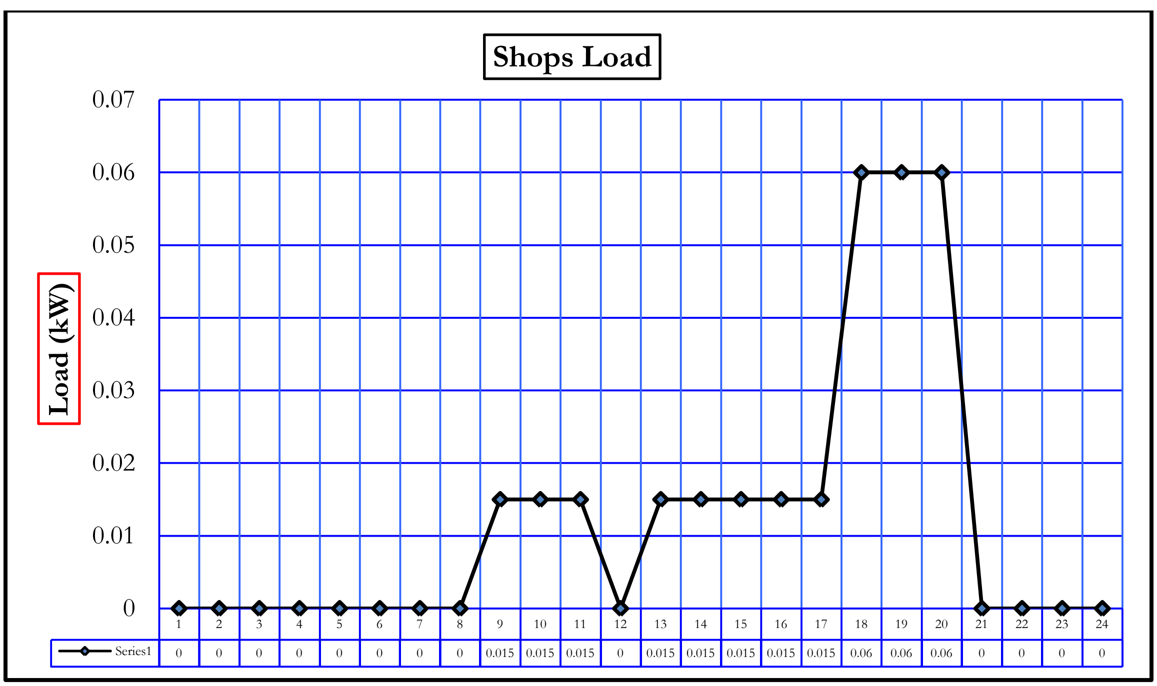

Figure 3-6 The 24 hour load profile of shops

In the community two barber shops are considered each having two hair clipping machine of 12W. Additionally, one 15W CFL for lighting between 18:00 to 21:00 is suggested for each. Figure 3-7 illustrates the load variation over the 24 hours in a day.

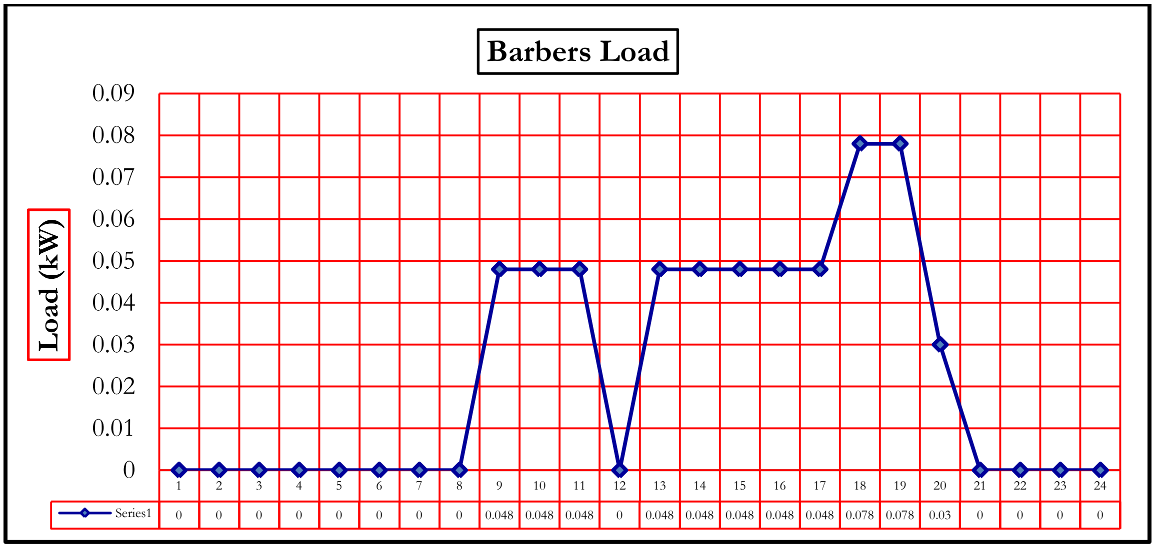

Figure 3-7 The 24 hour load profile of barbers

Figure 3-1 up to figure 3-7 shows the primary load profile of the community in different categories. Hence, the total primary load profile of the village can be considered as the sum of the whole loads indicated by the above graphs and it is showen in figure 3-8.

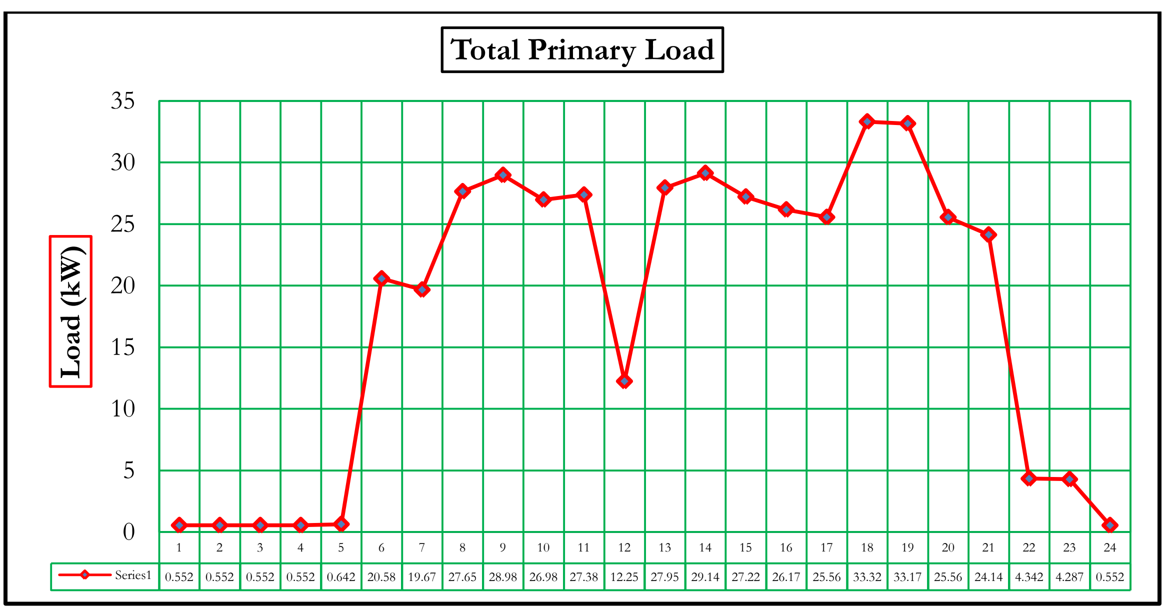

Figure 3-8 The 24 hour load profile of total primary loads in weekdays

The total primary load in weekend is expected to be less than weekdays. Because, some loads such as milling machines, school loads and clinics will not operate. Hence, by considering some load reduction in weekends, the 24 hour load trend curve indicated by figure 3-9 was obtained.

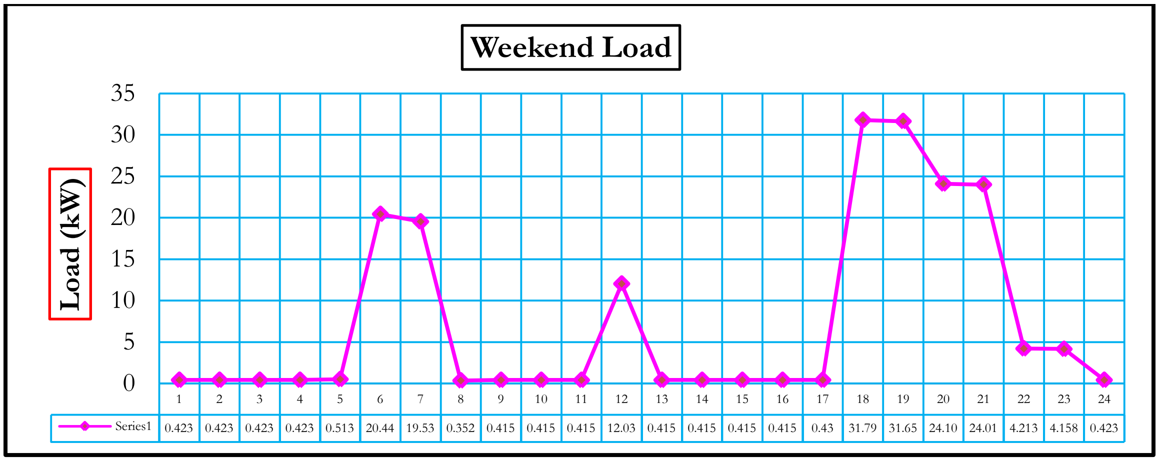

Figure 3-9 The 24 hour load profile of total primary loads in weekends

Water pumping system is required for the households, the schools and health care centers. A minimum of 100 l of water per day per family and 2400 l/day for each pair of one health center and one primary school is suggested [10], [47]. Therefore, to accomplish this, we need to have three 1.528kW of 40.416 l/m capacity (a total need of 4.584kW) water pumps so as to pump water for the community which operates for four hours with the energy demand of 18.336kWh. Again we need to have one 1.119 kW of 20 l/m capacity water pump for the school and clinic that operates for two hours with the energy demand of 2.238kWh. Hence the total peak deferrable load is 5.703kW which needs 20.574kWh energy.

A water storage capacity of 4 days is suggested requiring a storage capacity of 73.344 kWh for the community and 8.952kWh for primary school and health centers. Hence, the total storage capacity is equal to 82.296kWh.

Up to 30% deferrable load reduction can be expected in the rainy season [10], [47]. 15% load decrease for June, January and September while 30% for July and August are assumed [47]. There are no classes in July and August (annual break) and in January (semester break). With these assumptions, the monthly power consumption and energy demand of the water pumps are indicated by Table 3-1 and figure 3-10.

Table 3-1 Monthly deferrable loads

Month		Jan	Feb	March	April	May	June	Jul	Aug	Sept	Oct	Nov	Dec
Deff. Load	kW	4.8	5.7	5.7	5.7	5.7	4.8	4	4	4.8	5.7	5.7	5.7
	kWh	17.5	20.6	20.6	20.6	20.6	17.5	14.4	14.4	17.5	20.6	20.6	20.6

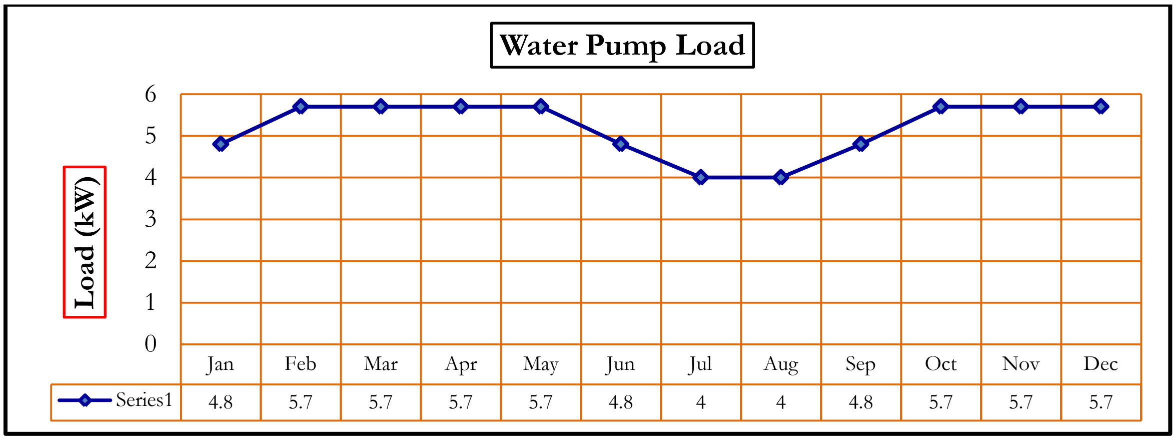

Figure 3-10 The monthly profile of deferrable loads (water pumps)

3.2 HOMER Model of the Hybrid System

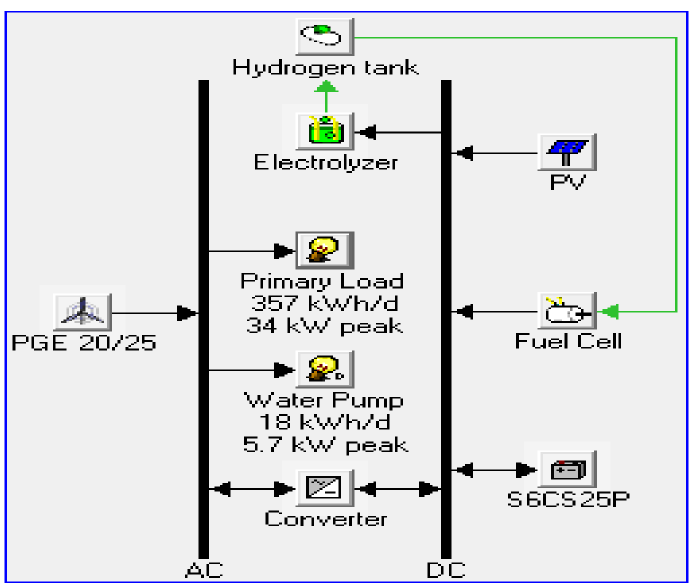

Figure 3-11 HOMER model of the hybrid power system

3.2.1 Primary Load Input

The 24 hour synthesized primary load profile which is generated by HOMER from the time series hourly input data's is given in figure 3-12.

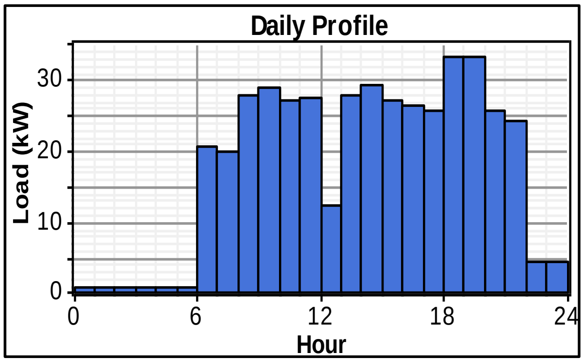

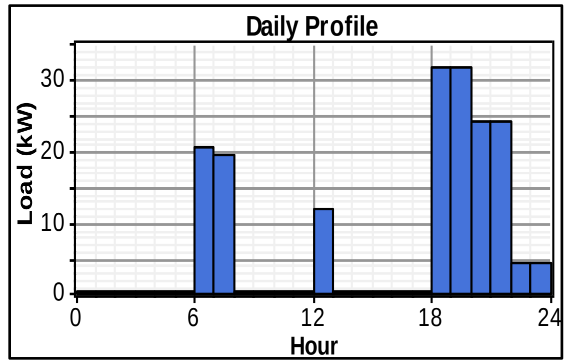

Figure 3-12 Primary load daily profiles (the first-weekday; the second-weekend)

3.2.2 Deferrable Load Input

The monthly deferrable load profile interred in to HOMER software is indicated by figure 3-13 which shows the monthly variability of the water pumping loads.

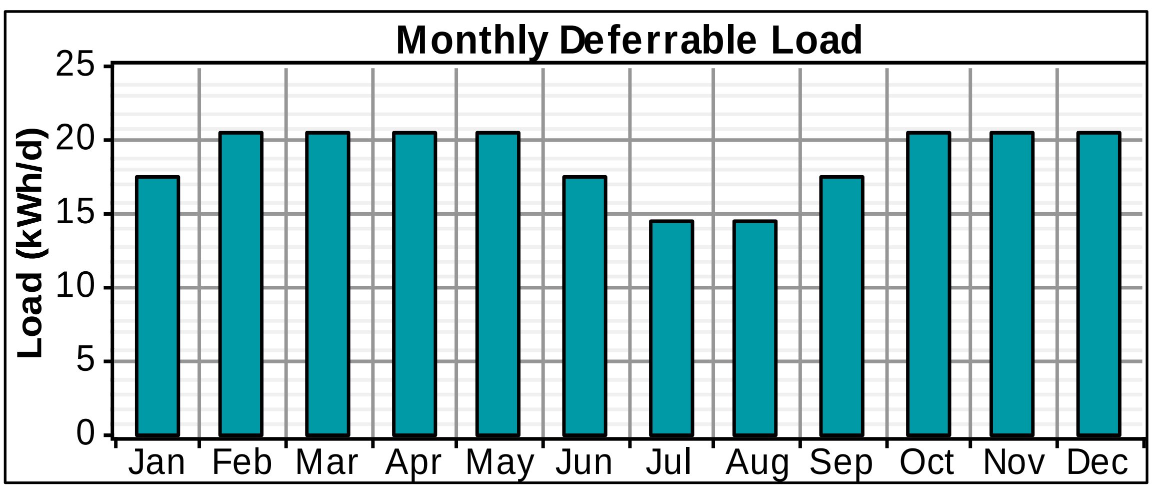

Figure 3-13 Monthly deferrable load profiles

3.2.3 Resource Inputs

The monthly average wind speed for the study area, determined in the ways described in chapter one was fed into HOMER. Figure 3-14 shows the average wind resource profile of each month at 10 m above the surface of the earth.

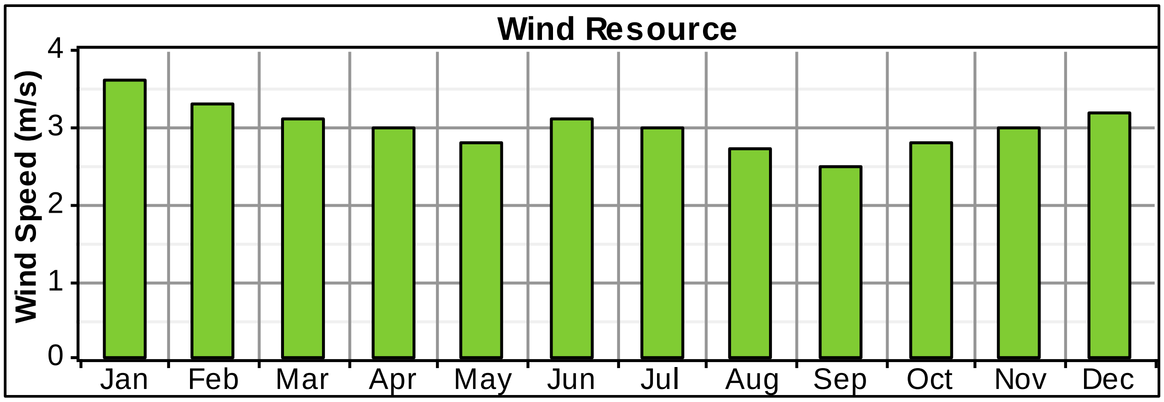

Figure 3-14 Monthly average wind speeds at 10m

The probability density function of the wind speed synthesized by HOMER is also given in figure 3-15 below. The software estimates a Weibull k = 1.87 and c = 3.39 m/s.

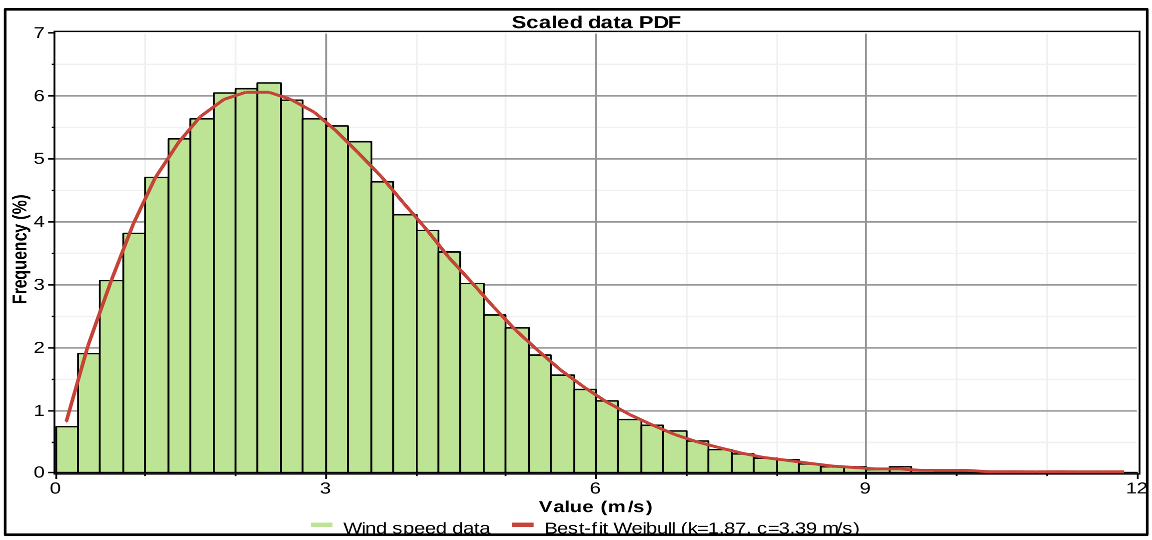

Figure 3-15 Wind speed probability density function at 10m

In a similar way, the solar energy potential for the study area was fed into HOMER and this is shown in figure 3-16. This figure also shows the clearness index which HOMER generates for the analysis. The clearness index is the fraction of solar radiation transmitted through the atmosphere which strikes the surface of the Earth and hence it is a measure of the clearness of the atmosphere. It is a dimensionless number between 0 and 1, defined as the surface radiation divided by the extraterrestrial radiation. Typical values for the monthly average clearness index range from 0.25 (a very cloudy month) to 0.75 (a very sunny month).

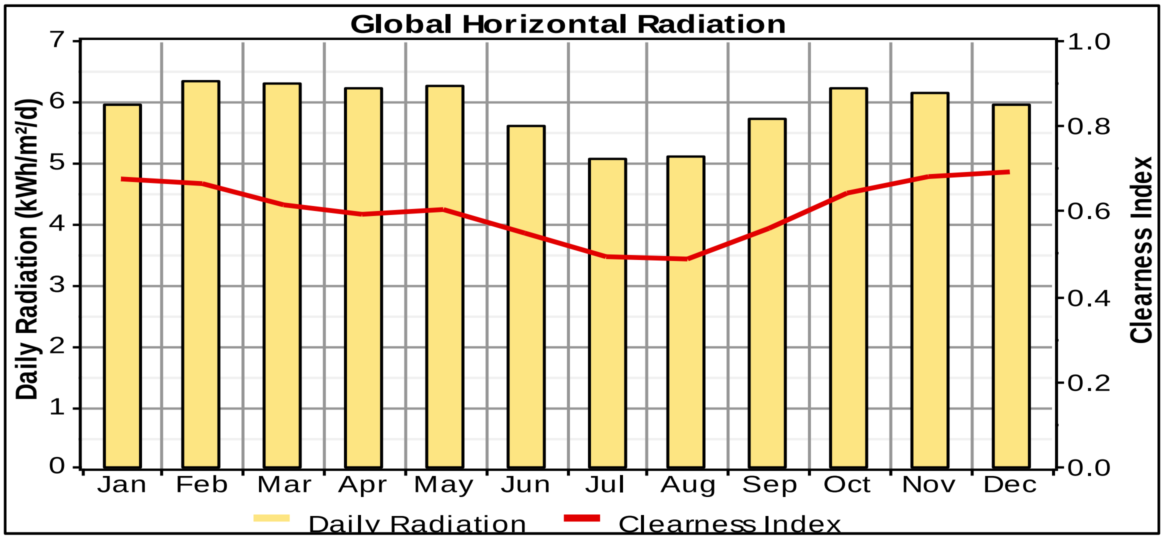

Figure 3-16 Monthly average radiations

The monthly temperature variation which is fed in to the HOMER software is indicated by figure 3-17. HOMER uses the ambient temperature to calculate the PV cell temperature and to consider temperature effect in the PV system.

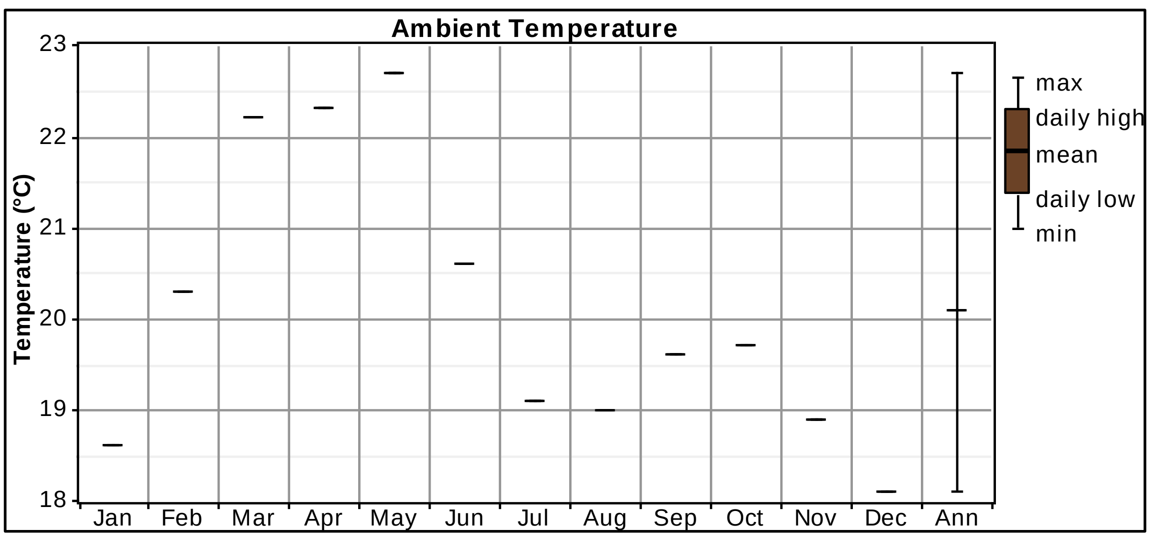

Figure 3-17 Monthly average ambient temperature

3.2.4 Summary of Additional Inputs for Simulation

The capital, replacement and operational and maintenance cost of each component in the hybrid system are given in Table 3-2. The table also contains the components average operational life year and the size and/or quantities considered in the study.

Table 3-2 Summary of additional inputs for HOMER simulation

	PV Array	Wind Turbine **(PGE20/25)**	Fuel Cell	Electrolyzer	Converter	Battery **(Surrette 6CS25P)**	Hydrogen Tank
Unit	kW	kW	kW	kW	kW	Ah	kg
Size	1	25	1	1	1	1156	1
Capital Cost ($)	**2,000**[1]	**55,000**[2]	**3,000**[3]	**1,000**[4]	**700**[5]	**855**[6]	**1,300**[7]
Replacement Cost ($)	2,000	36,667	2,000	667	700	555	867
O & M Cost ($/yr.)*	0 (0 %)	1,100 (2.5 %)	$ 0.02/hr	5 (0.5 %)	0 (0 %)	8.55 (1 %)	13 (1 %)
Size Considered	0, 50, 80 100, 110, 150, 200	-----------------	0, 5, 10, 15, 20, 25	0, 5,10, 15, 20, 25, 30, 50, 100	0, 30, 40, 50	-------------	0, 5, 10, 15, 20, 25, 30, 50
Quantities Considered	------------	0, 1, 2, 3	--------------	---------------	-------------	0,80, 100, 120, 140, 160, 180	------------
Life Time	25 yrs.	25 yrs.	40,000 hrs.	25 yrs.	15 yrs.	9,645 kWh	25 yrs.
*Considering O & M Cost as 0 - 10 % of the Capital Cost is a Standard Procedure.							

[1]PV cost is obtained from [36] & [26].
[2]Wind Turbine cost is obtained from [36] & [26].
[3]FC cost is obtained from WWW.homerenergy.com sample files and additional web search.
[4]Electrolyzer cost is obtained from WWW.homerenergy.com sample files and web search.
[5]Converter cost is obtained from [10], [47] and additional web search.
[6]Battery cost is obtained from [10], [47] and additional web search.
[7]Hydrogen Tank cost is obtained from WWW.homerenergy.com sample files & web search.

CHAPETR FOUR

4. DYNAMIC MODELING OF THE OPTIMUM HYBRID POWER SYSTEM

4.1 General Simulink Model of the Hybrid System

The general MATLAB/Simulink model of the optimum hybrid PV-Wind-Fuel Cell power system is given in figure 4-1. The detailed models of subsystems are presented in the coming subsequent sections.

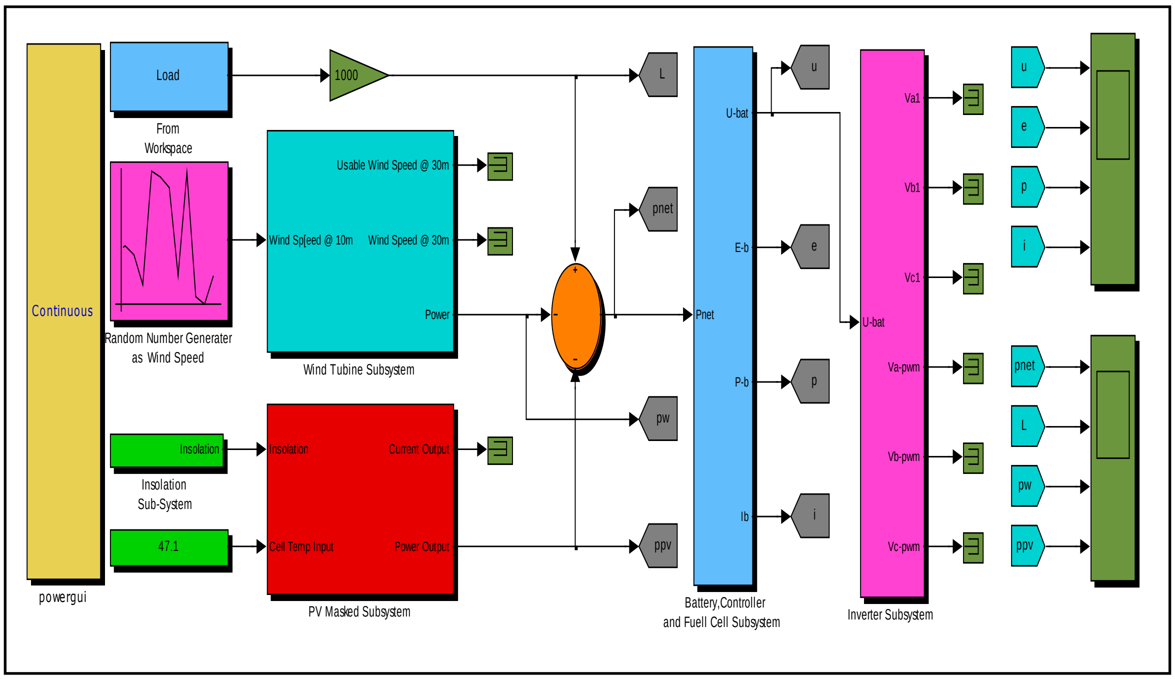

Figure 4-1 General MATLAB/Simulink model of PV/Wind/Fuel Cell hybrid system

4.2 Wind Turbine Subsystem Model

The wind turbine is modeled by the power curve equation indicated in eq. (4-1).

$$P_{wind}(t) = \frac{1}{2}\rho A_{rotor} v(t)^3 c_p \tag{4-1}$$

The air density (ρ) of the study area (Nifasso) is taken as 0.98 kg/m^3 (it is calculated based on the discussion presented in chapter two, section 2.3.6, pp. 22, eq. (2-12)). The rotor area of PGE 20/25 wind turbine is 305 m^2 [49]. Cp is taken as 59% = 0.59. The hub heights of PGE 20/25 wind turbine are 24/30/36 meter [49] and for this study, 36m is used. Gear and generator efficiency of 95 % is also considered (hence, cumulative efficiency of gear-generator = 0.95×0.95 = 90.25 %). With this detail's, the wind turbine in MATLAB/Simulink is given below in figure 4-2.

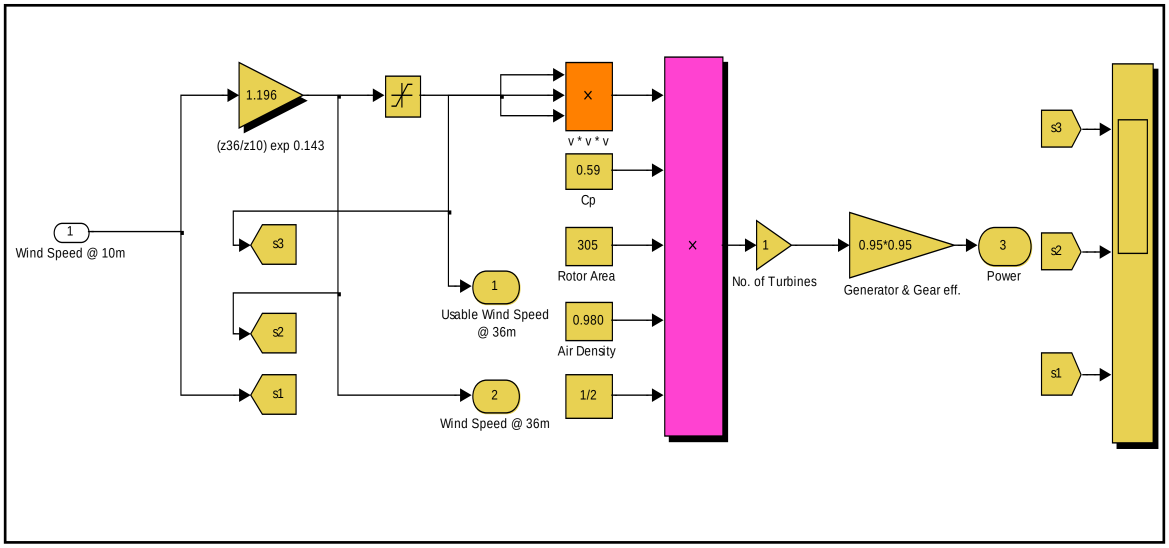

Figure 4-2 Expanded view of the wind turbine model

4.3 PV Subsystem Model

The equivalent circuit for the solar module arranged in N_P parallel and N_S series is shown in figure 4-3 below.

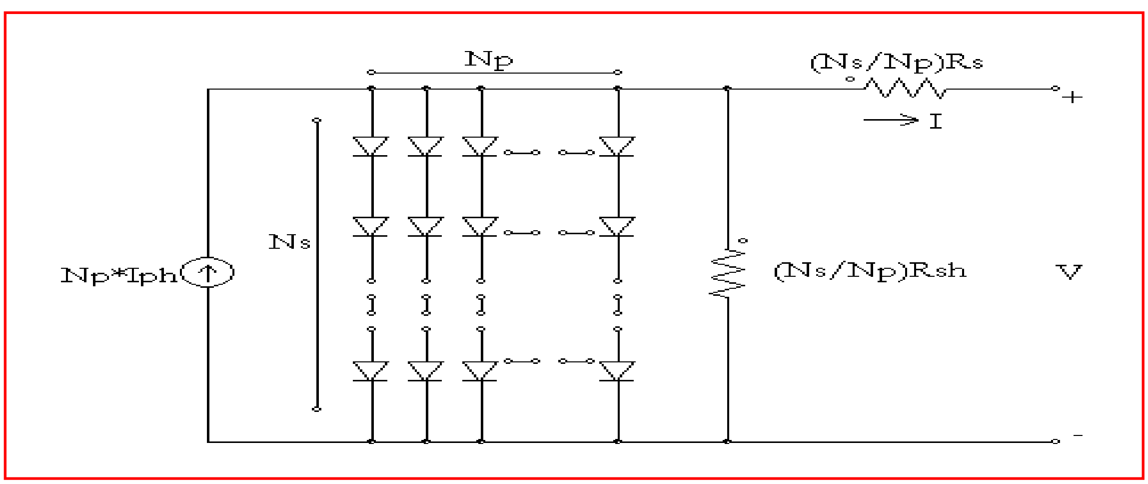

Figure 4-3 Circuit model of a generalized PV array [9]

The terminal equation for the current and voltage of the array becomes expressed in eq. (4-2) as stated in [9], [25] and [50].

$$I = N_p I_{PH} - N_P I_S \left[\exp\left(\frac{q\left(\frac{V}{N_s} + \frac{IR_s}{N_p} \right)}{KT_c a} \right) - 1 \right] - \frac{\frac{N_p V}{N_s} + IR_s}{R_{SH}} \quad (4\text{-}2)$$

Where: I_{PH} is a light generated current or photocurrent, I_S is the cell saturation of dark current, q (= 1.6 $\times 10^{-19}$C) is an electron charge, k (= 1.38 $\times 10^{-23}$J/K) is a Boltzmann's constant, T_C is the cell's working temperature, a is an ideal factor, R_{SH} is a shunt resistance, and R_S is a series resistance.

The photocurrent mainly depends on the solar insolation and cell's working temperature, which is described as:

$$I_{PH} = \left(I_{SC} + K_I \left(T_C - T_{\mathrm{Ref}}\right)\right)\lambda \quad (4\text{-}3)$$

Where: I_{SC} is the modules short-circuit current at a 25°C (T_{Ref}) and 1kW/m^2, K_I is the cells short-circuit current temperature coefficient, T_{Ref} is the cell's reference temperature, and λ is the solar insolation in kW/m^2.

$$T_C = T_{Air} + \frac{NOCT - 20}{80} S \quad (4\text{-}4)$$

S = insolation in mW/cm^2. (With T_{Air} = 20.1 ^{o}C, NOCT = 47 ^{o}C and S =80 mW/cm^2), T_c is calculated as 47.1 ^{o}C.

In order to know the values of Np and Ns, **KC175GT** solar module has been selected. The specification of this module can be found in the appendix C.

As the optimization result shows, we need to have 110kW PV modules to be installed (refer in chapter six, section 6.1.2, pp. 101, Table 6-1). Therefore, the number of modules required is equal to 110,000/175 = 629, approximated to 630.

- Module in series (Ns) = DC bus voltage/Voltage of the module = 120/20.9 = 6
- Strings in parallel (Np) = Total no of modules/Modules in series = 630/6 = 105

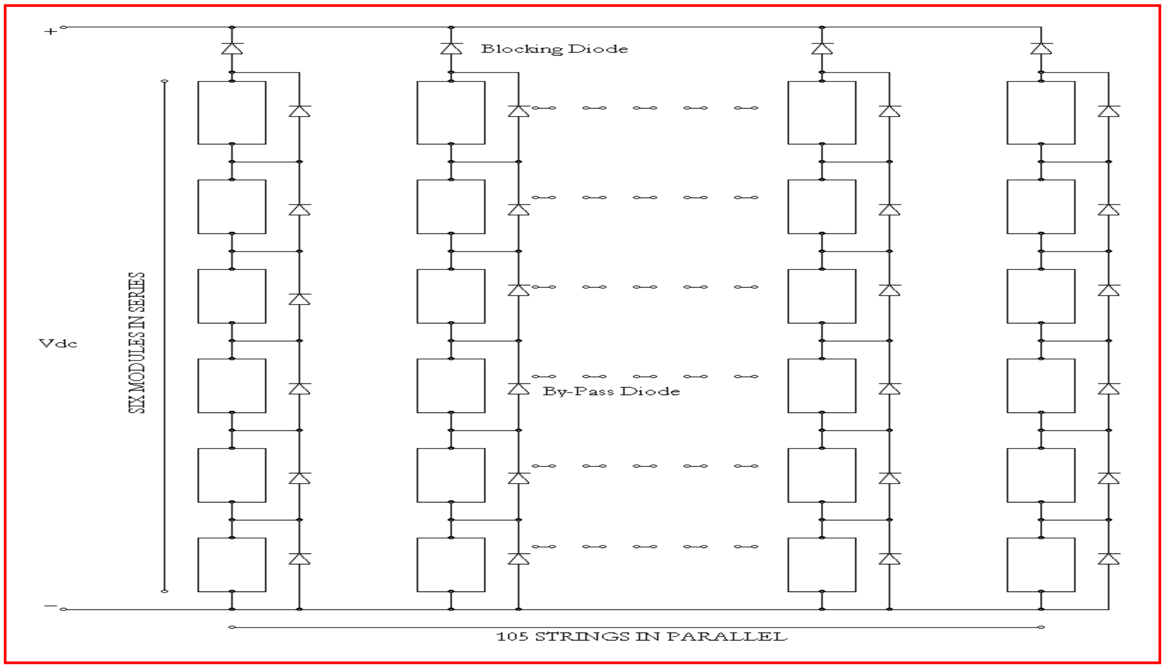

Figure 4-4 Modules arranged in 6 series and 105 series strings in parallel

In chapter two, section 2.2.5, page 14, it has been stated that for a typical module cell, R_S = 0.05 to 0.10 ohm and R_{SH} = 200 to 300 ohms. Therefore, for this study the average value of each, that is, R_S = 0.075 and R_{SH} = 250 is used (see figure 4-12).

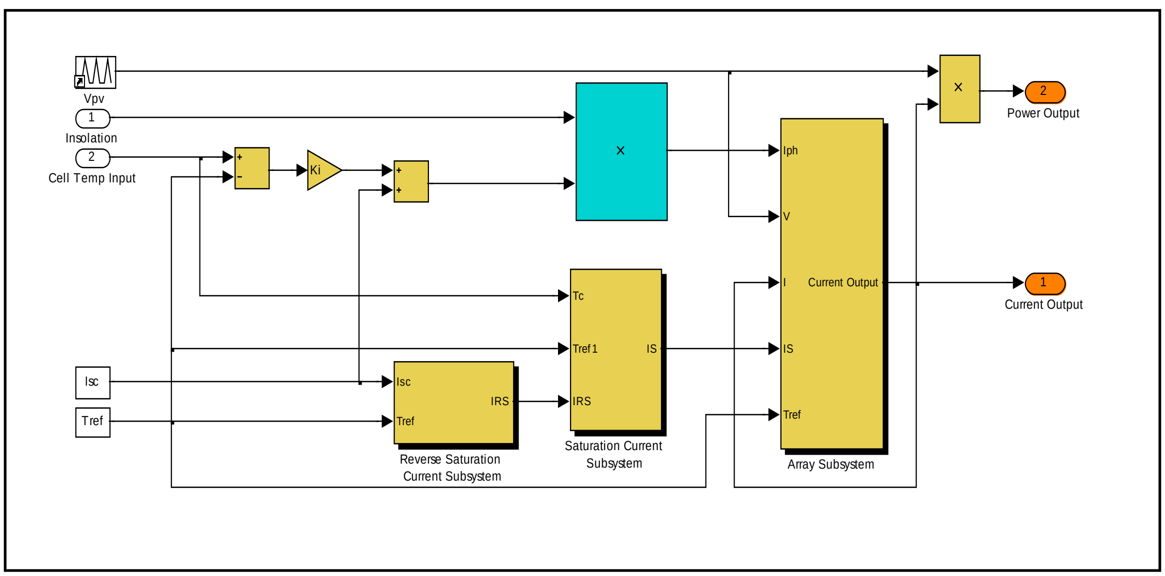

Figure 4-5 Masked model of PV modules

On the other hand, the cell's saturation current varies with the cell temperature, which is described as [50]:

$$I_S = I_{RS}\left(\frac{T_C}{T_{Ref}}\right)^3 \exp\left[\frac{qE_g\left(\frac{1}{T_{Ref}}-\frac{1}{T_C}\right)}{Ka}\right] \tag{4-5}$$

Where: I_{RS} is the cell's reverse saturation current at a reference temperature and a solar radiation and E_g is the band gap energy (an energy range in a solid where no electron states can exist and it is equal to 1.11 for Silicon semiconductor [50]) of the semiconductor used in the cell. The ideal factor *a* is dependent on PV technology and 1.3 is used for multicrystal solar module in this study from [50].

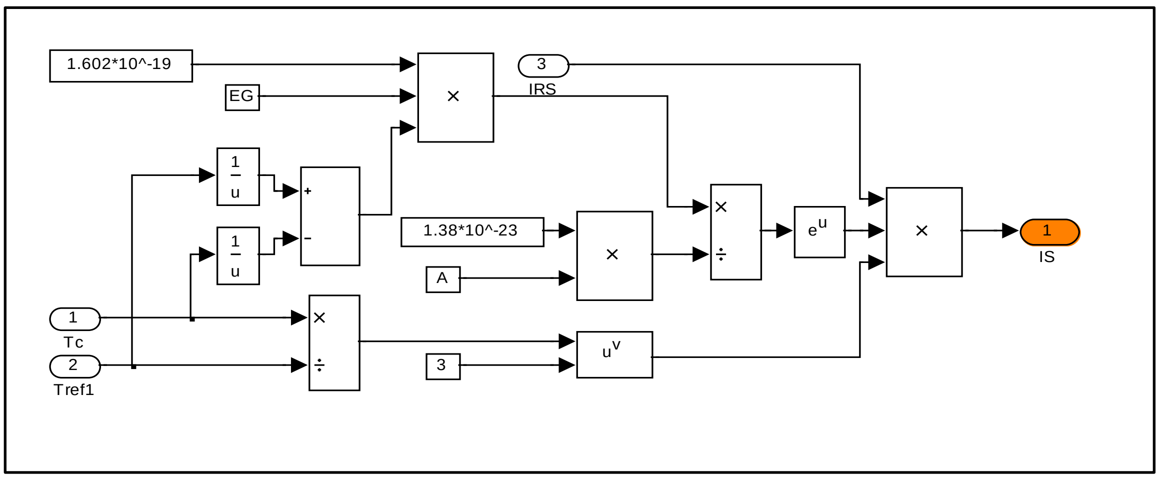

Figure 4-6 Expanded view of saturation current subsystem

Given the PV open-circuit voltage, V_{OC}, at reference temperature and ignoring the shunt leakage current, the reverse saturation current at reference temperature can be approximately obtained as [50]:

$$I_{RS} = \frac{I_{SC}}{\left[\exp\left(\frac{qV_{OC}}{N_S KaT_{Ref}}\right)-1\right]} \tag{4-6}$$

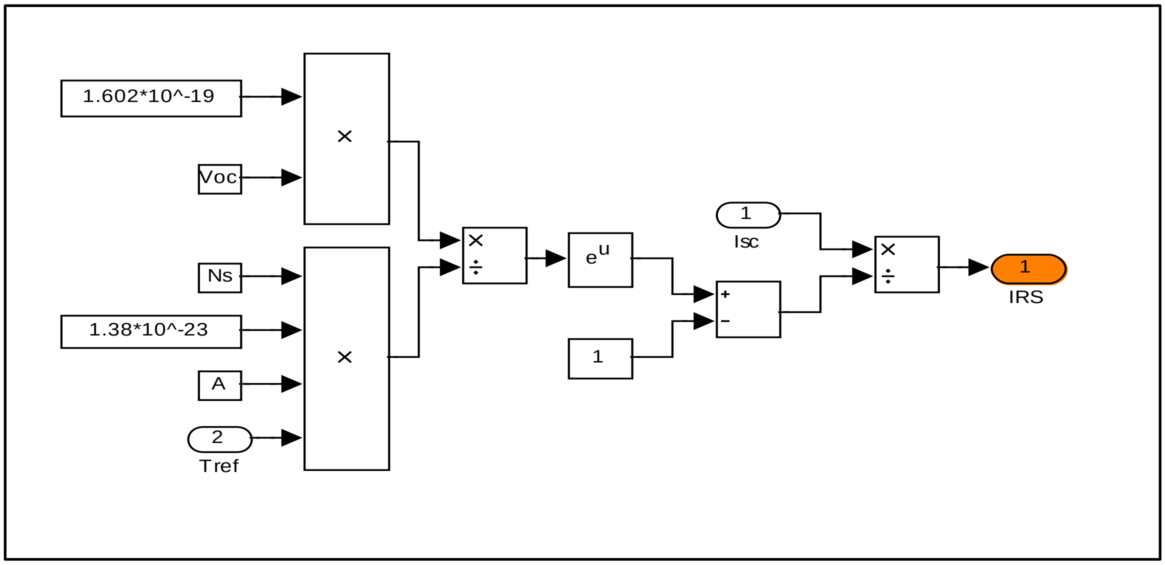

Figure 4-7Expanded view of reverse saturation current model

The detail of the array subsystem model in the Simulink is given in the figure 4-8.

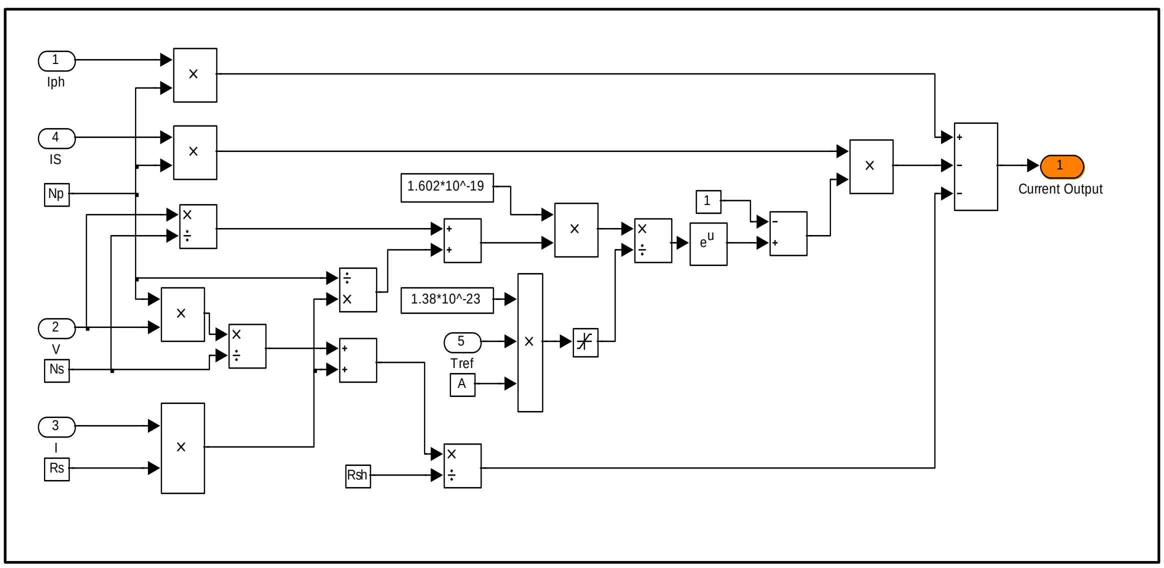

Figure 4-8 Expanded view of the array subsystem

For easy simulation, the solar radiation intensity for a sample day is assumed to be of a Gaussian function which is defined as [50]:

$$\lambda(t) = \lambda_{max} \exp\left[-\left(\frac{(t-t_c)^2}{2\sigma^2}\right)\right] \qquad (4\text{-}7)$$

Where: λ_{max} is the maximal radiation intensity at a given time, t_C is the center time, and σ is the standard deviation of Gaussian function.

Figure 4-9 shows a plot of the Gaussian function for the solar radiation intensity of a sample day for different months generated from the given monthly average radiation data (in $kWh/m^2/d$) inputs by HOMER. As the figure clearly shows, the maximum average value of the Gaussian function is 0.8.

Hence, with the conditions: $\lambda_{max} = 0.8kW/m^2$, $t_c = 12$, and $\sigma = 2$ a MATLAB/ Simulink model has been developed for simulation as indicated in figure 4-10. The output from this model is also indicated in figure 4-11 and it is the same as HOMER estimates.

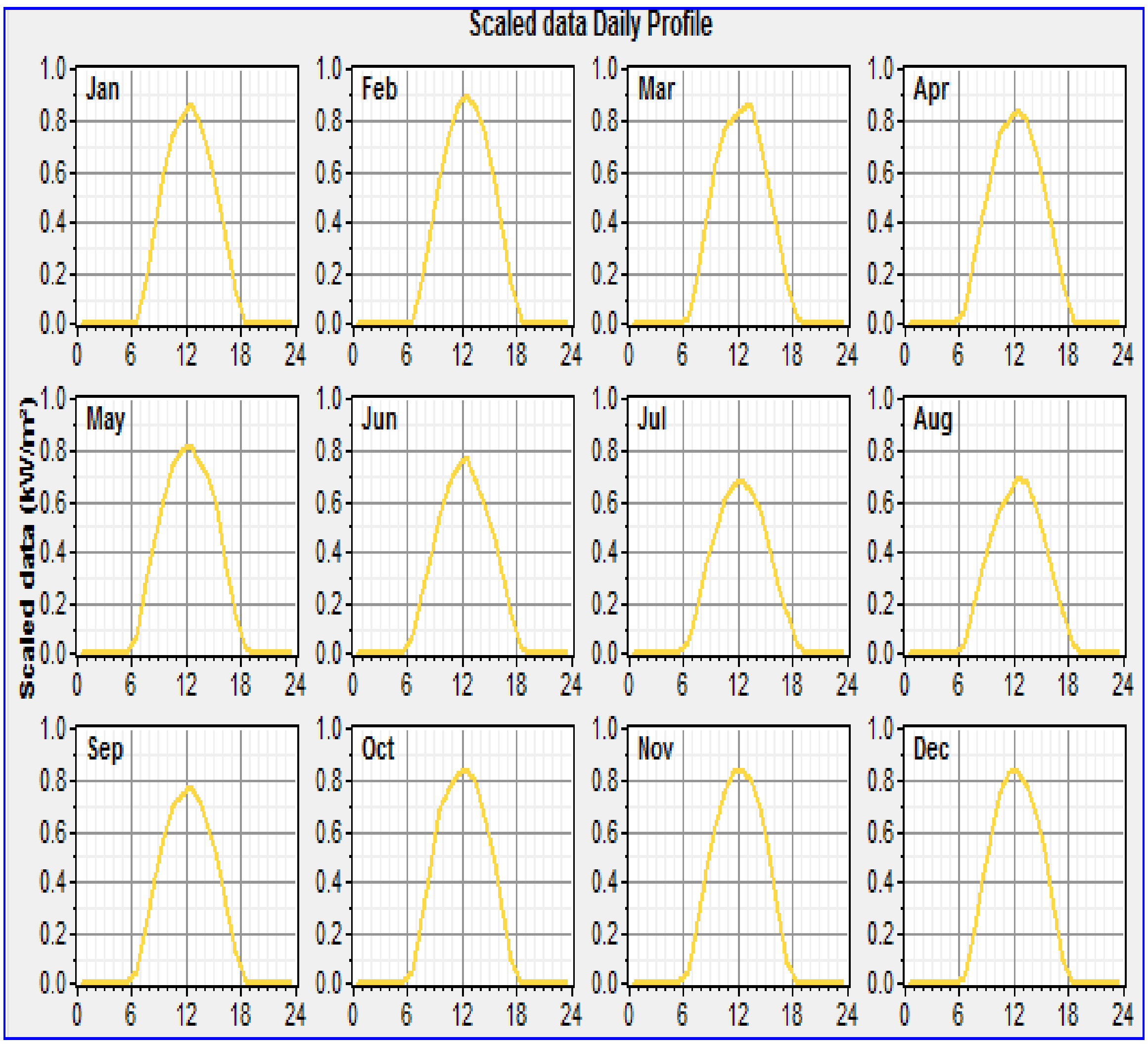

Figure 4-9 Scaled data solar insolation's in kW/m^2 in HOMER

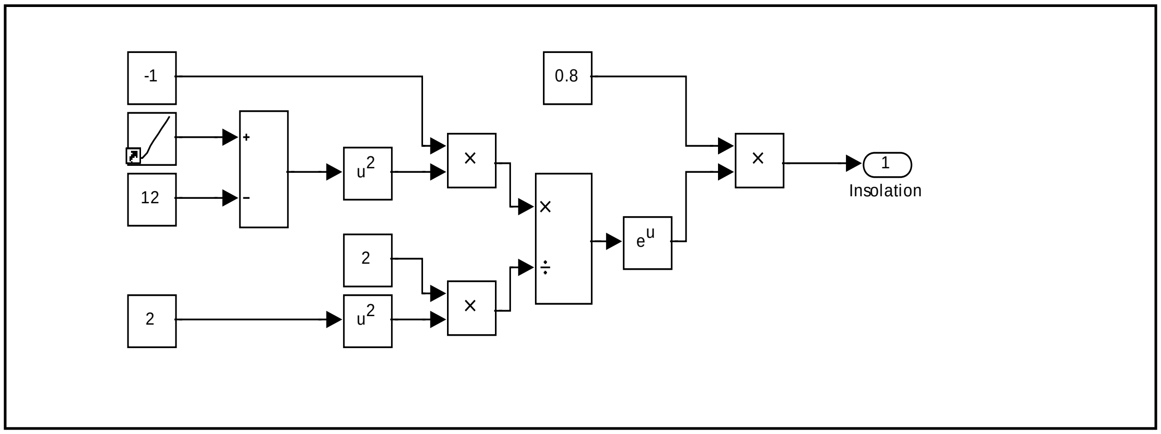

Figure 4-10 Expanded view of insolation subsystem model

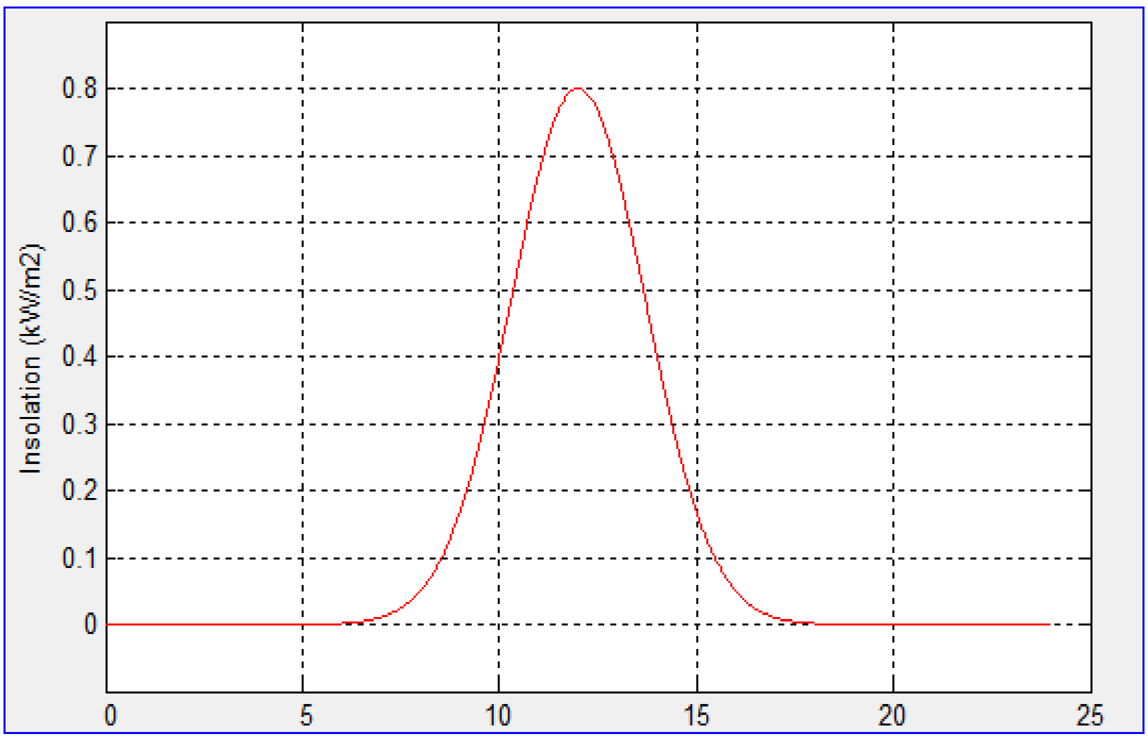

Figure 4-11 Insolation input signal generated by the model indicated in figure 4-10 (The reader is advised to see the similarity of this and the one indicated in figure 4-9)

So as to inter other constant values which are used in the modeling process, a user interface that interact the modeler has been designed by the author and it is presented in figure 4-12 below. Therefore, as the modeler clicks the masked PV subsystem model, the user interface interact the modeler and he/she has to inter the values of the parameter and click ok button. Finally, the user interface automatically transfers these values to the model for further processing and hence, the simulation will proceed as desired.

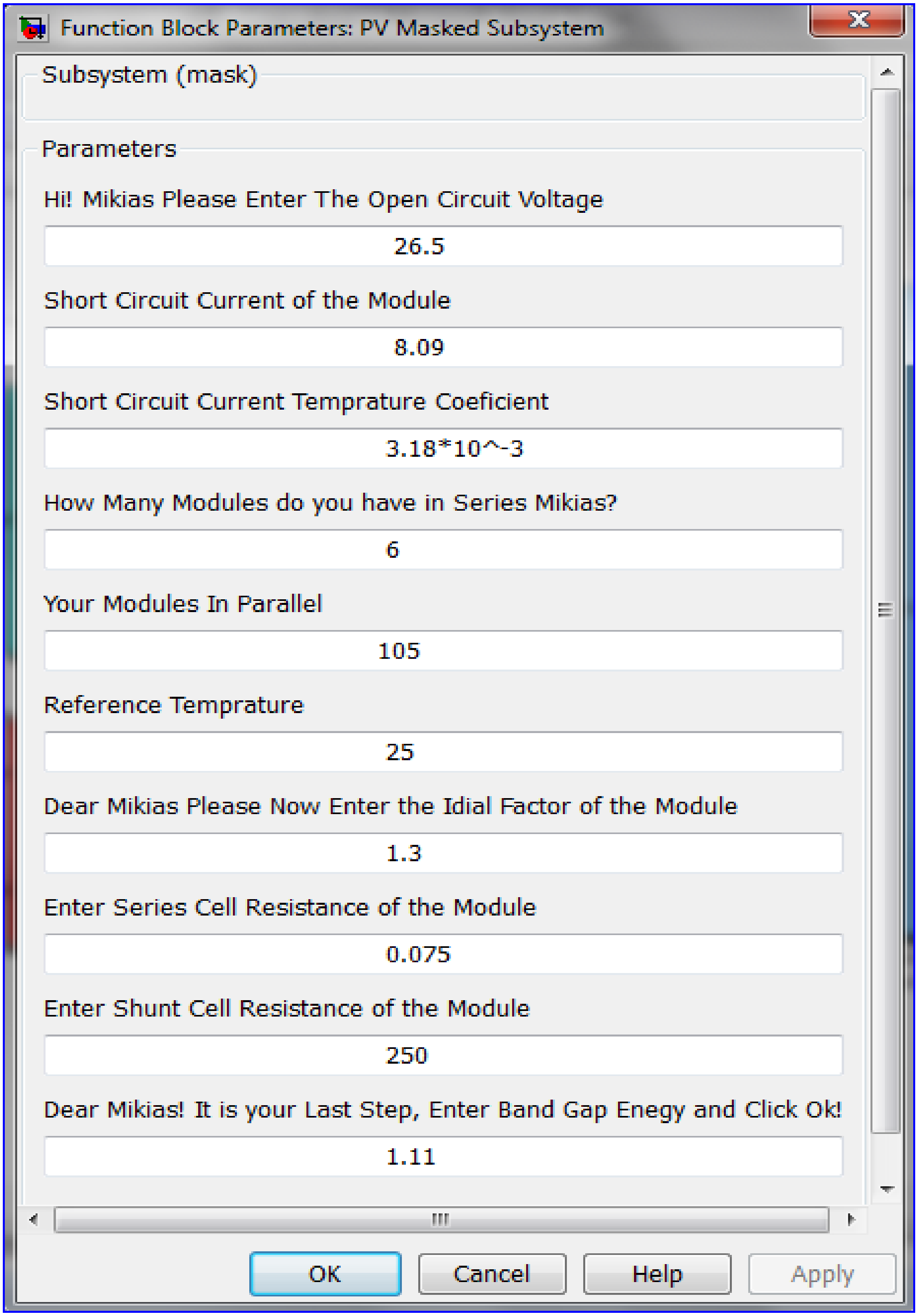

Figure 4-12 User interface designed to accept input values for PV masked model

4.4 Detail of the Battery Bank Subsystem

We can have the following equivalent circuit model indicated by figure 4-13 for a rechargeable battery bank connected with other elements at the DC bus.

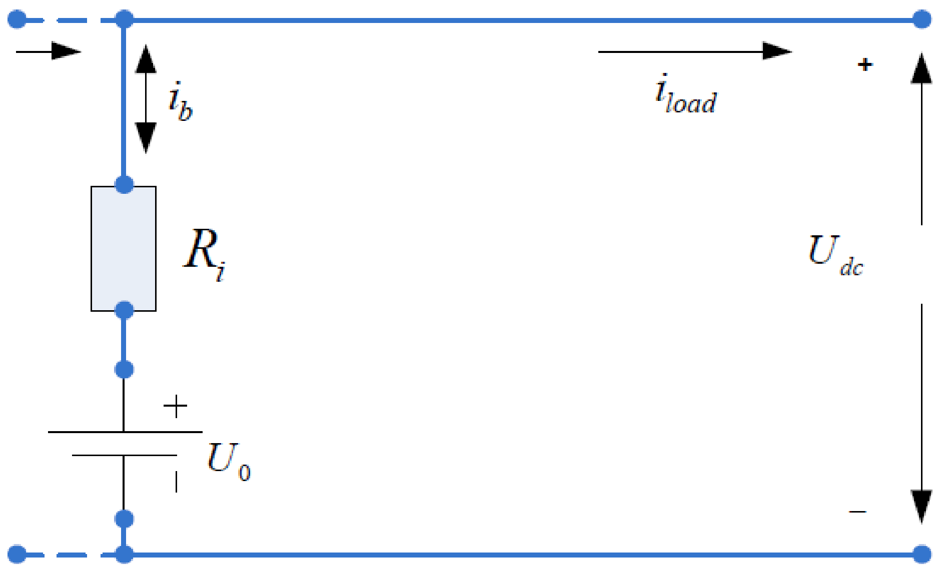

Figure 4-13 Simple equivalent circuit model of rechargeable lead acid battery [28]

Applying a simple KVL, the voltage at the battery terminal can be expressed as:

$$U_{dc} = U_o - R_i i_b(t) \tag{4-8}$$

The power that is drawn from the battery is also given as:

$$P_b(t) = U_{dc} i_b(t) \tag{4-9}$$

The energy which is left in the battery after the load has drawn power from the battery can also be expressed as:

$$e_b(t) = e_{b-init}(t) - \int p_b(t)dt \tag{4-10}$$

Where,

U_{dc} = DC voltage at the DC bus connection

U_o = Internal voltage of the battery bank

R_i = Internal resistance of the battery bank

$i_b(t)$ = Current output of the battery to the load

$e_b(t)$ = Energy delivered to the load when the battery is discharging; and stored energy when the battery is charging

$e_{b\text{-}init}(t)$ = Initial energy of the battery

$P_b(t)$ = Battery power delivered to the load

The DC bus voltage is 120V. Therefore, the total number of batteries, which is equal to 120 (refer in chapter six, section 6.1.2, pp. 101, Table 6-1), should have to be connected in such a way that 20 of them are linked in series and 6 such series strings in parallel (see Figure 4-14 below).

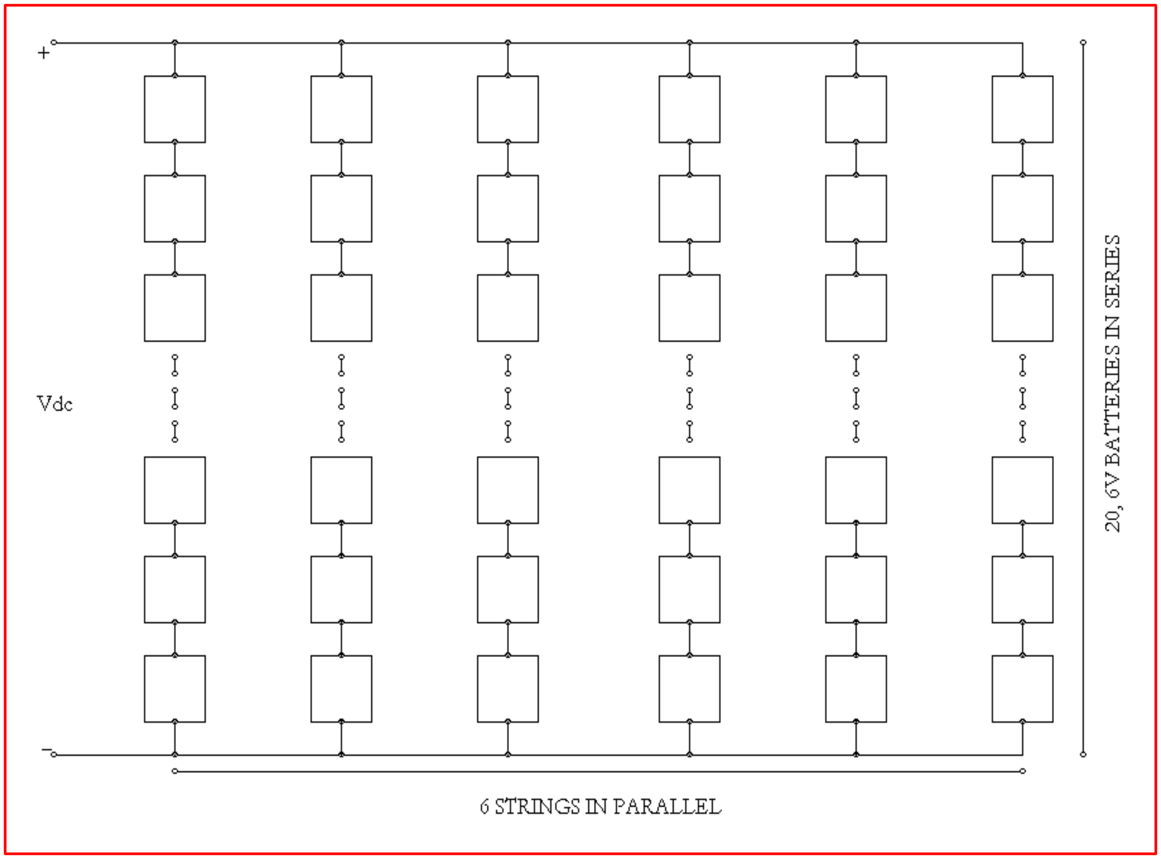

Figure 4-14 Schematic diagram of 20 (series) by 6 (series strings in parallel) battery connection

Based on eq. (4-8), eq. (4-9) and eq. (4-10) the battery bank subsystem can be modeled in MATLAB/Simulink as indicated in figure 4-15.

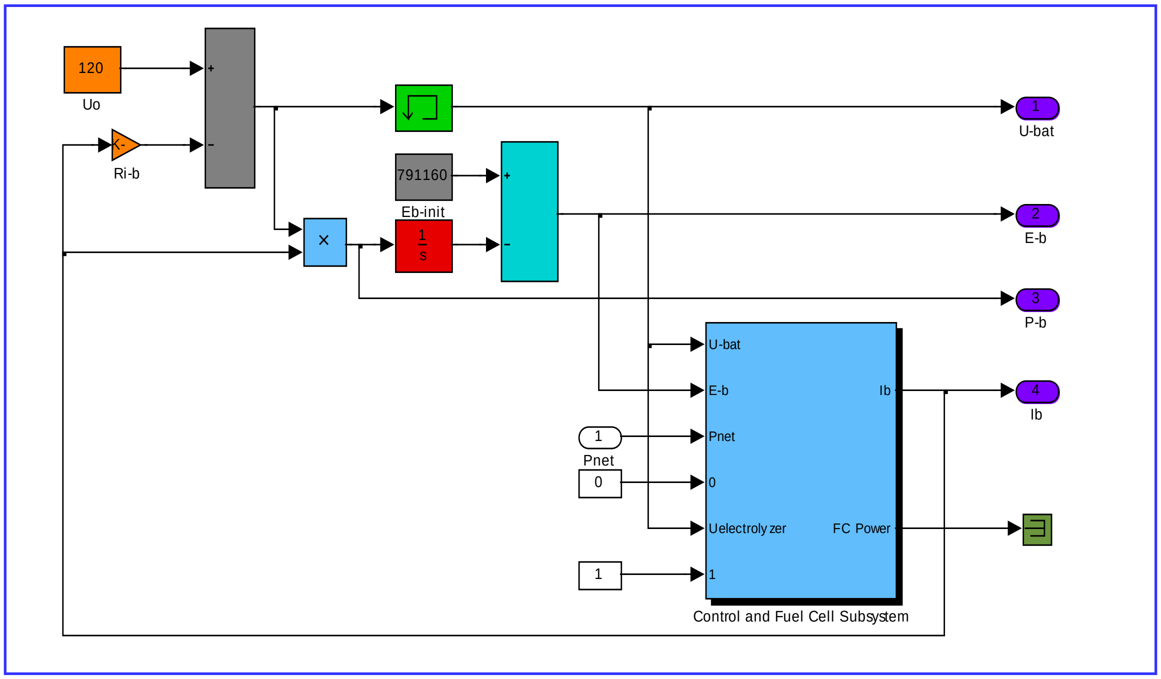

Figure 4-15 Expanded view of battery bank model

The control and fuel cell subsystem in figure 4-15 contains the model indicated in figure 4-16 which intern comprises power flow controller, fuel cell, electrolyzer and hydrogen tank subsystem models. The detailed expanded model of each is presented in the coming section.

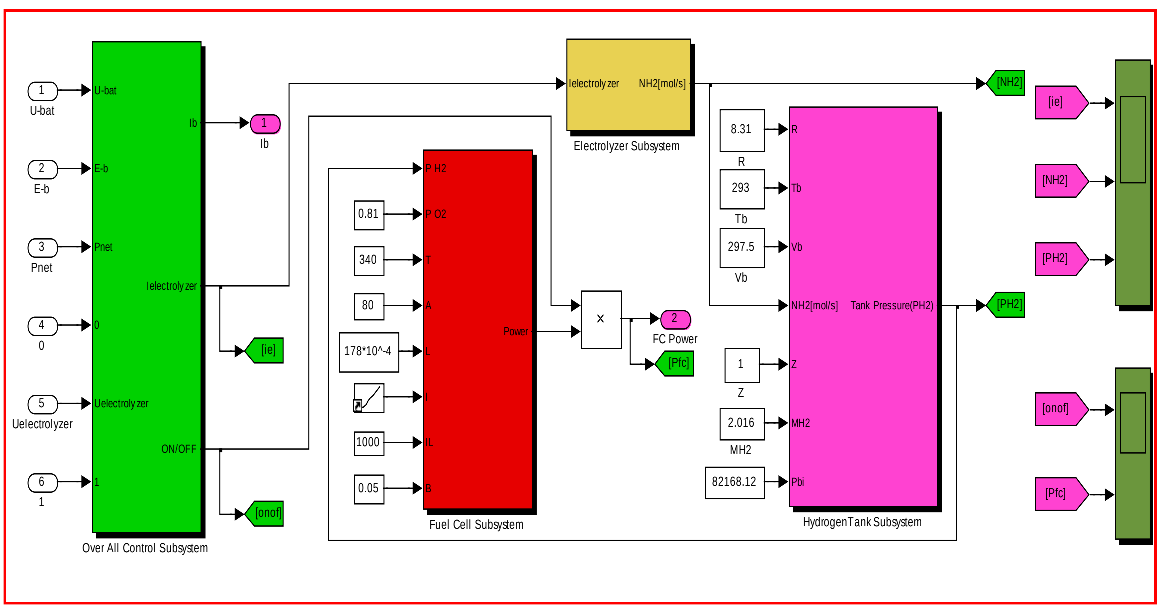

Figure 4-16 Power flow controller, fuel cell, electrolyzer and hydrogen tank subsystem models

4.5 Overall Power Flow Controller

The task of an overall power flow control unit are to facilitate the battery charging/discharging process, to enhance the hydrogen production by the electrolyzer and to determine the time at which fuel cell will operate to utilize the stored hydrogen for the production of electric power.

The charging/discharging of the battery can be indicated by the presence of current flow. If the battery is neither charging nor discharging, there will be no current flow and thus no power is available in the battery. In this thesis, the charging or discharging modes are identified by the sign of battery current and/or power. According to the convention used in this thesis work, a positive current or power shows the discharging mode (battery supply/deliver power) and a negative current or power indicates the charging of the battery (battery absorbs power).

When modeling for the simple electrical circuit that represents the rechargeable battery bank, three important points have to be considered. These are:

1. **<u>Battery state is neither minimum nor full</u>**

When the battery is neither at its lowest state nor at its full state $(E_{b\,min} < E_b(t) < E_{b\,peak})$, it can either charge or discharge depending on the load demand and other energy source conditions. Whenever there is more supply from other sources than the demand, it charges and when the demand exceeds the supply, it discharges.

2. **<u>Battery has been fully charged and load draws power from it</u>**

This is the case when the battery is fully charged and it is discharging when the load draws power from it. Depending on the energy sources and the load demand, the conditions which have to meet, in this case, are

$$E_b(t) = E_{b\,peak} \tag{4-11}$$

$$P_{load}(t) - P_{generated}(t) > 0 \tag{4-12}$$

Therefore, in this case, the battery current and power will have positive sign according to the convention used in this thesis work.

3. **Battery has been discharged to its minimum energy and it is charging**

When the battery has been discharged to its minimum state and there is more supply than there is demand, the battery charges. The conditions which must be fulfilled during this situation are:

$$E_b(t) = E_{b\ min} \quad (4\text{-}13)$$

$$P_{load}(t) - P_{generated}(t) < 0 \quad (4\text{-}14)$$

Hence, the current flow and the power will have negative sign according to the convention used in this thesis.

If none of the above three conditions happens at any time, the battery neither charges nor discharges. The energy of the battery, hence, remains constant and as a result the battery current- $i_b(t)$ and thus the battery power-$P_b(t)$ will be zero according to the convention developed so far.

When there is excess electricity, first it goes to charge the battery. If the battery reaches to its maximum capacity ($E_{b\text{-}peak}$) and still excess electricity exists, the electrolyzer will be turned on and hydrogen will be produced by the electrolysis of water.

When there is shortage, first the battery discharges to fulfill the load demand. If the battery reaches to its allowable minimum capacity ($E_{b\text{-}min}$), it will stop further discharging and the fuel cell will operate so as to convert the stored hydrogen in to electricity.

Therefore, we need to design such a controller that will perform the above tasks by supervising the power demand, power generated and energy content of the battery at any instant of time.

The general algorism which explains the above stated concepts is given in figure 4-17 and the equivalent digital control circuit model developed in MATLAB/Simulink is also given next to it in figure 4-18.

The numbers in the model indicated by figure 4-18 are calculated based on the optimization result. 120 Surrette S6CS25P batteries are needed (refer in chapter six, section 6.1.2, pp. 101, Table 6-1). The nominal capacity of one battery is 6.94kWh [49], hence, the peak nominal capacity of the battery bank is equal to 120×6940 = 832800Wh. Therefore, the battery bank is restricted to charge up this peak nominal value and, hence, further charging beyond this limit will be terminated even though there is surplus of power generation. The minimum energy content of the battery bank is allowed to be 40% of its nominal capacity as the depth of discharge is 60%. Hence, minimum energy capacity of the battery bank ($E_{b\text{-}min}$) is equal to (40/100) × 832800 = 333120Wh and, therefore, the battery bank will not discharge further below this minimum energy capacity as its deliverable energy is already elapsed. The initial energy content of the battery bank is assumed by considering 5% self-discharge and equal to (95/100) × 832800 = 791160Wh.

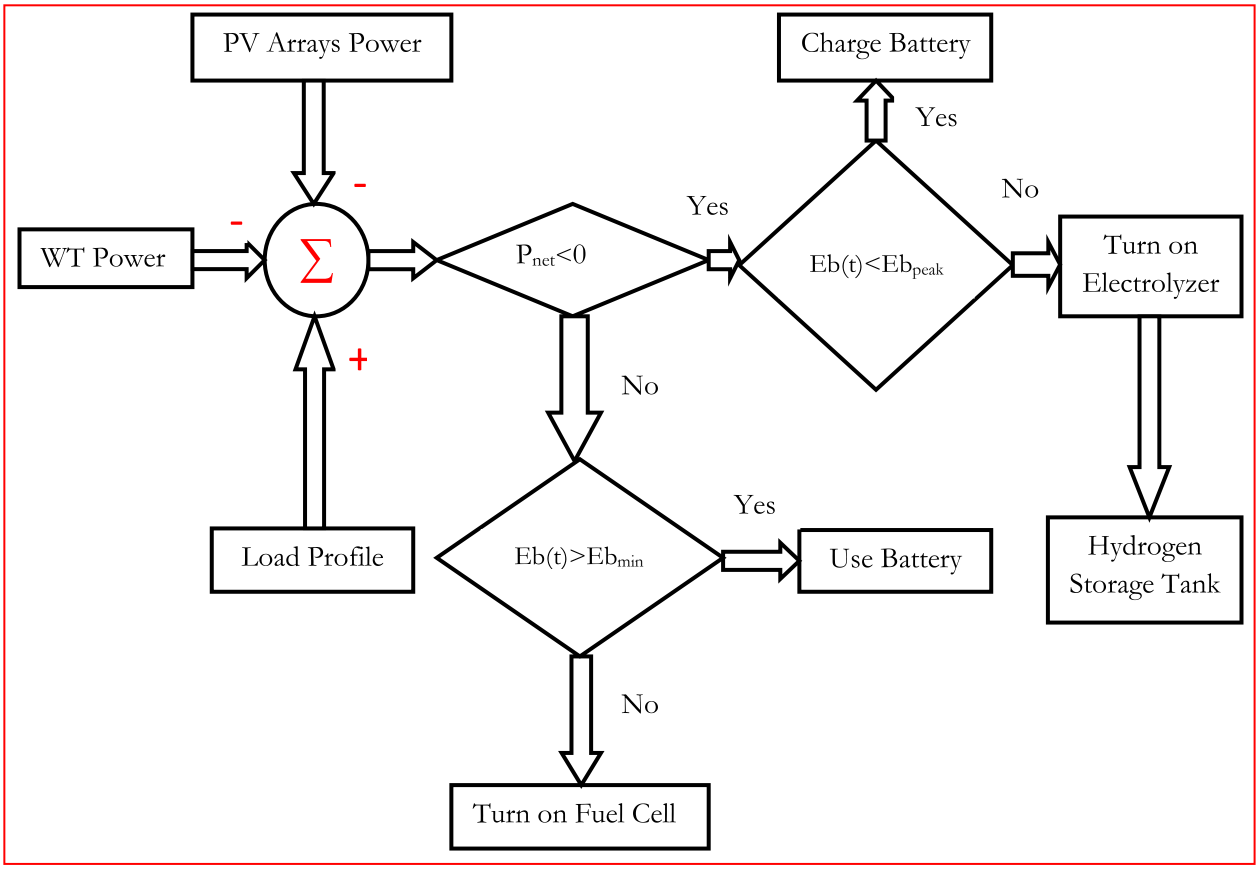

Figure 4-17 Algorithm of the overall control for the proposed hybrid alternative energy system.

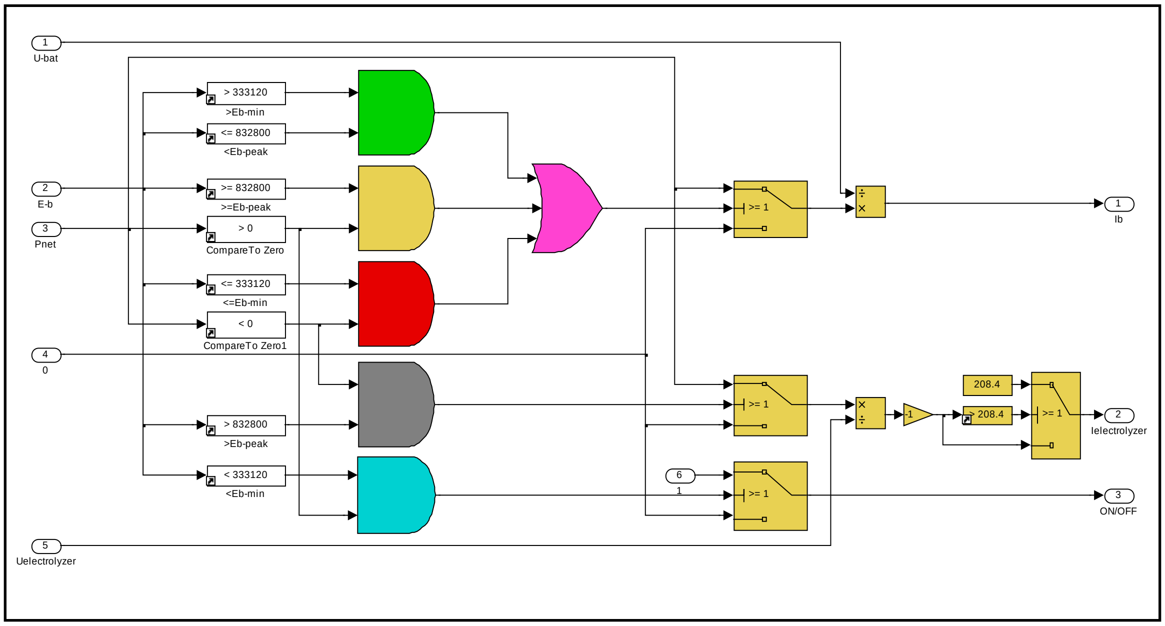

Figure 4-18 Overall controller models in MATLAB/Simulink

4.6 PEM Fuel Cell Model

The electrochemical equivalent circuit shown in figure 4-19 can be used for the analysis of the behavior of a PEM fuel cell. This electrochemical model is described by a set of equations and corresponding parameters, which are essential for the analysis of the performance of the PEMFC [4], [18], [27], [38].

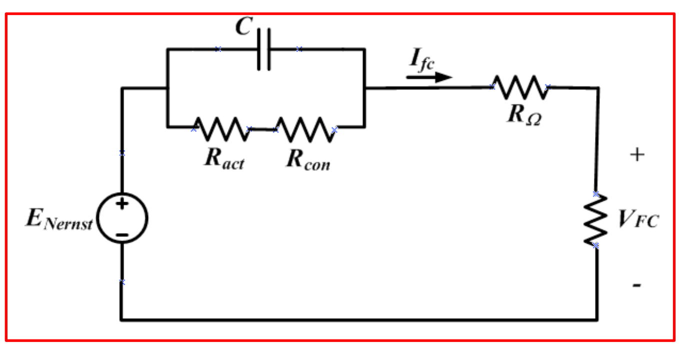

Figure 4-19 A simplified model of the PEM for only one cell [Maria, 2011]

The output voltage of a single fuel cell can be calculated by the expression indicated in eq. 4-15. According to the Nernst's equation and Ohm's law [37]:

$$V_{FC} = E_{Nernst} - V_{act} - V_{Ohmic} - V_{conc} \tag{4-15}$$

Where: E_{Nernst} is the thermodynamic potential of the cell in open circuit. The actual voltage of the PEM fuel cell is lower than the theoretical voltage due to various loss mechanisms, which are often called polarizations or losses. These losses or polarizations are [12]:

- Activation polarization (V_{act})
- Concentration polarization (V_{conc}) and
- Resistive or ohmic polarization (V_{ohm})

The ideal performance of a fuel cell is determined by the potential voltage level that it can theoretically produce. This potential voltage is called the Nernst potential and is defined by the Nernst equation.

The general MATLAB/Simulink model of a PEM fuel cell which considers polarizations is given below in figure 4-20. Then the detailed expanded models are presented sequentially and briefly underneath.

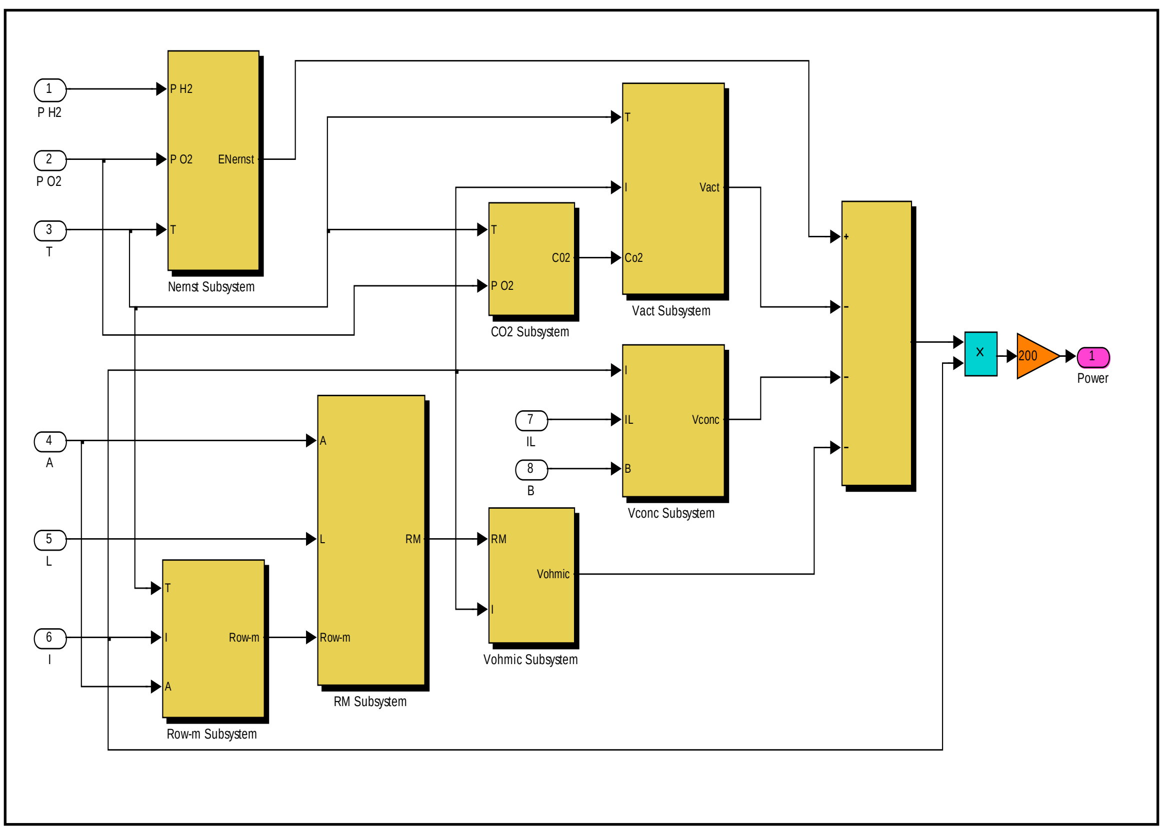

Figure 4-20 Fuel Cell model in MATLAB/Simulink

For the general reaction [12]:

$$aA + bB ===> cC + dD \tag{4-16}$$

The Nernst equation can be expressed as [12]:

$$E = E_o + \left(\frac{RT}{2F}\right)\ln\left(\frac{P_A^a P_B^b}{P_C^c P_D^d}\right) \tag{4-17}$$

Where E_o= the reversible standard potential for a cell reaction

E = the ideal equilibrium potential

T = temperature

F = Faraday's constant, and

P = pressure.

Therefore, for each of the fuel cell types, there is a theoretical voltage level that can be achieved which is determined by the Nernst equation for each of the electrochemical reactions that occur within the cell.

The overall reaction in hydrogen fuel cell is given by eq. (4-18) as stated in [12] and [2].

$$H_2 + ½\, O_2 ===> H_2O \tag{4-18}$$

Hence, the corresponding Nernst equation can be formulated as [12]:

$$E = E_0 + \left(\frac{RT}{2F}\right)\ln\left(\frac{P_{H_2} P_{O_2}^{1/2}}{P_{H_2O}}\right) \tag{4-19}$$

$$E = E_0 + \left(\frac{RT}{2F}\right)\left[\ln\left(P_{H_2}\right) + \frac{1}{2}\ln\left(P_{O_2}\right) - \ln\left(P_{H_2O}\right)\right] \tag{4-20}$$

With the assumption that the pressure of water is taken as zero when it is in liquid form and some other experimental investigations, eq. (4-21) can be used to determine the Nernst potential [31], [32].

$$E_{Nernst} = 1.229 - 0.85\times10^{-3}(T - 298.15) + 4.3085\times10^{-5}T\left[\ln(P_{H_2}) + \frac{1}{2}\ln(P_{O_2})\right] \quad (4\text{-}21)$$

PH_2 and PO_2 are the partial pressures of hydrogen and oxygen respectively. T is the fuel cell temperature in Kelvin.

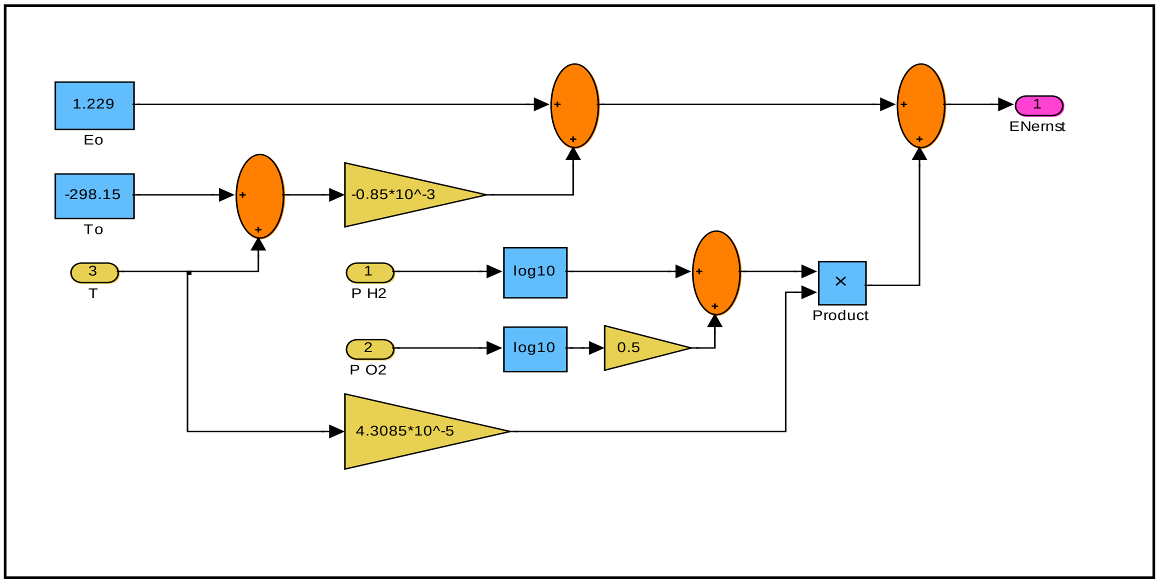

Figure 4-21Expanded model of Nernst subsystem

4.6.1 Activation Polarization Model

Thermodynamic analysis indicates that activation polarization occurs when the rate of an electrochemical reaction on an electrode surface is controlled by slow electrode kinetics and mathematically it can be formulated by eq. (4-22) [12].

$$V_{act} = \left(\frac{RT}{\alpha nF}\right)\ln\left(\frac{I}{I_0}\right) \quad (4\text{-}22)$$

Where: α is the electron transfer coefficient, *n* is the number of electrons participating in the reaction, *R* is the universal gas constant, *T* is the temperature, F is Faraday's constant, *I* is the current, and I_o is the exchange current density. The exchange current density is a measure of the maximum current that can be drawn with negligible polarization.

V_{act} also known as activation over-potential can be defined by eq. (4-23) which contains four coefficients [37].

$$V_{act} = \xi_1 + \xi_2 \times T + \xi_3 \times T \times \ln(i) + \xi_4 \times T \times \ln(C_{O_2}) \quad (4\text{-}23)$$

With CO_2 the concentration of oxygen in the catalytic interface of the cathode (mol.cm $^{-3}$) and the parametric coefficients for each cell model are represented by ξ_1, ξ_2, ξ_3 and ξ_4 [32], [37]:

$$V_{act} = -0.9514 + 0.00312T - 0.000187T\ln(i) + 7.4\times10^{-5}T\ln(C_{O_2}) \quad (4\text{-}24)$$

$$C_{O_2} = \frac{P_{O_2}}{5.08\times10^6 \times e^{-\left(\frac{498}{T}\right)}} \quad (4\text{-}25)$$

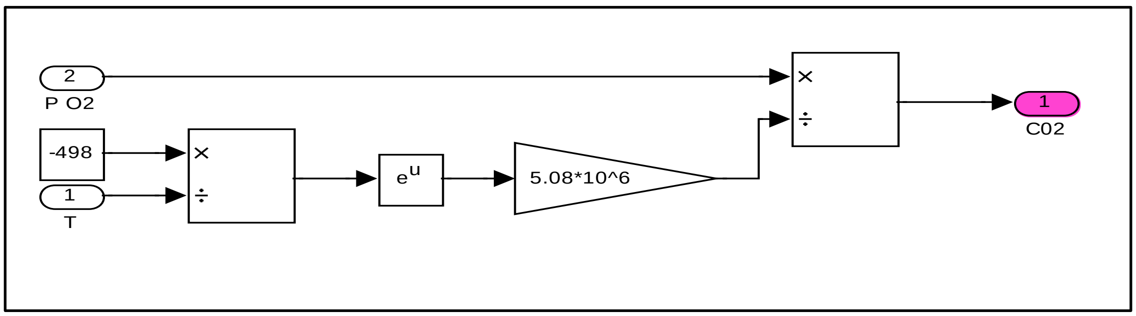

Figure 4-22 Expanded view of oxygen concentration subsystem

Therefore, we have

$$V_{act} = -0.9514 + 0.00312T - 0.000187T\ln(i) + 7.4\times10^{-5}T\ln\left(\frac{P_{O_2}}{5.08\times10^6 \times e^{-\left(\frac{498}{T}\right)}}\right) \quad (4\text{-}26)$$

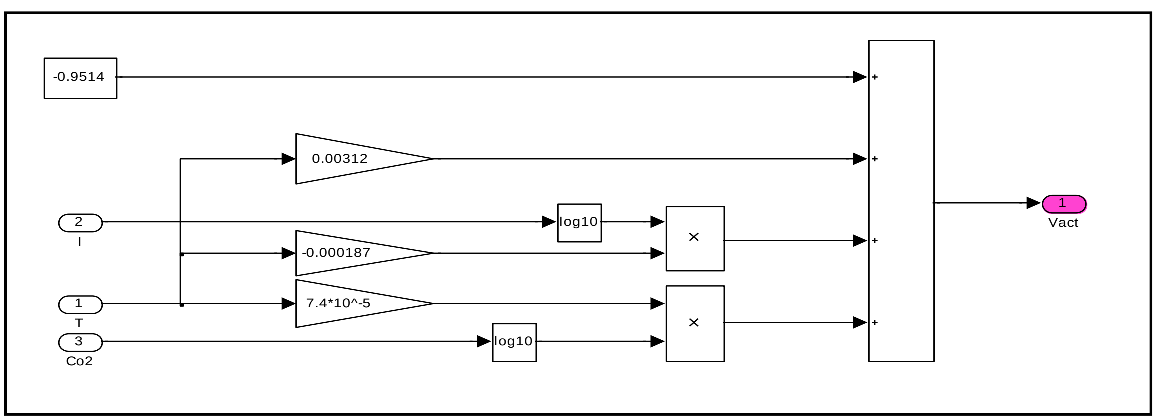

Figure 4-23 Expanded view of activation polarization model

4.6.2 Ohmic Polarization Model

Ohmic polarization is caused by resistance to the flow of ions in the electrolyte and resistance to the flow of electrons through the electrodes. The dominant losses are those associated with flow of ions through the electrolyte. These losses can be reduced by decreasing the distance between the electrodes (shortening the ionic flow distance) and/or enhancing the ionic conductivity of the electrolyte material. Ohm's law governs these losses by eq. (4-27) [12].

$$V_{ohmic} = i_{FC} \times R_{cell} \tag{4-27}$$

Where i_{FC} is the current and R_{cell} is the overall cell resistance; the overall cell resistance can be obtained experimentally.

Usually, the equivalent resistance can be formulated by eq. (4-28) [32].

$$R_M = \frac{\rho_M l}{A} \tag{4-28}$$

ρ_M is the specific resistance of the membrane. A is the valid area of the membrane, and l is the cell thickness. We can assume the membrane thickness to be 178×10^{-4}cm as stated in [32].

The expression in eq. (4-29) for the specific resistance is used from [32].

$$\rho_M = \frac{181.6\left[1 + 0.03\left(\frac{i_{FC}}{A}\right) + 0.062\left(\frac{T}{303}\right)^2\left(\frac{i_{FC}}{A}\right)^{2.5}\right]}{\left[\psi - 0.634 - 3\left(\frac{i_{FC}}{A}\right)\right]\exp\left[4.18\left(\frac{T-303}{T}\right)\right]} \tag{4-29}$$

The empirical formula indicated in equation (4-29) has been used so as to develop the model indicated by figure 4-24. Hence, the output from this model will be used as an input by the ohmic polarization model indicated by figure 4-25.

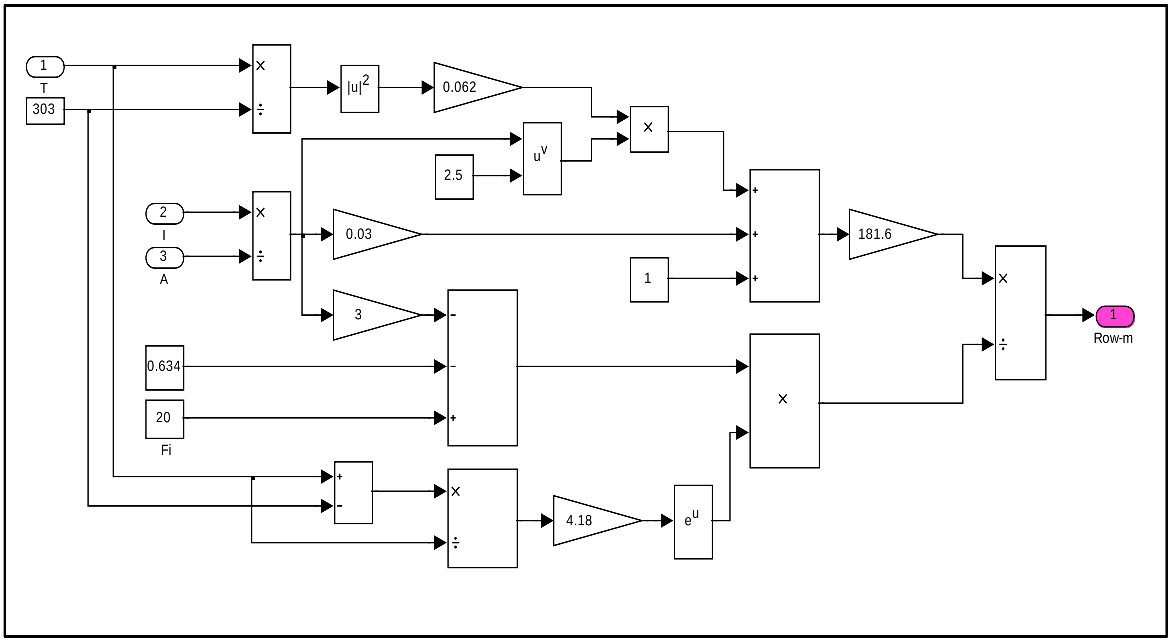

Figure 4-24 Expanded view of specific resistance model

Where: the term, $\left(\frac{181.6}{\psi - 0.634}\right)$, is the specific resistance (Ω.cm) at no current and at 30°C; the exponential term in the denominator is the temperature factor correction if the cell is not at 30°C. The factor ψ is an adjustable parameter with a possible maximum value of 23 and depends on the fuel cell type. Resistance to the transfer of protons through the membrane usually considered constant, as Rc (0.0003Ω). So the ohmic polarization loss will be [32], [37]:

$$V_{ohmic} = i_{FC}(R_M + R_C) \tag{4-30}$$

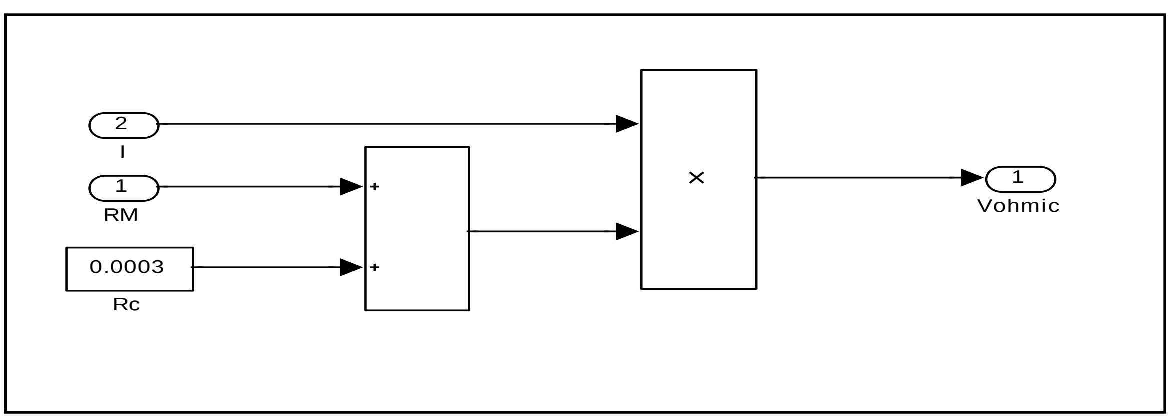

Figure 4-25 Expanded view of ohmic polarization

4.6.3 Concentration Polarization Model

Concentration polarization is caused by the formation of a reactant concentration gradient at the electrode surface. This concentration gradient is formed due to the rapid consumption of reactants at the electrode surface when the bulk fluid does not have sufficient time to replenish the reactants to their original concentration [12].

This loss of potential can be caused by a number of physical mechanisms including (1) diffusion in the gas phase within the electrode pores, (2) solution of reactants in to the electrolyte, (3) dissolution of the products out of the electrolyte, and (4) diffusion of reactants and products between electrolyte and electrochemical reaction sites within the fuel cell [12].

The overall effect of concentration over potential is given by eq. (4-31) as stated in [12].

$$V_{conc} = (B)\ln\left(1 - \frac{I}{I_L}\right) \tag{4-31}$$

Where: I_L is the limiting current, a measure of the maximum rate at which a reactant can be supplied to an electrode and it will be in the range from 500 to 1500 mA/cm^2, and B is a parametric coefficient that depends on the cell and its operation state and I represents the actual current of the cell [32].

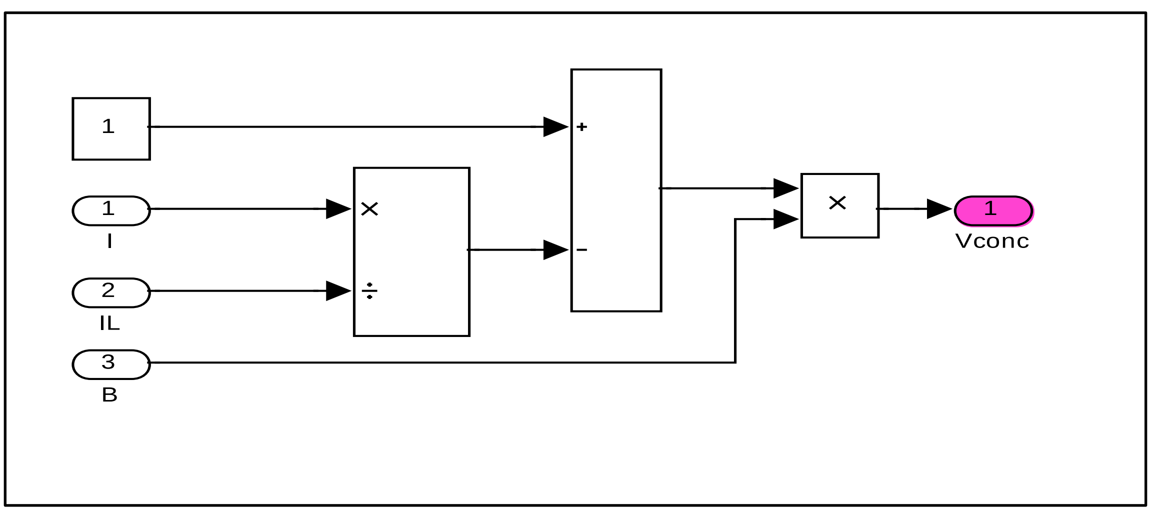

Figure 4-26 Expanded view of concentration polarization model

4.7 The Electrolyzer Model

The electrolyzer can be modeled according to the simple mathematical formula indicated in eq. (4-32). This empirical equation relates the quantity of hydrogen produced from electrolysis to the current entering to the electrolyzer [31].

$$N_{H2} = 5.18\times10^{-6} \times I_{electrolyzer} (kmoles/s) = 5.18\times10^{-3} \times I_{electrolyzer} (moles/s) \tag{4-32}$$

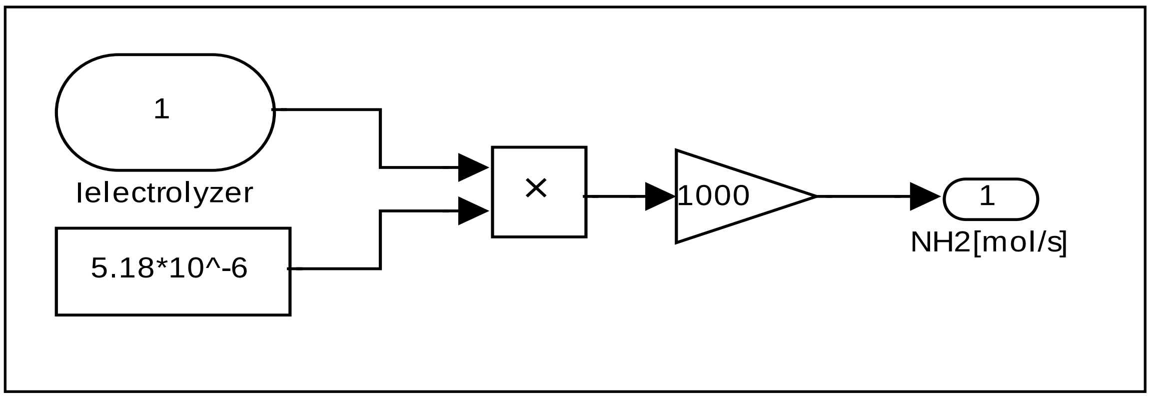

Figure 4-27 Expanded view of electrolyzer model

4.8 Hydrogen Storage Tank Model

The parameters and equations used in the hydrogen storage tank system modeling in this research work are according to the discussion presented in [41] and set of theories presented in chapter two.

One of the hydrogen storage techniques is physical hydrogen storage, which involves using tanks to store in compressed hydrogen gas which comes from the electrolyzer. The hydrogen storage model is based on eq. (4-34) and it directly calculates the tank pressure variation using the ratio of hydrogen flow to the tank [41] (For more detail in hydrogen storage, refer in chapter two, section 2.6, starting from page 28).

$$P_b - p_{bi} = z\frac{N_{H_2} R T_b}{M_{H_2} V_b} \tag{4-33}$$

Therefore, the pressure of hydrogen in the storage tank is given by mathematical formula indicated in eq. (4-34), which is the rearranged form of eq. (4-33).

$$P_b = z\frac{N_{H_2} R\, T_b}{M_{H_2} V_b} + P_{bi} \tag{4-34}$$

Where: MH_2 = molar mass of hydrogen [kg kmol^{-1}]

NH_2 = hydrogen moles per second delivered to the storage tank from the electrolyzer [mol s^{-1}]

P_b = pressure of tank [Pa]

P_{bi} = initial pressure of the storage tank [Pa]

R = universal (Rydberg) gas constant [J/ (kmolK)]

T_b = operating temperature [K]

V_b = volume of the tank [m^3]

z = compressibility factor as a function of pressure (typical value is 1)

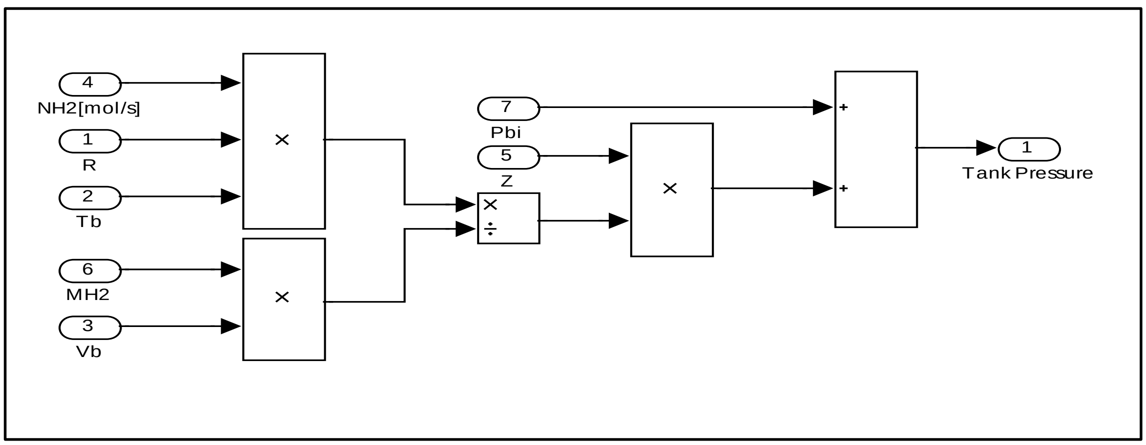

Figure 4-28 Expanded view of hydrogen tank model

4.9 PWM Inverter Modeling

4.9.1 Inverter in General

DC to AC converters are known as inverters. The function of an inverter is to change DC input voltage to a symmetrical AC output voltage of desired magnitude and frequency. The output voltage could be fixed or variable at a fixed or variable frequency. Variable output voltage can be obtained by varying the input DC voltage and maintaining the gain of the inverter constant. On the other hand, if the DC input voltage is fixed, and it is not controllable, a variable output voltage can be obtained by varying the gain of the inverter, which is normally accomplished by pulse width modulation (PWM) control within the inverter. The inverter gain may be defined as the ratio of the AC output voltage to the DC input voltage [42].

The output voltage wave forms of the inverters should be sinusoidal. However, the outputs of wave forms of practical inverters are non-sinusoidal and contain certain harmonics. For low and medium power applications square wave or quasi square wave voltages may be acceptable; and for high power applications, low distorted sinusoidal wave forms are required. With the availability of high speed power semiconductor devices, the harmonic content of output voltage can be minimized or reduced significantly by switching techniques [42].

An inverter is called a voltage fed inverter (VFI) if the input voltage remains constant, a current fed inverter (CFI) if the input current is maintained constant and a variable DC linked inverter if the input voltage is controllable.

4.9.2 Three-Phase PWM Inverter in Particular

A three-phase output can be obtained from a configuration of six IGBTs as shown in figure 4-29. Two types of control signals can be applied to the IGBTs: 180 degree or 120 degree conduction. The 180 degree conduction has better utilization of the switches and is the preferred method.

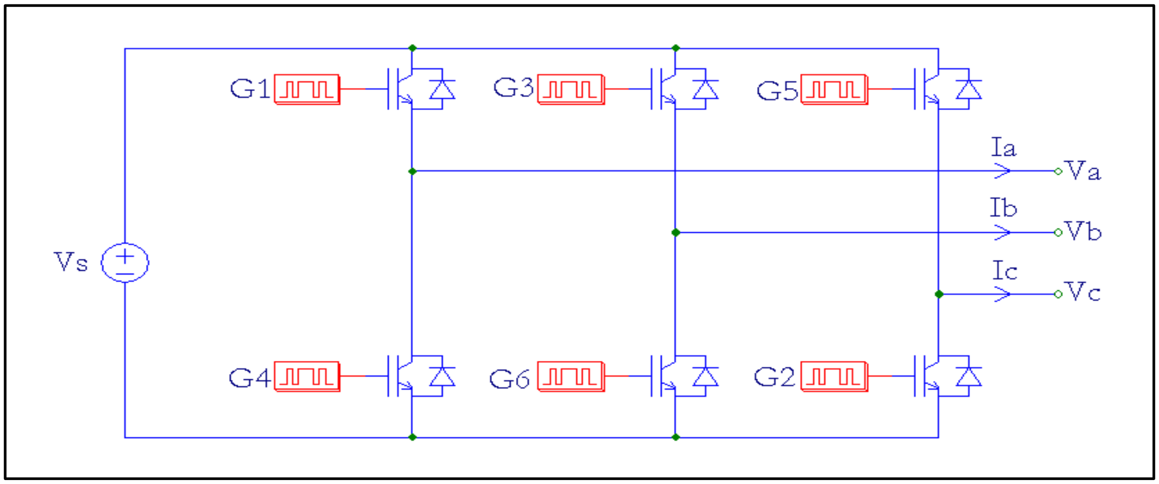

Figure 4-29 Three phase inverter configuration

4.9.3 180 and 120 Degree Conduction: A comparisons!

Table 4-1 below compares the peak, rms, total rms, distortion factor (DF), and total harmonic distortion (THD) of phase voltage and line voltage for both 180 degree and 120 degree conduction of switches and one can see that the 180 degree conduction have more merits than the 120 degree conduction.

Table 4-1 180^o and 120^{o}conduction of switches in line and phase voltage outputs [8]

Conduction Period	Fundamental Voltage		Characteristic		
	Peak	rms	Total rms	Distortion Factor (DF)	Total Harmonic Distortion (THD)
	V_1	V_{1rms}	V_{rms}	μ	THD
180^0	[v]	[v]	[v]		
Phase Voltage $V_{L\text{-}N}$	$\frac{2}{\pi}V_S$ =0.637V_s	$\frac{\sqrt{2}}{\pi}V_S$ =0.450V_s	$\frac{\sqrt{2}}{3}V_S$ =0.471V_s	$\frac{3}{\pi}$ =0.955	$\sqrt{\left(\frac{\pi^2}{9}-1\right)}$ =0.311
Line Voltage $V_{L\text{-}L}$	$\frac{2\sqrt{3}}{\pi}V_S$ =1.10V_s	$\frac{\sqrt{6}}{\pi}V_S$ =0.78V_s	$\sqrt{\frac{2}{3}}V_S$ =0.816V_s	$\frac{3}{\pi}$ =0.955	$\sqrt{\left(\frac{\pi^2}{9}-1\right)}$ =0.311
120^0	[v]	[v]	[v]		
Phase Voltage $V_{L\text{-}N}$	$\frac{\sqrt{3}}{\pi}V_S$ =0.551V_s	$\frac{\sqrt{6}}{2\pi}V_S$ =0.390V_s	$\frac{1}{\sqrt{6}}V_S$ =0.408V_s	$\frac{3}{\pi}$ =0.955	$\sqrt{\left(\frac{\pi^2}{9}-1\right)}$ =0.311
Line Voltage $V_{L\text{-}L}$	$\frac{3}{\pi}V_S$ =0.955V_s	$\frac{3}{\sqrt{2}\pi}V_S$ =0.673V_s	$\frac{1}{\sqrt{2}}V_S$ =0.707V_s	$\frac{3}{\pi}$ =0.955	$\sqrt{\left(\frac{\pi^2}{9}-1\right)}$ =0.311

4.9.4 180 Degree Conduction Inverter Modeling

Figure 4-30 shows inverter quasi-square output voltage waveforms for a 180° switch conduction pattern. Each switch conducts for 180°, such that no two series connected (leg or arm) semiconductor switches across the voltage rail conduct simultaneously.

The generation of the three-phase voltages can be analyzed analytically by using the rotating voltage space vector technique. With this approach, the output voltage state from each of the three inverter legs (or poles) is encoded as summarized in Table 4-2, where a '1' signifies the upper switch in the leg is on, while a '0' means the lower switch is on in that leg. The resultant binary number (one bit for each of the three inverter legs), represents the output voltage vector number (when converted to decimal). The quasi-square output waveform in figure 4-30 is generated by stepping instantaneously from one vector position to another in an anticlockwise direction.

Table 4-2 Quasi-square-wave six conduction states - 180° conduction [8]

Interval	Three Conducting Switches								Leg State	Voltage Vector
1	G_1	G_2	G_3						110	V_6
2		G_2	G_3	G_4					010	V_2
3			G_3	G_4	G_5				011	V_3
4				G_4	G_5	G_6			001	V_1
5					G_5	G_6	G_1		101	V_5
6						G_6	G_1	G_2	100	V_4

The square wave phase voltages with respect to the fictitious DC center tap can be expressed using Fourier series by eq. (4-35) to eq. (4-40) [8]:

The phase voltage of phase a:

$$V_{an} = \frac{2V_S}{\pi}[\sin \omega t + \frac{1}{5}\sin 5\omega t + \frac{1}{7}\sin 7\omega t + \frac{1}{11}\sin \omega t + ...] \tag{4-35}$$

The fundamental component becomes:

$$V_{an} = \frac{2V_S}{\pi}[\sin \omega t] = 0.637 V_s \sin \omega t \tag{4-36}$$

The phase voltage of phase b:

$$V_{bn} = \frac{2V_S}{\pi}[\sin(\omega t - \frac{2\pi}{3}) + \frac{1}{5}\sin(5\omega t - \frac{2\pi}{3}) + \frac{1}{7}\sin(7\omega t - \frac{2\pi}{3}) + \frac{1}{11}\sin(11\omega t - \frac{2\pi}{3}) + ...] \tag{4-37}$$

The fundamental component becomes:

$$V_{bn} = \frac{2V_S}{\pi}[\sin(\omega t - \frac{2\pi}{3})] = 0.637 V_s \sin(\omega t - \frac{2\pi}{3}) \tag{4-38}$$

The phase voltage of phase c:

$$V_{cn} = \frac{2V_S}{\pi}[\sin(\omega t + \frac{2\pi}{3}) + \frac{1}{5}\sin(5\omega t + \frac{2\pi}{3}) + \frac{1}{7}\sin(7\omega t + \frac{2\pi}{3}) + \frac{1}{11}\sin(11\omega t + \frac{2\pi}{3}) + ...] \quad (4\text{-}39)$$

The fundamental component becomes:

$$V_{cn} = \frac{2V_S}{\pi}[\sin(\omega t + \frac{2\pi}{3})] = 0.637 V_s \sin(\omega t + \frac{2\pi}{3}) \quad (4\text{-}40)$$

The inverter line to line output voltage waveforms Fourier series expansion results in the eq. (4-41) to eq. (4-49) as stated in [8].

$$V_{ab} = V_a - V_b \quad (4\text{-}41)$$

$$V_{ab} = \frac{2\sqrt{3}V_S}{\pi}[\sin\omega t - \frac{1}{5}\sin 5\omega t - \frac{1}{7}\sin 7\omega t + \frac{1}{11}\sin 11\omega t + ...] \quad (4\text{-}42)$$

The fundamental component becomes:

$$V_{an} = \frac{2\sqrt{3}V_S}{\pi}[\sin\omega t] = 1.10 V_s \sin\omega t \quad (4\text{-}43)$$

$$V_{bc} = V_b - V_c \quad (4\text{-}44)$$

$$V_{bc} = \frac{2\sqrt{3}V_S}{\pi}[\sin(\omega t - \frac{2\pi}{3}) - \frac{1}{5}\sin(5\omega t - \frac{2\pi}{3}) - \frac{1}{7}\sin(7\omega t - \frac{2\pi}{3}) + \frac{1}{11}\sin(11\omega t - \frac{2\pi}{3}) + ...] \quad (4\text{-}45)$$

The fundamental component becomes:

$$V_{an} = \frac{2\sqrt{3}V_S}{\pi}[\sin(\omega t - \frac{2\pi}{3})] = 1.10 V_s \sin(\omega t - \frac{2\pi}{3}) \quad (4\text{-}46)$$

$$V_{ca} = V_c - V_a \quad (4\text{-}47)$$

$$V_{ca} = \frac{2\sqrt{3}V_S}{\pi}[\sin(\omega t + \frac{2\pi}{3}) - \frac{1}{5}\sin(5\omega t + \frac{2\pi}{3}) - \frac{1}{7}\sin(7\omega t + \frac{2\pi}{3}) + \frac{1}{11}\sin(11\omega t + \frac{2\pi}{3}) + ...] \quad (4\text{-}48)$$

The fundamental component becomes:

$$V_{an} = \frac{2\sqrt{3}V_S}{\pi}[\sin(\omega t + \frac{2\pi}{3})] = 1.10V_s\sin(\omega t + \frac{2\pi}{3}) \qquad (4\text{-}49)$$

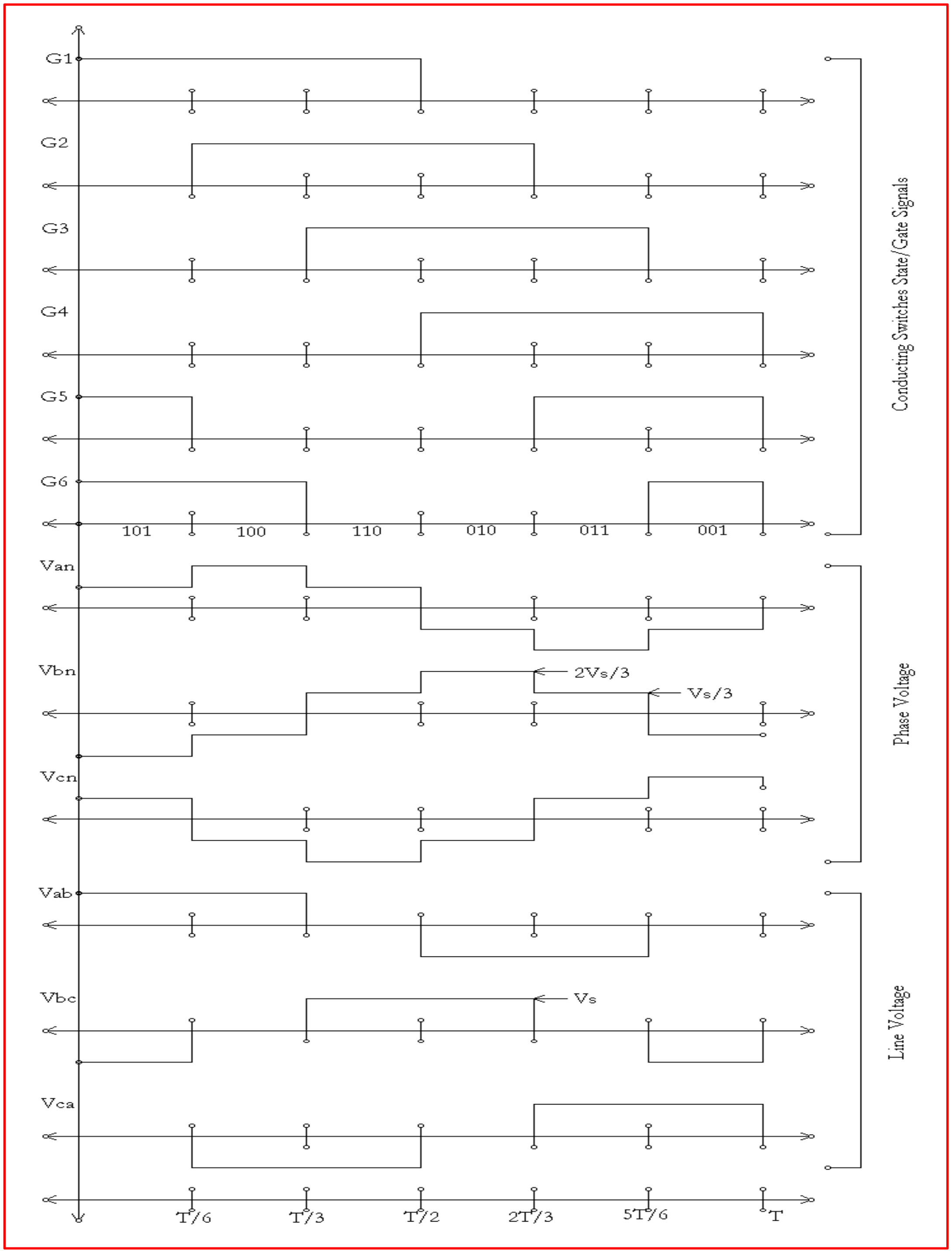

Figure 4-30 Inverter quasi-square output voltage waveforms [8]

4.9.5 Voltage Control of 180^o Conduction Inverter by Sinusoidal PWM

Sinusoidal PWM technique can be used in three-phase inverters, in which three sine waves phase shifted by 120° with the frequency of the desired output voltage is compared with a very high frequency carrier triangle, the two signals are mixed in a comparator whose output is high when the sine wave is greater than the triangle and the comparator output is low when the sine wave or typically called the modulation signal is smaller than the triangle. The modulation signals are selected so meet some specifications, like harmonic elimination, higher fundamental component and so on.

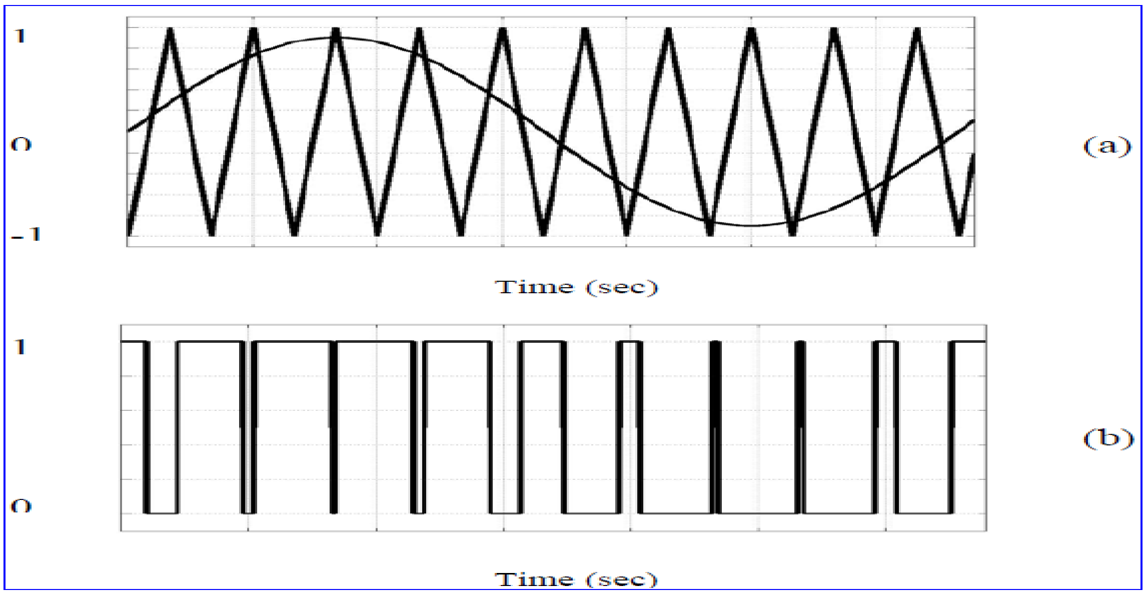

Figure 4-31 PWM illustration by the sine-triangle comparison method (a) sine-triangle comparison (b) switching pulses.

Now the need is so as to design and model a three phase inverter which inverts 120V DC to three phase (220AC line to neutral) sinusoidal voltage waveforms using sine-triangle PWM voltage control technique.

With the reference of Table 4-1 and the set of equations from eq. (4-35) to eq. (4-40), the peak of the sinusoidal signal that can be achieved from the direct inversion of 120V DC bus voltage from the battery bank terminal is equal to 0.637×120 = 76.44. But, the desire is $220 \times \sqrt{2} = 311$. To come up to this, the internal design of currently existed commercial inverters uses two techniques. The first approach is boosting the lower DC to the required higher DC then inverting; the second approach is just inverting the DC voltage level directly and then step upping the inverted AC signal to the required level. In this thesis work the second approaches is followed and figure 4-31 below shows the inverter-transformer set-up of the three phase inverter in PSIM. The MATLAB/Simulink model is indicated in figure 4-33.

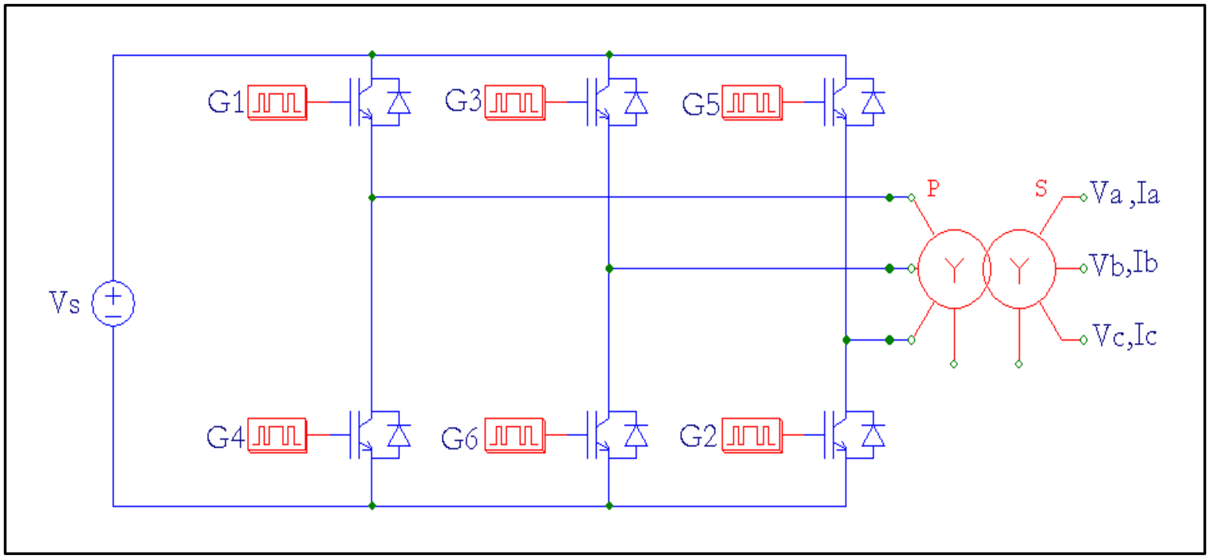

Figure 4-32 Inverter with a step up transformer in PSIM

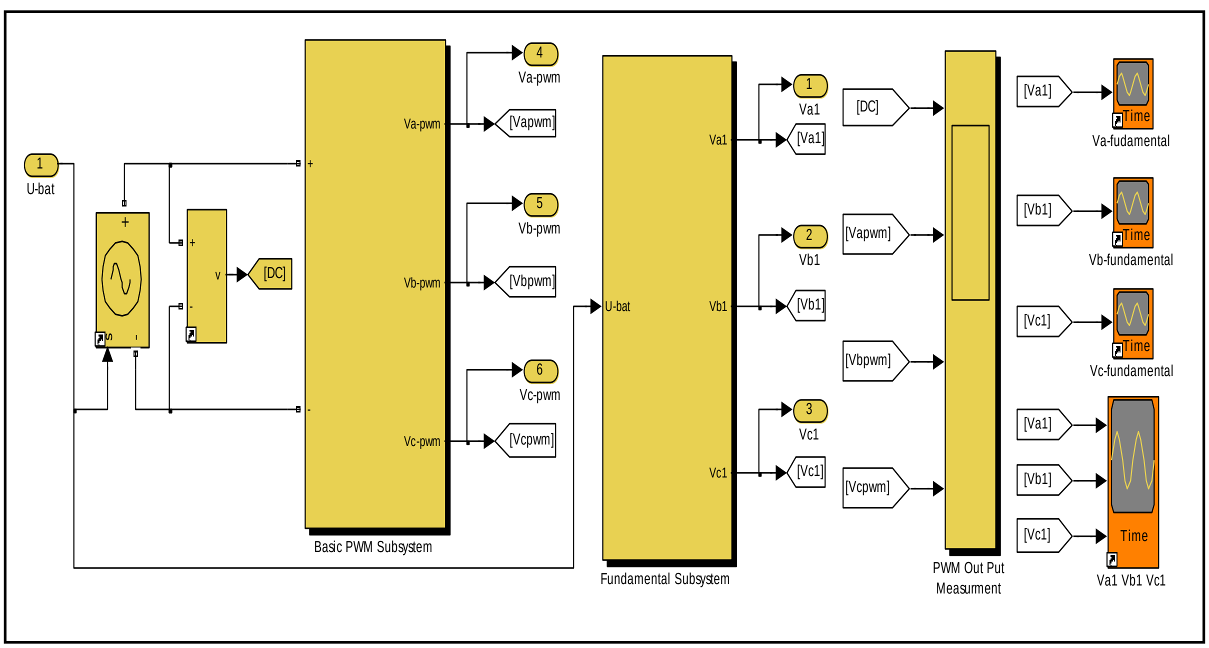

Figure 4-33 General inverter models in MATLAB/Simulink

In figure 4-33 showen above, both the basic PWM and fundamental component models of the three phase inverter are modeled. The detailed expanded model of each are also presented below in figure 4-35 and figure 4-36.

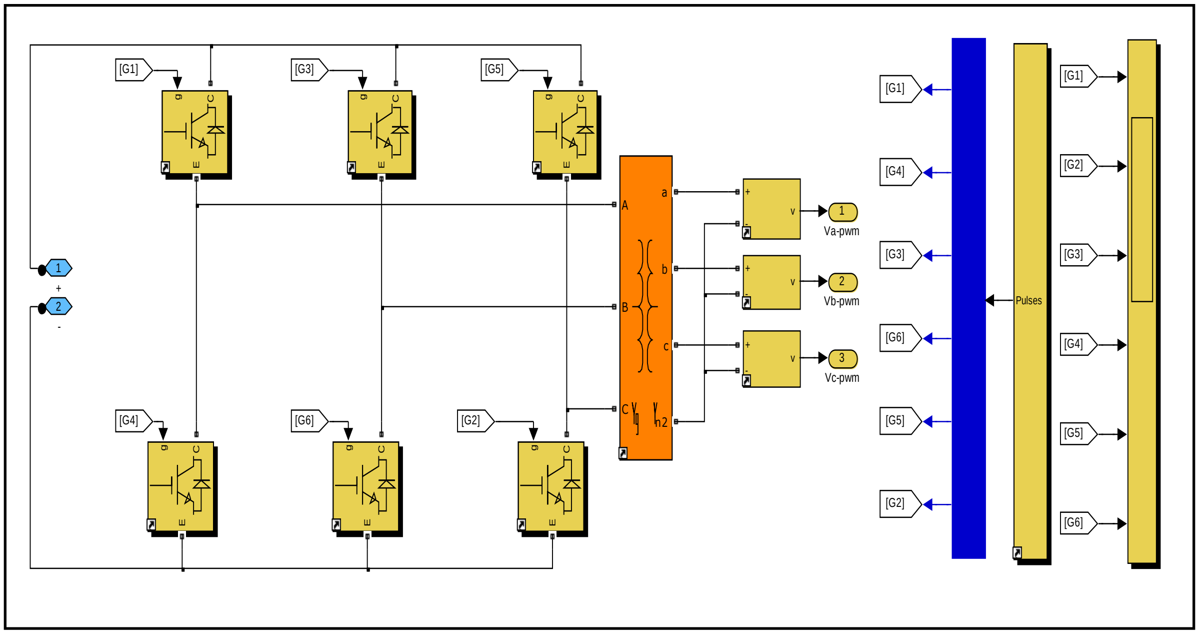

Figure 4-34 Detailed model of basic PWM-Transformer-Pulse Generator set-up of the inverter

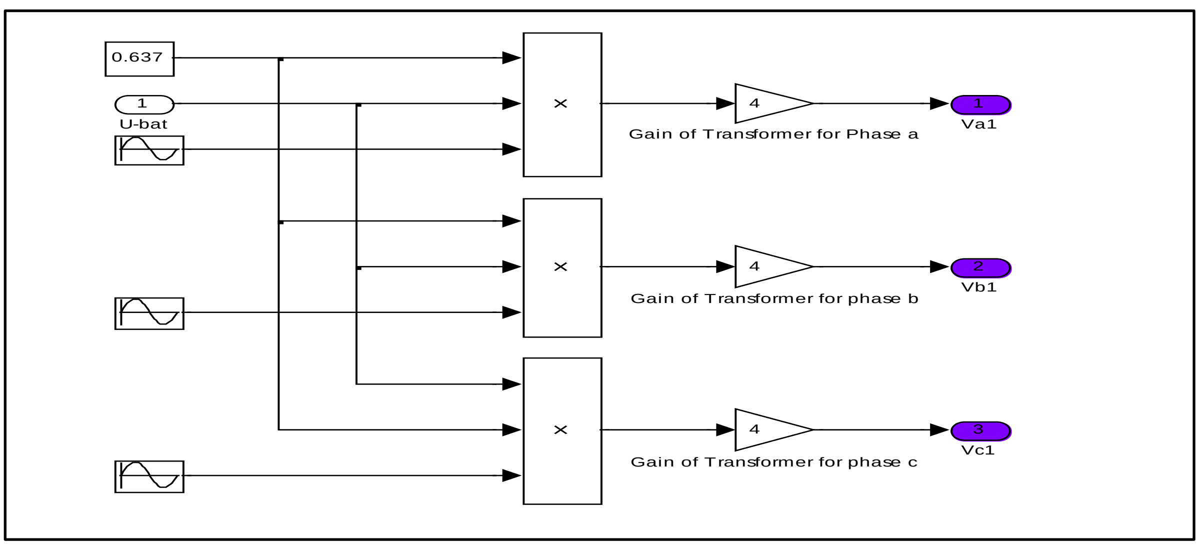

Figure 4-35 Detail of fundamental component model (from Fourier series expansion equation)

CHAPTER FIVE

5. GRID EXTENSION DESIGN AND COMPARISON WITH THE HYBRID POWER SYSTEM

5.1 Design of Grid Extension

5.1.1 Voltage Level Selection

Whenever there is an alternative to tap from either 33 kV or 15 kV, top most priority should be for tapping from 33 kV. If the substation is to be upgraded from 15 kV to 33 kV line then the tapping voltage level should be taken as 33 kV to be constructed with 33 kV accessories. If the upgrade of substation is delayed then the town could be energized by 15 kV using 15 kV transformers and after the substation upgrading is complete the town will be energized by 33 kV [15].

- Hence as the Shewarobit substation was upgraded to 33 kV, the voltage level under consideration for this study is 33 kV.

5.1.2 Route of Medium Voltage Line

The major points that shall be taken into consideration while deciding the route of medium voltage line are [15]:

- The line shall run, as much as possible, along a road. This will facilitate construction and maintenance of the line.
- The number of angle poles shall be minimized.
- An intersection of high way and railway tracks shall be avoided as far as possible.

Where unavoidable the medium voltage line shall intersect the road, railway track, and river or telephone line at right angles. With this consideration, the route of the MV power transmission line is indicated by the figure 5-1 below. And the total length span was found to be 10 kms.

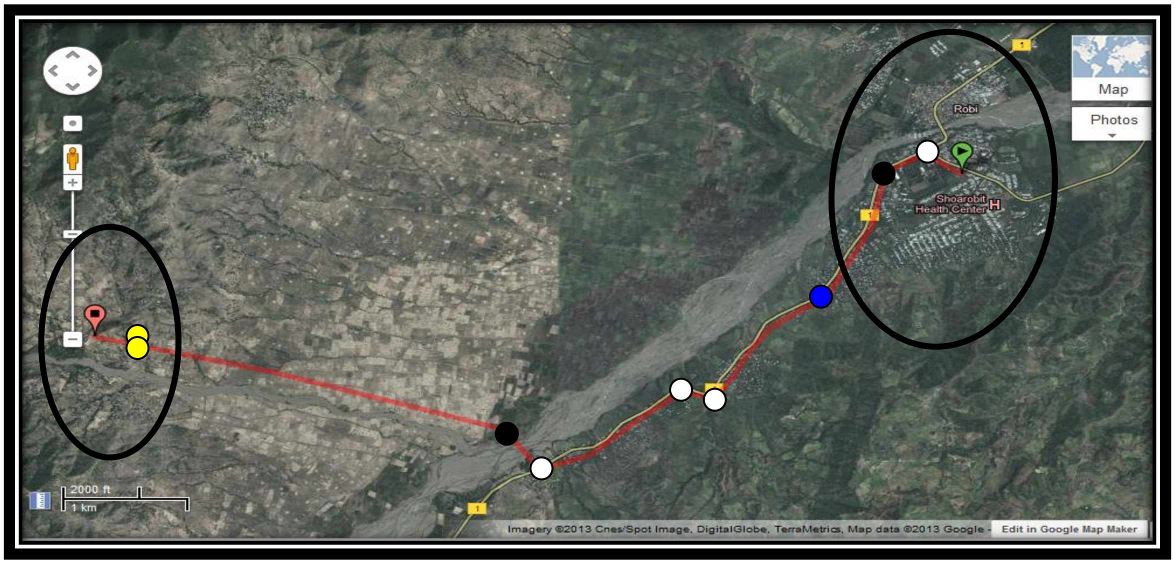

Figure 5-1 Proposed route for the MV power transmission line (Red Line)

5.1.3 Network Support (Pole Type) Selection

Due to the recently occurring wooden pole shortage and MV line network constructed with wooden pole has poor quality; UEAP has started using Concrete and Steel poles as major network construction pole types. Due to mostly occurring pole type change requests, the following guideline is prepared to assist the supervisors and the contractors in properly identifying and providing clear information that will facilitate decision making process [15].

- **Concrete Poles:** are the first choices for the construction of the network because concrete poles cannot be affected by insects, it is durable, and have good resistance to wind, fire and moist or marshy areas given that there is good foundation. Therefore, concrete poles are the most preferred.
- **Steel Poles:** Similar to the concrete poles, steel poles are durable and have resistance to wind, fire and moist or marshy areas given that there is good foundation**.** In areas where concrete poles are hard to transport, steel poles could be used.
- **SA Wooden Poles:** Wooden poles are currently scarce and due to that wooden pole should be the last option for network support in areas where it is impossible to transport either concrete or steel pole. The recently imported

strong and high quality South African wooden poles are available and must be used in places where the concrete /steel poles are impossible to erect.

- **Other Wooden Poles:** wooden poles that are manufactured nationally by the country can be used as the last options in places where the above three options is unavailable.

- Therefore, for this study, 10/11m 300 dan and 10/11m 500 dan concrete pole types are used.

5.1.4 Conductor Types and Cross-Sections

The factors governing the selection of conductor materials are low resistivity, high tensile strength, low cost and easy availability. The cross-sections and type of conductor recommended for 15/33kV medium voltage (MV) network is AAAC 95 [15].

- As EEPCo is currently using AAAC 95 mm^2 type of conductor, it is assumed for this study.

5.1.5 Required MV/LV (Step Down) Transformer Capacity

The total load of the transformer's LV network is calculated taking into account the load variation. After the load has been calculated, the "next bigger" transformer size is chosen, i.e. 50 kVA, 100 kVA, or 200 kVA [15].

- For this study a three phase 100 kVA, 33 kV/0.4 kV three phase transformer is selected because our peak load is 39.703kW (34kW of primary load plus 5.703 kW of the water pump (see section 3.2, figure 3-11, pp. 39)).

  For 15 year horizon, the load demand is equal to:
  Future load, $P = P_o \times D \times (1+R/100)^t$
  P_o is the current peak load (39.703 kW), D is the diversity factor taken as 0.7 [15] and R is the annual load growth rate considered as 5% [15]. Substituting these values gives:

$$P = 39.703 \times 0.7 \times (1+5/100)^{15}$$

$$P = 57.78 \text{ kW}$$

Considering 10% loss [15],

$$P = 1.1 \times 57.78 = 63.56 \text{ kW}$$

Therefore, this power (63.56 kW) should have to be delivered by the step down transformer.

The transformer kVA rating is then:

kVA = P/cos ϕ (Where cos ϕ = Power factor between 0.85 to 1 [15])

Hence, if we take cos ϕ = 0.85, kVA = 63.56/0.85 = 74.78

Therefore, the transformer capacity should be equal to 100 kVA.

5.1.6 High Voltage Protection

A lightning arrester is a device that protects transformers and other electrical apparatus from voltage surges. The lightning arrester provides a path over which the surge can pass before it has a chance to attack and seriously damage the transformer or other equipment. The elementary lightning arrester consists of an air gap in series with a resistive element. The voltage surge causes a spark which jumps across the air gap, passes through the resistive element (silicon carbide, for example) which is usually a material that allows a low-resistance path for the high-voltage surge, but presents a high resistance to the flow of line energy. This material is usually known as the “valve” element. The “earth terminal” at the bottom of all the three lighting arresters are joined together and connected to the earth wire [5].

- 33 kV lighting arrestors (3 in numbers) should have to be connected at the top of the H-pole structure for the protection of the transformer against lighting over-voltage.

5.1.7 System Earthing

One of the key factors in any electrical protection scheme is earthing. If any acceptable measure of safety is to be attained, correct grounding design and implementation must be followed. An earthing system to be totally effective shall satisfy the following conditions as stated in [15].

- Provide a low impedance path to ground for personal and equipment protection.
- Withstand and dissipate repeated fault and surge currents.
- Provide corrosion allowance or corrosion resistance to various soil chemicals to ensure continuous performance during the life of the equipment being protected.
- Provide rugged mechanical properties for easy driving with minimum effort and rod damage.

Further, for protection of person and equipment, the effort shall be done to aim for a ground resistance of less than 4ohm. In the circumstances where it is difficult to obtain the designed ground resistance, some methods of lowering the ground resistance shall be employed. These include deep driven rod system, chemical treatment of the soil using charcoal and salt layers around the rod and due to the inherent property of absorbing and retaining moisture clay can be used in areas where soil resistivity is high, of the order of 300ohm meters and above. The protective earth wire shall have a conductor cross section of Cu 35mm^2 [15].

The transformer body and the neutral terminal shall be connected together and then the body shall be connected to the earthling wire provided. Two cross arms of 33kV transformer adjacent to distribution transformer shall be earthed. The transformer body and surge arresters shall be connected to system earth point as short conductors as possible. The distribution transformer substation earthing wires shall be connected to the earthing electrode [15].

5.1.8 Short Circuit Protection

In order to protect the transformer from high fault current, 33kV dropout fuse containing 2A fuse link element should be installed on the 33kV side of the transformer. Besides this, HRC fuses of 100A capacity are also needed to be installed on the low voltage side of the transformer so as to protect the transformer from high current. This high current might be caused by overloading and/or faults on the LV networks.

5.1.9 Pole Top Accessories

Overhead line accessories will be installed after erection of poles is completed. The main accessories which are installed on the top of a pole are tie straps, cross arm, pins and insulators (both pin types and disc types according to their usage). Figure 5-2 shows all the components of the pole top accessories.

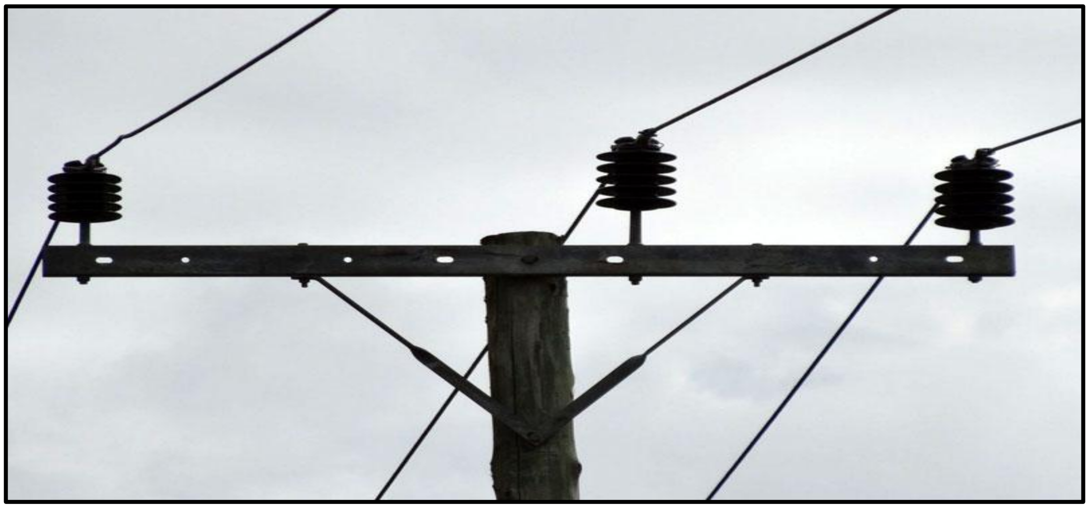

Figure 5-2 Pole and its top accessories [21]

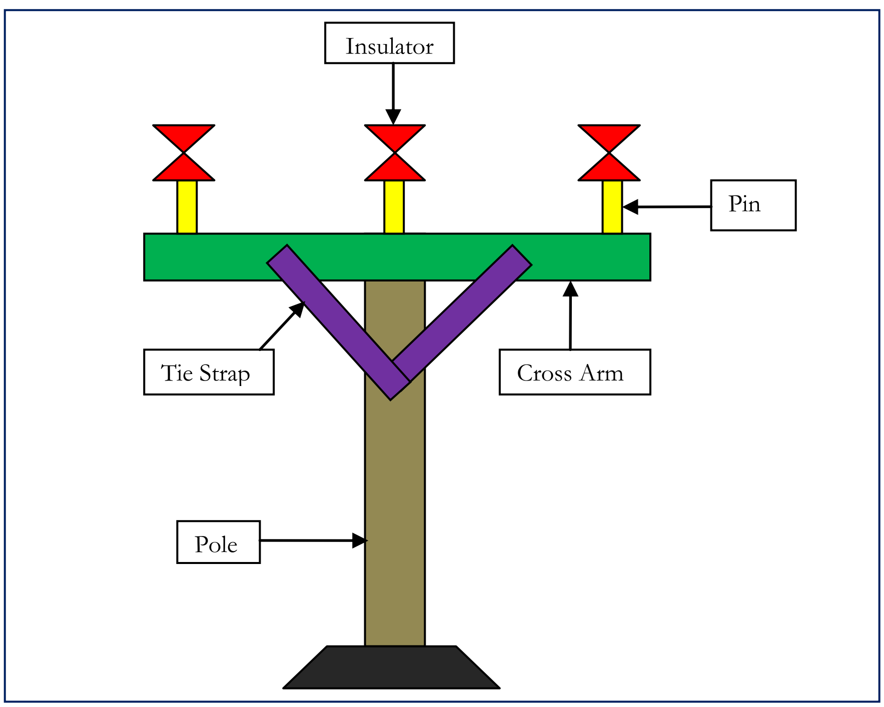

Figure 5-3 Pole and detailed names of its top accessories

5.1.10 Section Switch Installation

A section switch indicated below in figure 5-4 needs to be constructed near to the taping point of the MV line [15]. The main usage of this is to disconnect power in any occasions that needs power interruption.

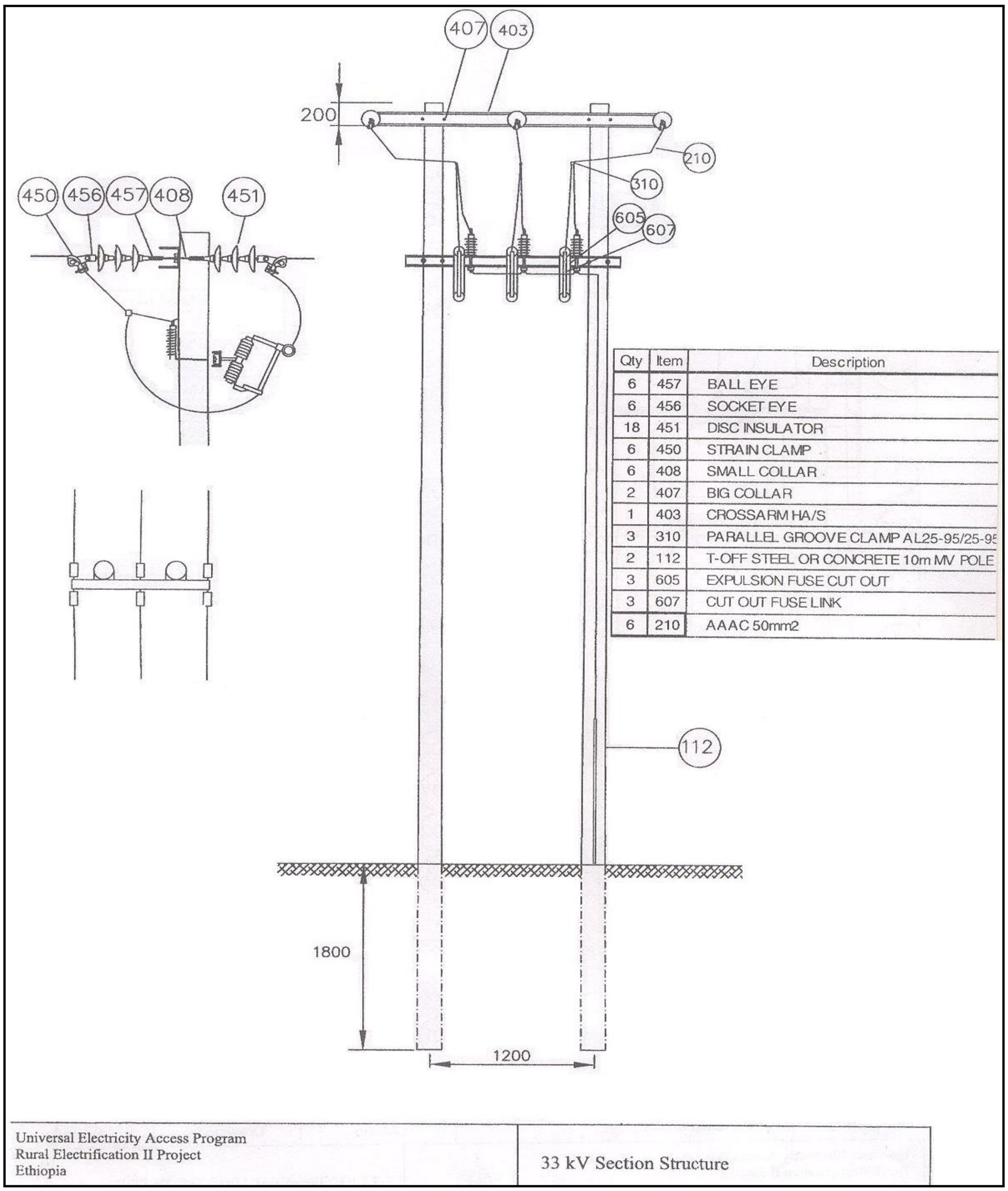

Qty	Item	Description
6	457	BALL EYE
6	456	SOCKET EYE
18	451	DISC INSULATOR
6	450	STRAIN CLAMP
6	408	SMALL COLLAR
2	407	BIG COLLAR
1	403	CROSSARM HA/S
3	310	PARALLEL GROOVE CLAMP AL25-95/25-95
2	112	T-OFF STEEL OR CONCRETE 10m MV POLE
3	605	EXPULSION FUSE CUT OUT
3	607	CUT OUT FUSE LINK
6	210	AAAC 50mm2

Figure 5-4 Section switch assembly [15]

5.1.11 Guys

Situations arise where the conductor tries to force the pole from its normal position. This happens because of abnormal loads of wind as well as because of broken lines, uneven spans, corners, dead-ends and hills. When these cases of strain arise, the pole is strengthened and kept in position by guys. Guys are braces or cables fastened to the pole [5]. The most commonly used form of guying is the anchor guy installation indicated by figure 5-6, figure 5-7, figure 5-8, and figure 5-10.

In figure 5-1 (page 78), the white, black, blue, and red spots on the proposed route of MV transmission line indicates the poles that needs guying support. In the figure, the green spot is proposed to be the taping point. The white spots are proposed to be heavy angle assembly with guy wire[8]. The black spots are proposed to be light angle 2 assembly with guy wire[9]. The blue spot is proposed to be light angle 1 assembly with guy wire[10]. The yellow spots are proposed to be towers for the transformer erection and the red spot at the end is proposed to be dead end assembly with guy wire.

a *b* *c*

Figure 5-5 a: 33kV dropout fuse, b: 100A HRC fuse and c: 33kV lightning arrestor [21]

8Heavy angle assembly with guy wire is needed when MV line turns 30^0 to 60^0 [15].
9Light angle 2 assembly with guy wire is needed when MV line turns 15^0 to 30^0 [15].
10Light angle 1 assembly with guy wire is needed when MV line turns 2^0 to 15^0 [15].

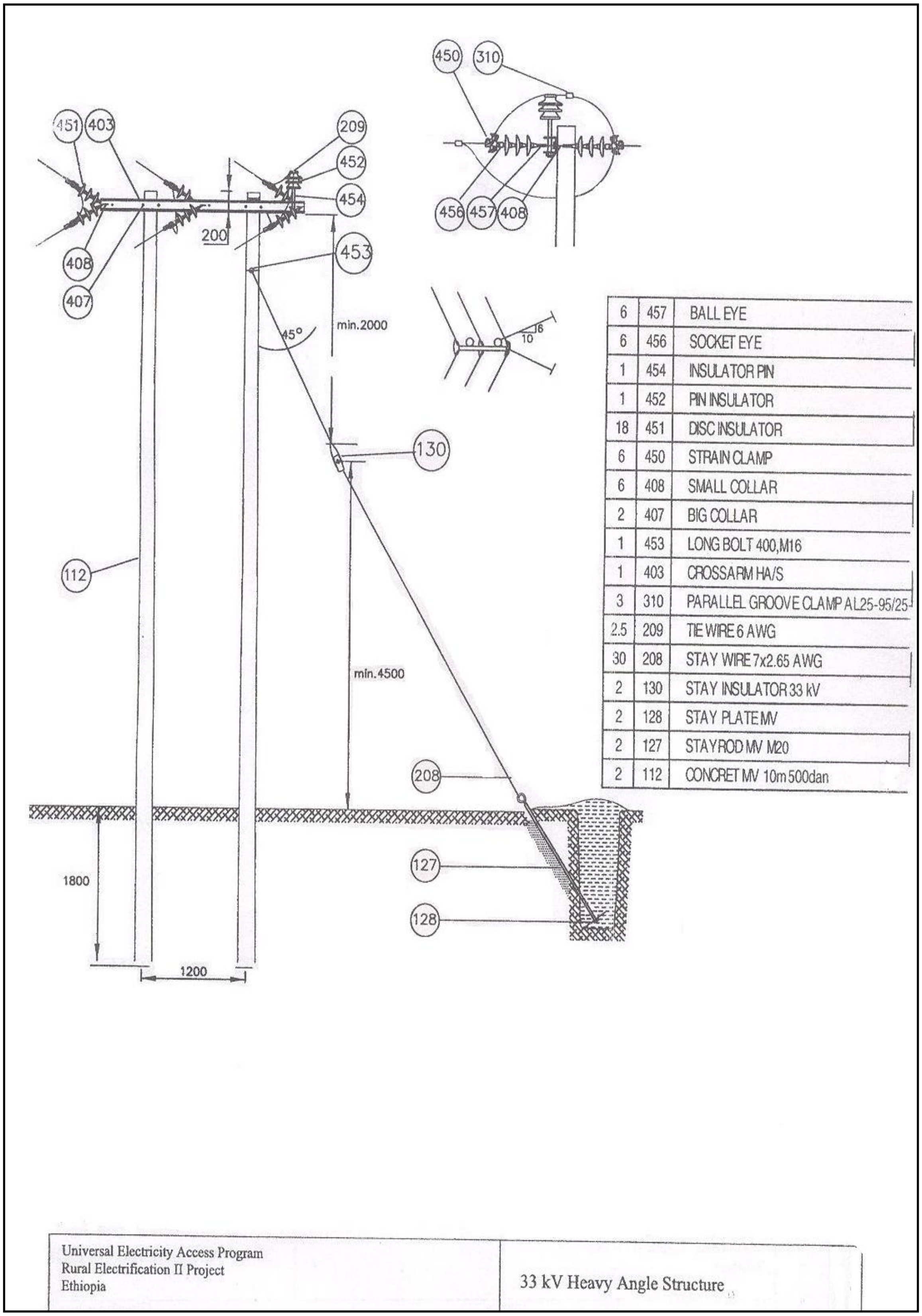

Figure 5-6 Heavy angle assembly with guy wire [15]

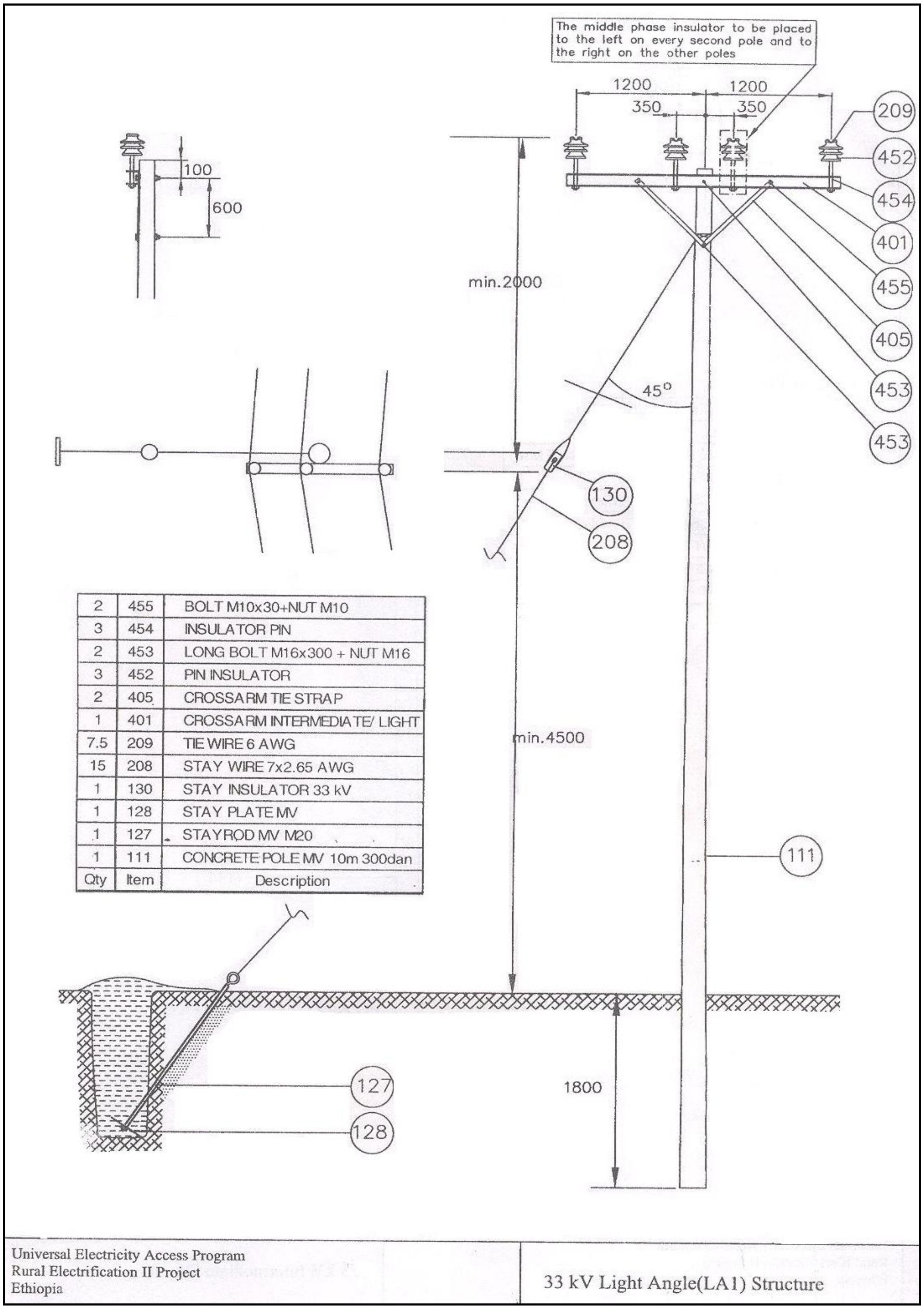

Qty	Item	Description
2	455	BOLT M10x30+NUT M10
3	454	INSULATOR PIN
2	453	LONG BOLT M16x300 + NUT M16
3	452	PIN INSULATOR
2	405	CROSSARM TIE STRAP
1	401	CROSSARM INTERMEDIATE/ LIGHT
7.5	209	TIE WIRE 6 AWG
15	208	STAY WIRE 7x2.65 AWG
1	130	STAY INSULATOR 33 kV
1	128	STAY PLATE MV
1	127	STAYROD MV M20
1	111	CONCRETE POLE MV 10m 300dan

Figure 5-7 Light angle 1 assembly with guy wire [15]

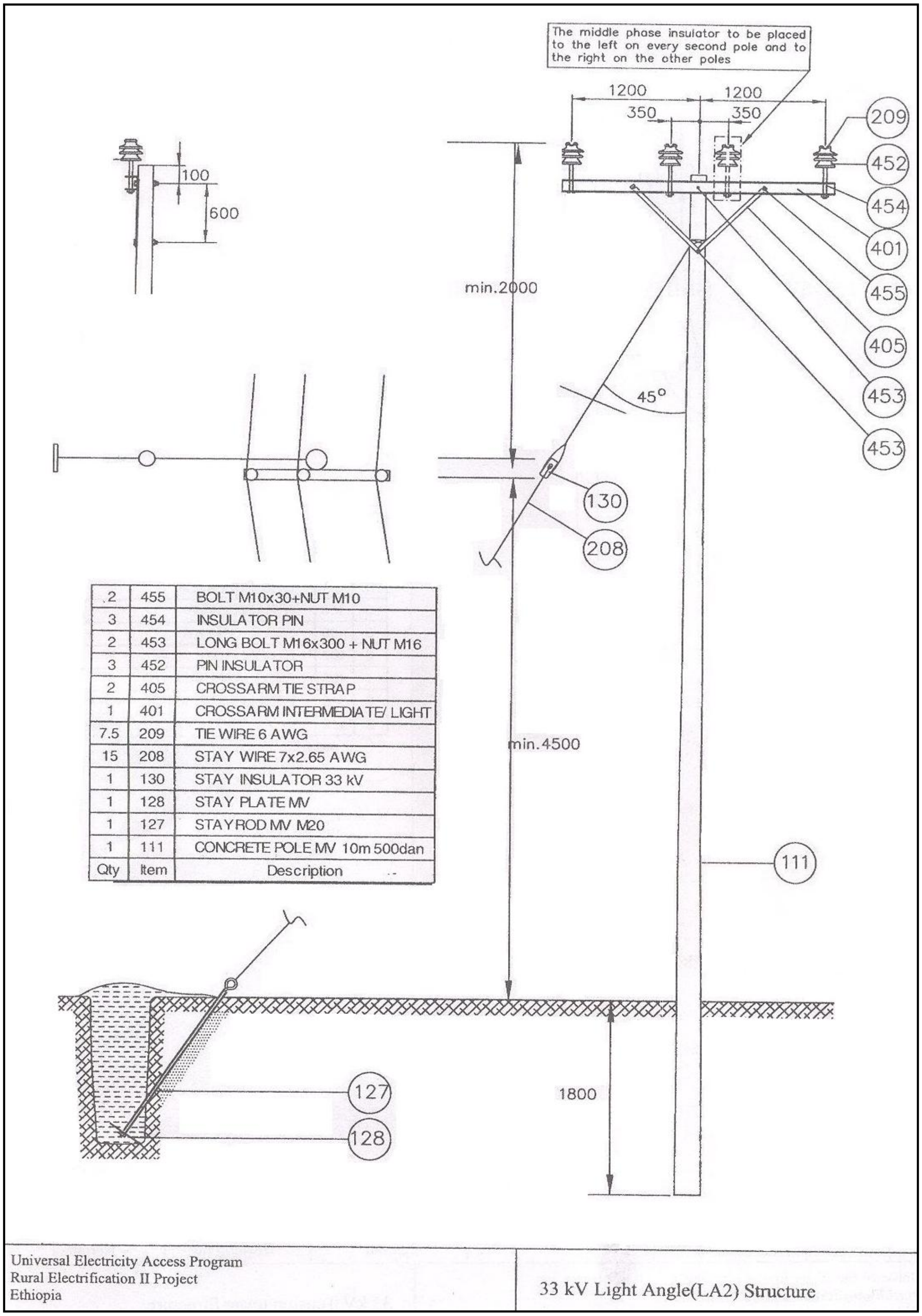

Qty	Item	Description
2	455	BOLT M10x30+NUT M10
3	454	INSULATOR PIN
2	453	LONG BOLT M16x300 + NUT M16
3	452	PIN INSULATOR
2	405	CROSSARM TIE STRAP
1	401	CROSSARM INTERMEDIATE/ LIGHT
7.5	209	TIE WIRE 6 AWG
15	208	STAY WIRE 7x2.65 AWG
1	130	STAY INSULATOR 33 kV
1	128	STAY PLATE MV
1	127	STAYROD MV M20
1	111	CONCRETE POLE MV 10m 500dan

Figure 5-8 Light angle 2 assembly with guy wire [15]

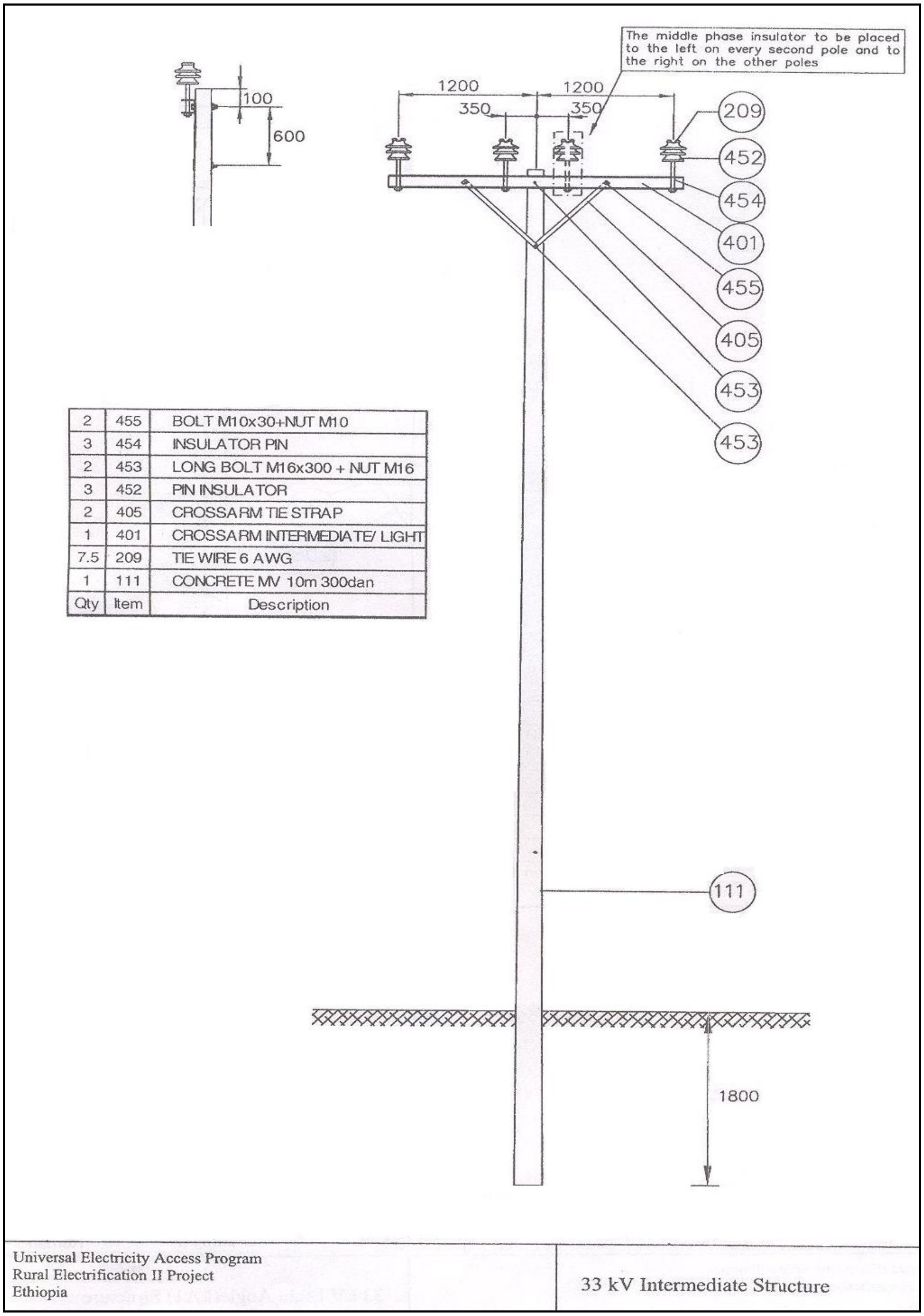

Qty	Item	Description
2	455	BOLT M10x30+NUT M10
3	454	INSULATOR PIN
2	453	LONG BOLT M16x300 + NUT M16
3	452	PIN INSULATOR
2	405	CROSSARM TIE STRAP
1	401	CROSSARM INTERMEDIATE/ LIGHT
7.5	209	TIE WIRE 6 AWG
1	111	CONCRETE MV 10m 300dan

Figure 5-9 Normal suspension assembly [15]

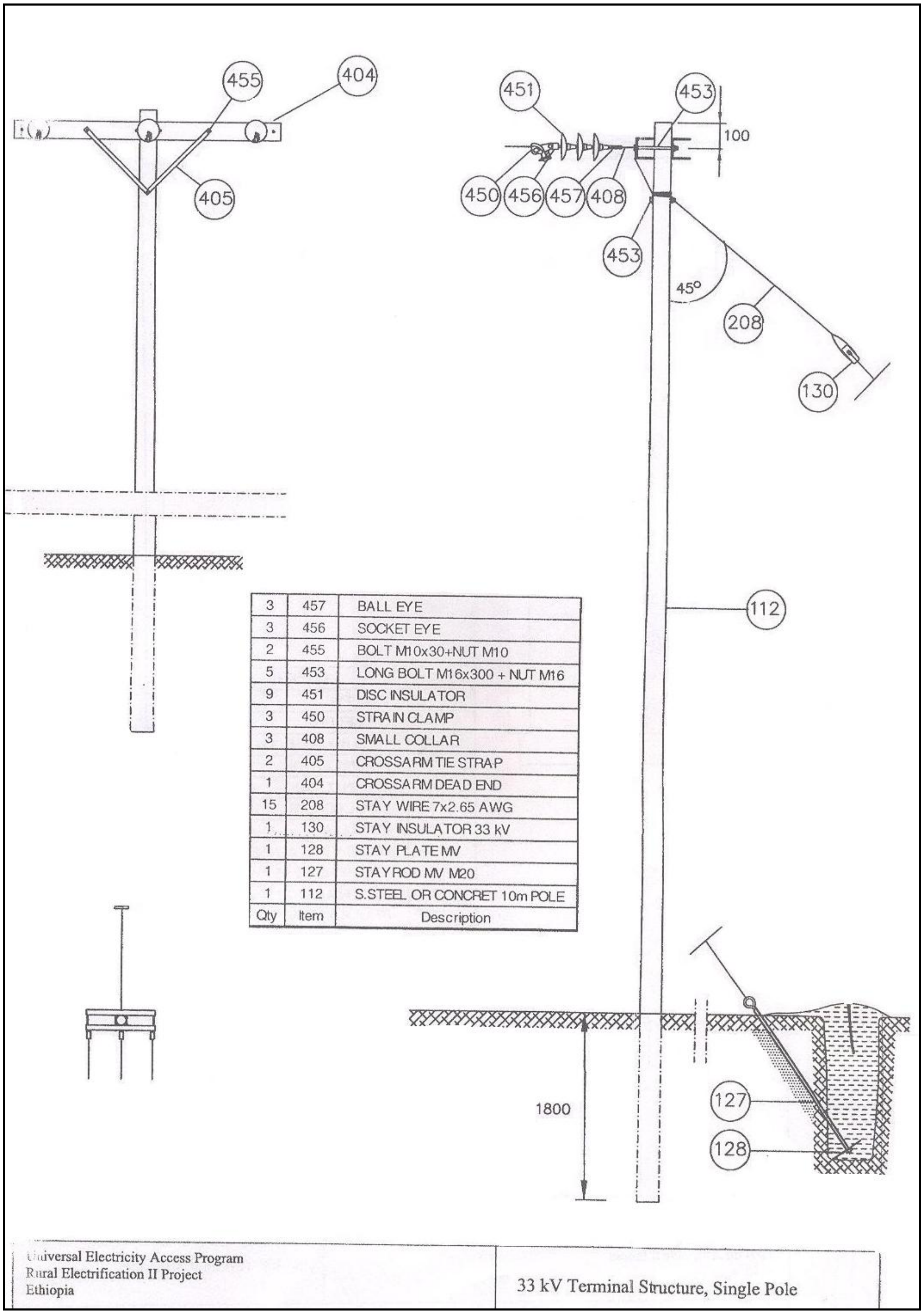

Qty	Item	Description
3	457	BALL EYE
3	456	SOCKET EYE
2	455	BOLT M10x30+NUT M10
5	453	LONG BOLT M16x300 + NUT M16
9	451	DISC INSULATOR
3	450	STRAIN CLAMP
3	408	SMALL COLLAR
2	405	CROSSARM TIE STRAP
1	404	CROSSARM DEAD END
15	208	STAY WIRE 7x2.65 AWG
1	130	STAY INSULATOR 33 kV
1	128	STAY PLATE MV
1	127	STAYROD MV M20
1	112	S.STEEL OR CONCRET 10m POLE

Figure 5-10 Dead end assembly with guy wire [15]

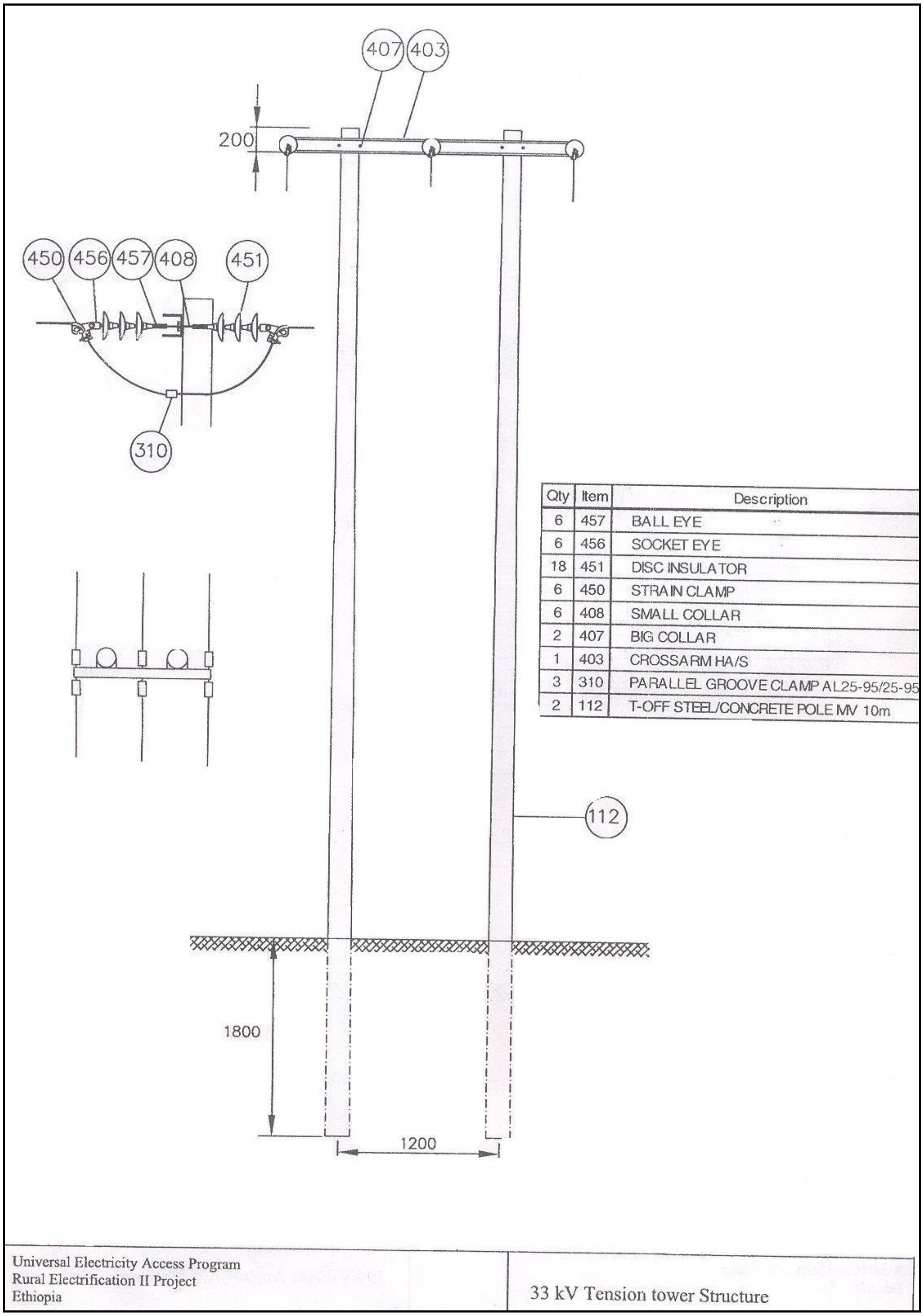

Qty	Item	Description
6	457	BALL EYE
6	456	SOCKET EYE
18	451	DISC INSULATOR
6	450	STRAIN CLAMP
6	408	SMALL COLLAR
2	407	BIG COLLAR
1	403	CROSSARM HA/S
3	310	PARALLEL GROOVE CLAMP AL25-95/25-95
2	112	T-OFF STEEL/CONCRETE POLE MV 10m

Figure 5-11Tension tower assembly [15]

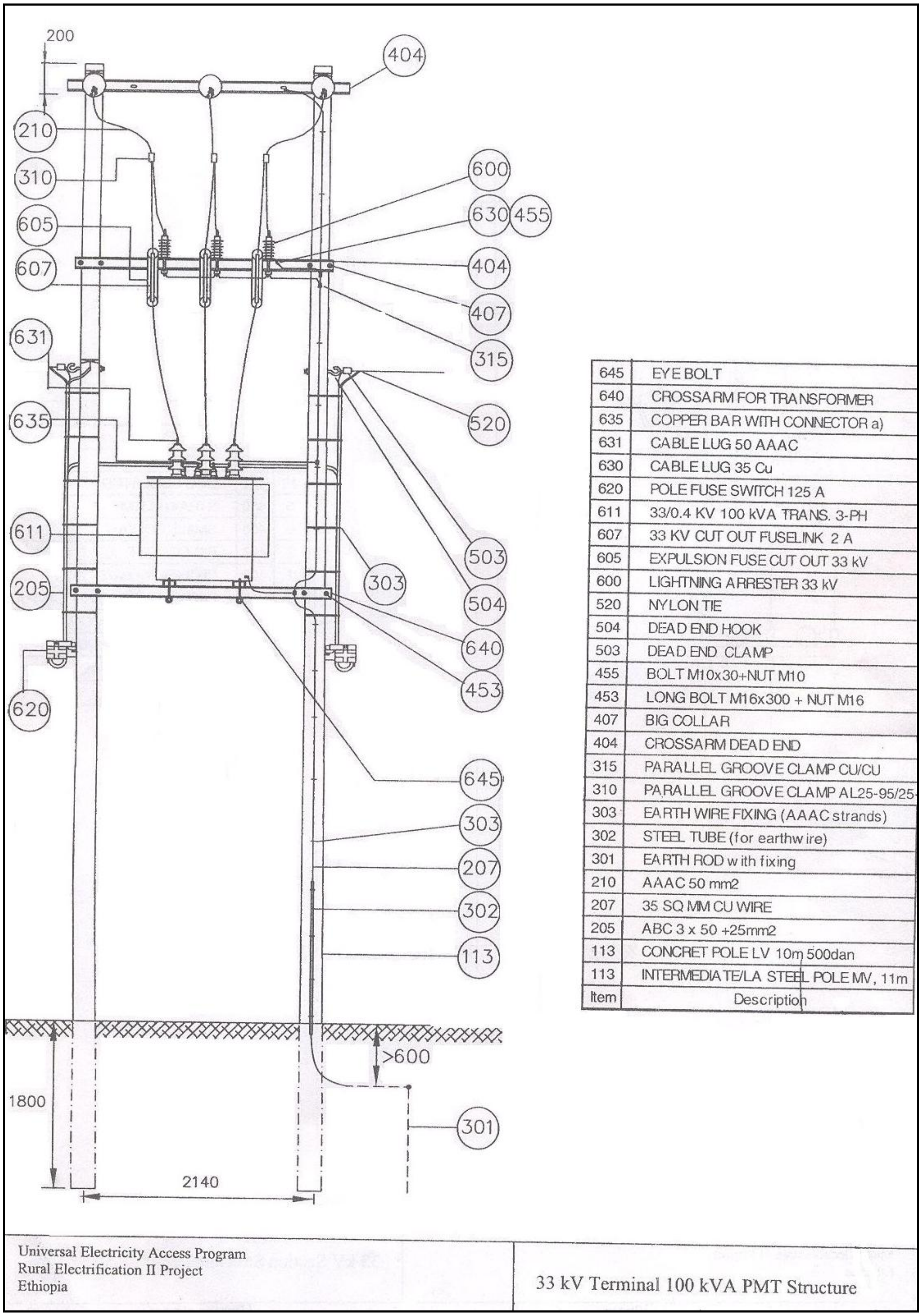

Item	Description
645	EYE BOLT
640	CROSSARM FOR TRANSFORMER
635	COPPER BAR WITH CONNECTOR a)
631	CABLE LUG 50 AAAC
630	CABLE LUG 35 Cu
620	POLE FUSE SWITCH 125 A
611	33/0.4 KV 100 kVA TRANS. 3-PH
607	33 KV CUT OUT FUSELINK 2 A
605	EXPULSION FUSE CUT OUT 33 kV
600	LIGHTNING ARRESTER 33 kV
520	NYLON TIE
504	DEAD END HOOK
503	DEAD END CLAMP
455	BOLT M10x30+NUT M10
453	LONG BOLT M16x300 + NUT M16
407	BIG COLLAR
404	CROSSARM DEAD END
315	PARALLEL GROOVE CLAMP CU/CU
310	PARALLEL GROOVE CLAMP AL25-95/25-
303	EARTH WIRE FIXING (AAAC strands)
302	STEEL TUBE (for earthwire)
301	EARTH ROD with fixing
210	AAAC 50 mm2
207	35 SQ MM CU WIRE
205	ABC 3 x 50 +25mm2
113	CONCRET POLE LV 10m 500dan
113	INTERMEDIATE/LA STEEL POLE MV, 11m

Figure 5-12 100kVA 3 phase transformer assembly with its accessories [15]

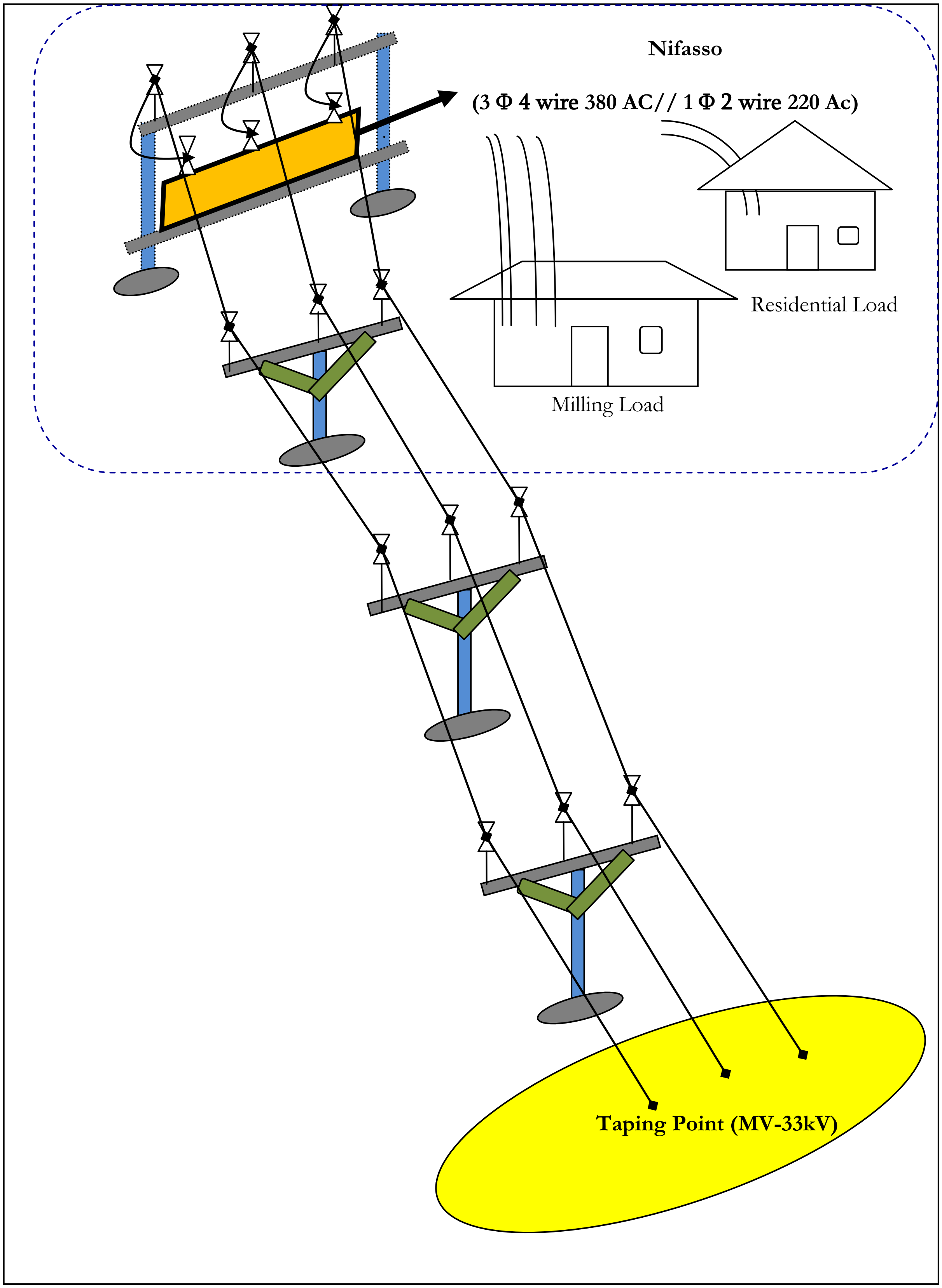

Figure 5-13 Simplified block diagram of grid extension

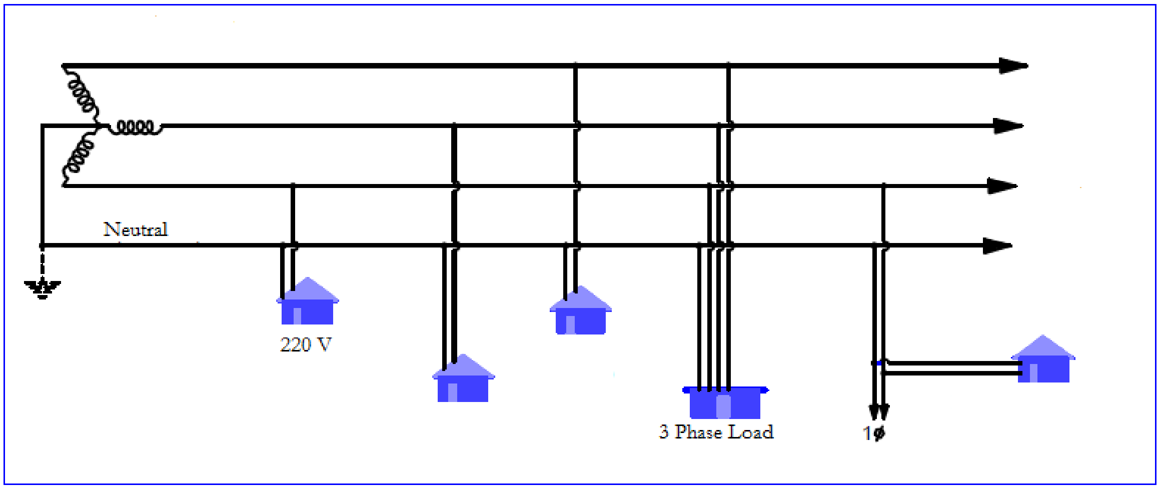

Figure 5-14 Low voltage distribution network configurations

5.2 Estimation of Grid Extension Cost

The cost of extending the grid generally categorized as: construction cost, transportation cost, material cost and administration and control. The detailed estimation of these cost categories are presented in Table 5-1, Table 5-2 and Table 5-3 below.

5.2.3 Material Cost

Table 5-1 Material cost of grid extension

Material cost estimation for 33kV MV line to electrify Nifasso (in ETB)					
No.	Description	Unit	Qty.	Unit Price	Total price
1	Concrete Pole 300 dan 10/11m	no	87	2,677.75	232,964.25
2	Concrete Pole 500 dan 10/11m	no	11	2,806.80	30,874.80
3	2.5m Cross arm	no	85	729.62	62,017.70
4	Heavy angle/Tension tower Cross arm 2.5m	no	5	769.79	3,848.95
5	T-off Cross arm / Dead end Cross arm 2.5m	no	10	280.16	2,801.60
6	Big Collar (Flat Bar) for 300dan/Long bolt 16mm, 40cm with nut and washer	no	89	13.42	1,194.38
7	Big Collar (Flat Bar) for 500dan/Long bolt 16mm, 40cm with nut and washer	no	11	13.42	147.62
8	Tie Strap	no	188	31.41	5,904.89

9	Bolt and nut M10.5cm	no	375	2.74	1,027.13
10	Long bolt 16mm, 40cm with nut and washer	no	124	13.93	1,726.70
11	Small collar, 12 mm	no	39	7.90	308.22
12	Ball eye, 16mm	no	39	15.39	600.29
13	Disc insulator, 16mm (chain insulator)	no	117	75.01	8,776.17
14	Socket eye, 16mm	no	39	27.29	1,064.23
15	Strain clamp 25…95mm^2	no	39	55.43	2,161.77
16	33kV Pin type Insulator	no	270	134.79	36,393.30
17	33kV Pin Threaded with nut & washer	no	270	64.36	17,376.39
18	Galvanized steel (guy) wire	kg	49.41	43.34	21,141.43
19	33kV stay insulator	no	10	16.19	161.90
20	PG clamp Al/Al 25…95mm^2	no	15	12.61	189.12
21	AAAC95mm^2	km	30.03	14,976.34	449,739.43
22	Tie wire 6 AWG	kg	15	41.71	625.65
23	Drop out fuse	no	3	848.10	2544.3
24	Drop out fuse element, 2A	no	3	14.57	43.71
25	Mid span joint 95mm^2	no	27	16.02	432.54
26	Cement	kg	9375	2.60	24,375.00
27	Sand	m^3	13.17	200.00	2,634.00
28	Coarse aggregate	m^3	26.28	150.00	3,942.00
29	Stay rod, M 20 with washer	no	10	148.09	1,480.90
30	Base plate	no	10	208.56	2,085.60
31	Gravel stone	m^3	0.474	150.00	71.10
Note: Drop out fuse is for section switch purpose			**Total**		**896,551.55**

1	Suspension = 82	4	Tension Tower = 1
2	Light Angle 1 = 1 and Light Angle 2 = 2	5	Heavy Angle = 4
3	Dead End = 1		

Material cost estimation for Transformer to electrify Nifasso (in ETB)					
No.	Description	Unit	Qty.	Unit Price	Total Price
1	Concrete Pole 300 dan11mt	no	2	2,677.75	5,355.50
2	Cross arm for transformer fixture,2.5m	set	1	806.24	806.24
3	Long bolt with nut,M12x300mm	no	7	8.10	56.70
4	Washer 3/4	kg	3	9.31	27.93
5	33 kV pin threaded	no	3	59.14	177.42

6	33 kV pin type insulator	no	3	134.79	404.37
7	Tie wire 6 AWG	kg	0.33	41.71	13.89
8	Drop out fuse 33 kV	no	3	848.10	2,544.30
9	33kV lightning arrestor	no	3	739.87	2,219.61
10	PG clamp Al/Al 25…95mm^2 or Al/Cu	no	6	21.87	131.20
11	Transformer, 100kVA	no	1	40,668.73	40,668.73
12	Pole mount fuse switch				
12a	Pole mount fuse switch 3x125A, for Ntoo HRC fuse OR	no	2	3,617.01	7,234.02
12b	Pole mount fuse switch 3x400A, for NT 1/2/3 (Size 01) HRC fuse	no	2	3,617.01	7,234.02
13	HRC fuse 100A	no	6	39.18	235.08
14	Dead End Hook	no	2	20.33	40.66
15	Dead End Clamp	no	2	43.45	86.90
16	Nylon tie	no	20	0.42	8.40
17	PG clamp Cu/cu 10…35mm^2	no	5	15.26	76.30
18	CU wire stranded 35mm^2 for Earthing	kg	4	57.21	256.30
19	Steel tube 1/2" 2mt	no	1	112.95	112.95
20	Eye bolt	no	4	11.85	47.4
21	Earthing rod 50mmx3mm,4mt	no	1	194.08	194.08
22	Suspension Cross arm	no	1	431.25	431.25
23	Bolt and nut M10.5cm	no	7	0.89	6.23
24	ABC Conductor (3×50 +25mm^2)	m	6	32.56	195.36
25	Tie strap	no	2	38.98	77.96
26	Fuse element, 2A	no	3	14.57	43.71
27	AAAC 50mm^2	m	18	6.25	112.50
28	Big Collar (Flat Bar)	no	4	14.36	54.24
29	Cement	kg	350	2.60	910.00
30	Sand	m^3	0.50	200.00	100.80
31	Gravel stone	m^3	0.02	150.00	3.00
32	Coarse aggregate	m^3	1.01	150.00	151.20
33	Dead end Cross arm	no	2	229.82	459.64
34	Cable Lug with connector b (MV)	no	3	50.24	150.72
35	Cable Lug with connector a (LV)	no	4	43.48	173.92
Total					**70,801.40**

5.2.1 33 kV Line Construction Cost

The line construction cost contains surveying of MV line routes and detailed design calculations, network support (Poles) foundation or pole pit excavation, network assembly and final construction cost such as built in document preparation as indicated in Table 5-2.

Table 5-2 33kV line construction cost

A: Assembly and profile drawing cost (in ETB)					
No.	Description	Unit	Qty.	Unit Price	Total Price
1	Surveying of MV routes , profile drawing and detail design calculation	km	9.10	944.16	8,591.86
2	Suspension Assembly	ass	82	1,440.49	118,120.18
3	Light Angle 1 Assembly (with guy wire)	ass	1	1,645.03	1,645.03
4	Light Angle 2 Assembly (with guy wire)	ass	2	1,645.03	3,290.06
5	Tension Tower Assembly	ass	1	2,808.70	2,808.70
6	Heavy Angle Assembly (with guy wire)	ass	4	3,035.76	12,143.04
7	Dead end Assembly (with guy wire)	ass	1	1,663.70	1,663.70
8	Section Switch Assembly	ass	1	2,808.70	2,808.70
Total					**151,071.27**

B: Foundation cost (in ETB)						
No.	Pole and assembly type	Unit	Qty.	Foundation unit price	Concrete back fill unit price	Total
1	Suspension & Light Angle 1 (1×300dan)	ass	83	843.23	244	90,240.09
2	Light Angle 2 (1×500dan)	ass	2	988.65	286.07	2,549.44
3	Tension Tower (2×300dan)	ass	1	1,686.46	488	2,174.46
4	Heavy Angle & Dead End (2×500dan & 1×500dan)	ass	5	1,270.43	349.38	8,099.05
5	Transformer & Section Switch Assembly (2×300dan)	ass	2	1,690.96	489.3	4,360.52
Total						**107,423.56**

C: Final construction cost (in ETB)					
1	Tapping point arrangement	per town	1	805.74	805.74
2	Conductor stringing (three phase)	km	9.1	2,025.08	18,428.23
3	Transformer erection with earthing	no	1	4,794.63	4,794.63
4	Built in document preparation	per town	1	4,144.04	4,144.04
5	Test & commissioning	km	9.10	264.95	2,411.05
Total					**30,583.69**

5.2.2 Transportation Cost

Table 5-3 Material transportation cost of grid extension

No.	Description			Accessories Transport (ETB)	Pole Transport (ETB)	Total (ETB)
1	Suspension Assembly	no	82×300dan	75	692.11	62,903.02
2	L.A-1 assembly	no	1×300dan	78	692.11	770.11
3	L.A-2 assembly	no	2×500dan	78	692.11	1,540.22
4	H.A assembly	no	8×500dan	138	692.11	6,640.88
5	Tension Tower Assembly	no	2×300dan	132	692.11	1,648.22
6	Dead End Assembly	no	1×500dan	69	692.11	1,522.22
7	Section Switch Assembly	no	2×300dan	132	692.11	1,648.22
8	Transportation of AAAC 95 mm^2 and Tie wire needed for stringing of 1km 3 phase	km	9.1+Tie wire	1,365		13,663.65
9	Transformer with all its accessories and switch gear	set	1	1,542		1,542
10	Transformer pole transportation	pair	1		1,384.22	1,384.22
Total						**93,262.76**

Adding up of results of Table 5-1, Table 5-2 and Table 5-3 gives the overall total to be = 1,484,663.65 ETB. With an exchange rate of 1 USD = 18.79 ETB, the investment cost of grid extension is = 8,681.22 $/km. O and M cost/year/ km is taken as 10 % of the capital cost [44] = USD 868.12.

The cost breakdown can be summarized in Table 5-4 and Figure 5-15 given below.

Table 5-4 Overall total cost of grid extension (in ETB)

Material Cost	967,352.95	65 %
Construction Cost	289,078.52	20 %
Transportation Cost	93,262.76	5 %
Administration & Control	134,969.42	10 %
Overall Total	1,484,663.65	100 %

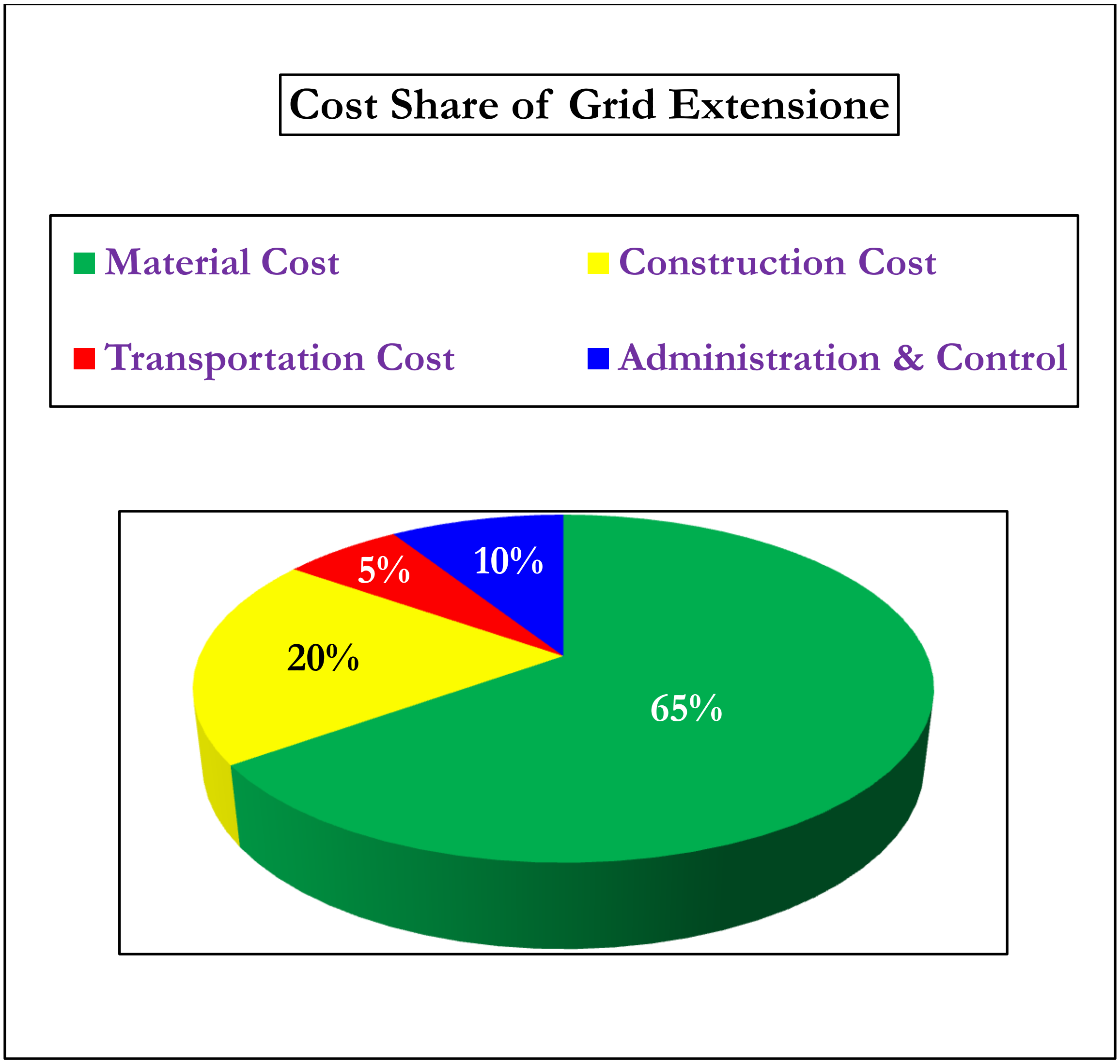

Figure 5-15 Cost share of grid extension

5.3 Cost Comparisons of the HPS against Grid Extension

HOMER assumes that load can be supplied either by the standalone system or by grid extension. The cost of the standalone system is independent of the grid extension distance, whereas the cost of extending the grid does depend on the grid extension distance. The distance at which the costs equate is the breakeven grid extension distance.

The input to HOMER so as to compare the cost of a standalone hybrid power system with grid extension are indicated by figure 5-16 which is the homer input dialog box in which the user inters the data’s.

Hence, as the figure 5-16 indicates it contains the investment cost of the grid extension per km as 8,681.22 $/km, the O & M cost as 868.12 $/yr./km and the current EEPCo average energy sale tariff as 0.028 $/kWh.

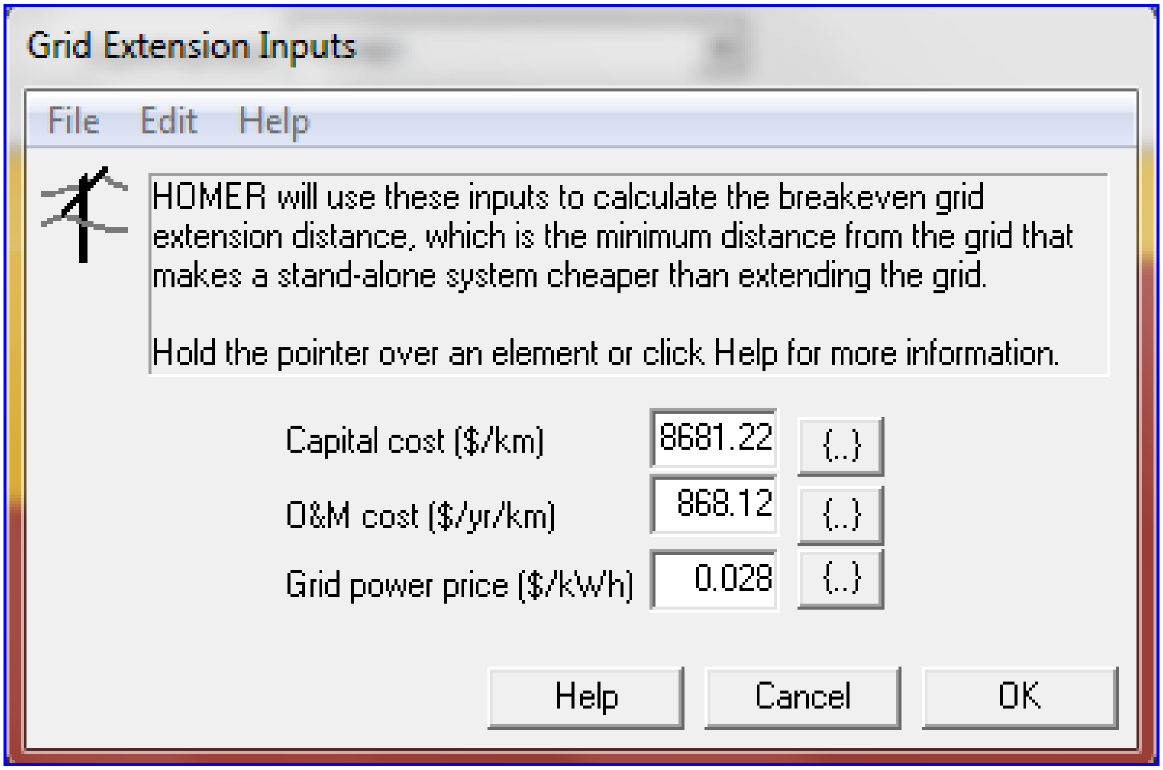

Figure 5-16 HOMER input for comparison of grid extension

Finally, after running the simulation, the cost comparison graph of the standalone system against grid extension was obtained and the result is discussed in chapter six.

CHAPTER SIX

6. RESULTS AND DISCUSSIONS

6.1 HOMER Simulation Results

6.1.1 Optimization Results

Figure 6-1 below shows some optimization results (which are part of the numerous alternative solutions from rank 1 up to 26) that are the possible configurations able to feed the system total load. Despite the numerous alternatives with equal renewable fraction, the choice of optimal system type is restricted by the varying nature of initial capital, net present cost, excess electricity and COE of each set-up. Accordingly, the one which is marked in blue color (the fifth rank) in which fuel cell operates for 2,731 hours/year is the best optimum PV-Wind-Fuel Cell hybrid system configuration.

PV (kW)	PGE25	FCell (kW)	S6CS25P	Conv. (kW)	Elec. (kW)	H2 Tank (kg)	Disp. Strgy	Initial Capital	Operating Cost ($/yr)	Total NPC	COE ($/kWh)	Ren. Frac.	Capacity Shortage	FCell (hrs)
150			160	40			CC	$ 464,800	5,796	$ 538,893	0.310	1.00	0.01	
150			160	40			LF	$ 464,800	5,796	$ 538,893	0.310	1.00	0.01	
150		10	100	40	30	10	LF	$ 486,500	4,436	$ 543,207	0.313	1.00	0.01	2,057
150		5	120	40	20	10	LF	$ 478,600	5,087	$ 543,624	0.312	1.00	0.01	2,939
110	1	5	120	40	25	15	LF	$ 465,100	6,215	$ 544,550	0.313	1.00	0.01	2,731
150		10	100	40	25	15	LF	$ 488,000	4,469	$ 545,128	0.314	1.00	0.01	2,072
150		5	120	40	15	15	LF	$ 480,100	5,091	$ 545,175	0.314	1.00	0.01	2,844
150			160	40		5	CC	$ 471,300	5,846	$ 546,032	0.314	1.00	0.01	
150			160	40		5	LF	$ 471,300	5,846	$ 546,032	0.314	1.00	0.01	
150		5	120	40	30	5	LF	$ 482,100	5,064	$ 546,832	0.315	1.00	0.01	2,836
150			160	50			CC	$ 471,800	5,982	$ 548,270	0.316	1.00	0.01	
150			160	50			LF	$ 471,800	5,982	$ 548,270	0.316	1.00	0.01	
150		5	140	40	10	5	LF	$ 479,200	5,462	$ 549,019	0.316	1.00	0.01	2,271
150		5	120	40	25	10	LF	$ 483,600	5,124	$ 549,097	0.315	1.00	0.01	2,994
110	1	5	120	40	30	15	LF	$ 470,100	6,246	$ 549,951	0.316	1.00	0.01	2,759
150		10	100	40	30	15	LF	$ 493,000	4,516	$ 550,727	0.316	1.00	0.01	2,114
150		5	120	40	20	15	LF	$ 485,100	5,148	$ 550,903	0.316	1.00	0.01	2,989
110	1	5	120	40	25	20	LF	$ 471,600	6,275	$ 551,814	0.317	1.00	0.01	2,774
150		5	120	40	15	20	LF	$ 486,600	5,146	$ 552,379	0.318	1.00	0.01	2,867
150		10	100	40	25	20	LF	$ 494,500	4,528	$ 552,380	0.318	1.00	0.01	2,089
150		10	100	50	30	10	LF	$ 493,500	4,622	$ 552,585	0.318	1.00	0.01	2,057
150		5	120	50	20	10	LF	$ 485,600	5,273	$ 553,001	0.318	1.00	0.01	2,939
110	1		180	40			CC	$ 456,900	7,528	$ 553,128	0.318	1.00	0.01	
110	1		180	40			LF	$ 456,900	7,528	$ 553,128	0.318	1.00	0.01	
150			160	40		10	CC	$ 477,800	5,896	$ 553,171	0.319	1.00	0.01	
150			160	40		10	LF	$ 477,800	5,896	$ 553,171	0.319	1.00	0.01	

Figure 6-1 Some of the optimization results

6.1.2 System Architecture and Cost Summary

A hybrid power system containing PV, wind and fuel cell power sources marked in blue color in figure 6-1 can be summarized by Table 6-1 below.

Table 6-1 System architecture and cost summary

System Architecture		Cost Summary	
110kW PV Array	120×Surrette 6CS25P	Total NPC	$ 544,550
1×PGE 20/25	25kW Electrolyzer	Initial Capital	$ 465,100
5kW Fuel Cell	15kg Hydrogen Tank	Operating Cost	$ 6,215/yr.
40kW Converter	LF Dispatch Strategy	Levelized COE	$ 0.313/kWh

As it can be seen clearly in the fifth rank that is marked in blue in figure 6-1 the capacity shortage is reported as 0.01 which is nearly zero. Furthermore, the system report shows that there is an excess electricity of 43,460 kWh/yr. (18.9 %).

Figure 6-2 given below shows the detailed net present cost share by each components of the optimal hybrid set-up supported by a bar graph. Hence, the net present cost share of each component in decreasing order can be recognized as PV, battery, wind turbine, converter, electrolyzer, hydrogen tank and fuel cell.

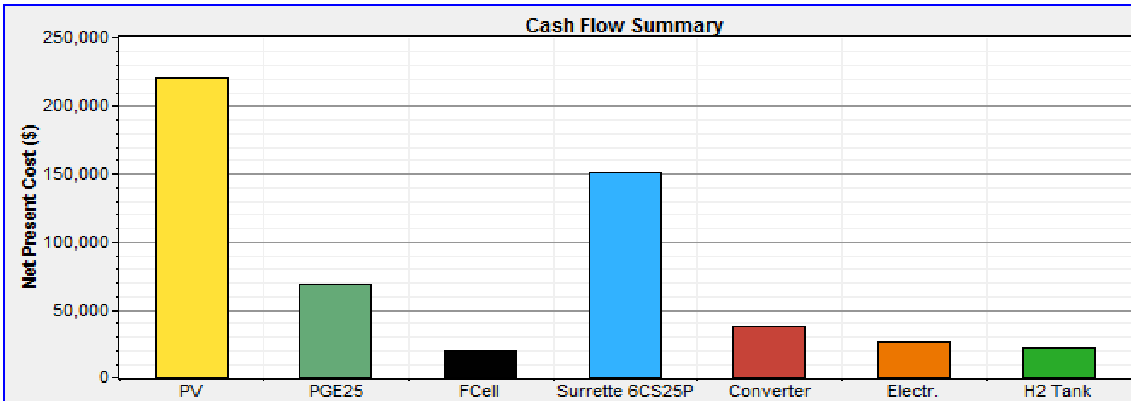

Component	Capital ($)	Replacement ($)	O&M ($)	Fuel ($)	Salvage ($)	Total ($)
PV	220,000	0	0	0	0	220,000
PGE 20/25	55,000	0	14,062	0	0	69,062
Fuel Cell	15,000	4,259	349	0	-683	18,926
Surrette 6CS25P	102,600	49,547	13,116	0	-14,225	151,038
Converter	28,000	11,683	0	0	-2,175	37,509
Electrolyzer	25,000	0	1,598	0	0	26,598
Hydrogen Tank	19,500	0	1,918	0	0	21,418
System	465,100	65,490	31,042	0	-17,082	544,550

Figure 6-2 The optimum hybrid power system cost share by each components

6.1.3 Electric Power Production and Consumption

Table 6-2 Electric power production and consumption

Production			Consumption		
Power Unit	kWh/yr.	%	Load Type	kWh/yr.	%
PV Array	183,017	80	AC Load	129,291	79
Wind Turbine	33,461	14	Deferrable Load	6,703	4
Fuel Cell	13,395	6	Electrolyzer	27,511	17
Total	229,874	100	Total	163,505	100

Figure 6-3 displays the monthly average electric production by each power units. Hence, as it can be seen clearly, most of the electric production is being shared by the PV followed by the wind turbine. But, the power production share by the fuel cell, even though it is significant, it is small as compared with the PV and wind turbine power unit outputs.

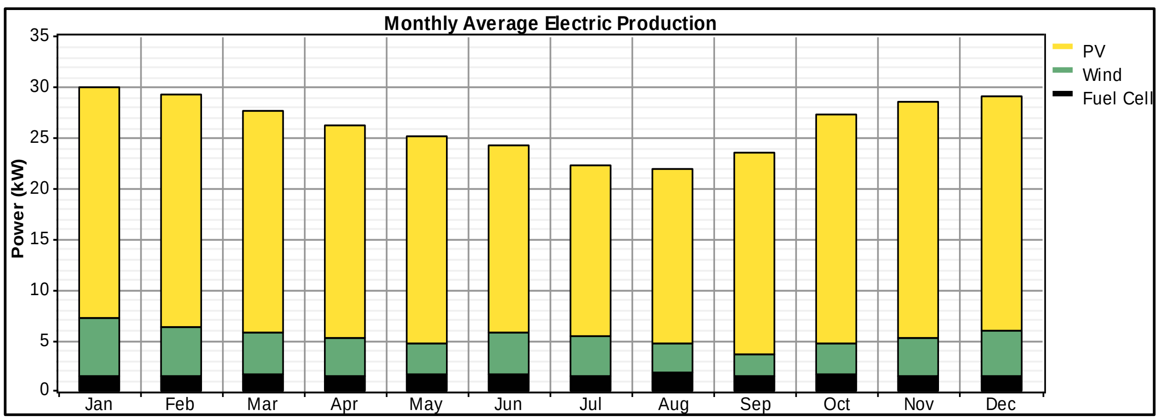

Figure 6-3 Monthly average electric production by the optimal hybrid PV-Wind-FC power units

6.1.4 Hydrogen Production by the Electrolyzer

The monthly average hydrogen production by the electrolyzer is given in figure 6-4 below. Recall that an electrolyzer converts the excess electricity in to hydrogen via by the electrolysis of water. As the simulation result reports that the total hydrogen production and total hydrogen consumption was found to be 684 kg/yr. and 670 kg/yr. respectively. Besides this, the hydrogen tank autonomy (expressed in hour) which is defined as the ratio of the energy capacity of the hydrogen tank to the electric load was reported as 32.

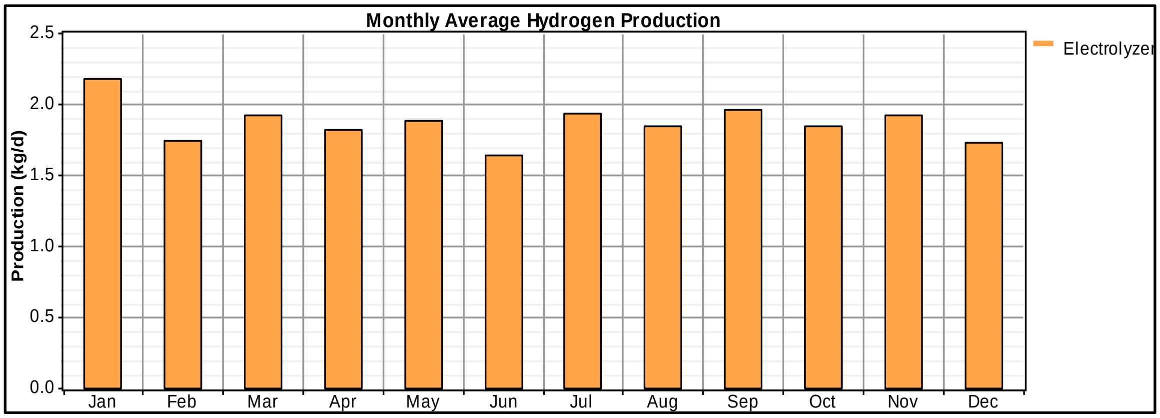

Figure 6-4 Monthly average hydrogen production by the electrolyzer

6.1.5 Sensitivity Analysis Result

Figure 6-5 shows sensitivity of the optimal system type under the imposed price variation of sensitive components. The PV capital cost multiplier on the Y axis and FC capital cost multiplier on the X axis are considered as sensitivity variables. In the graph, the total net present costs (NPCs) of the most cost effective systems are also displayed.

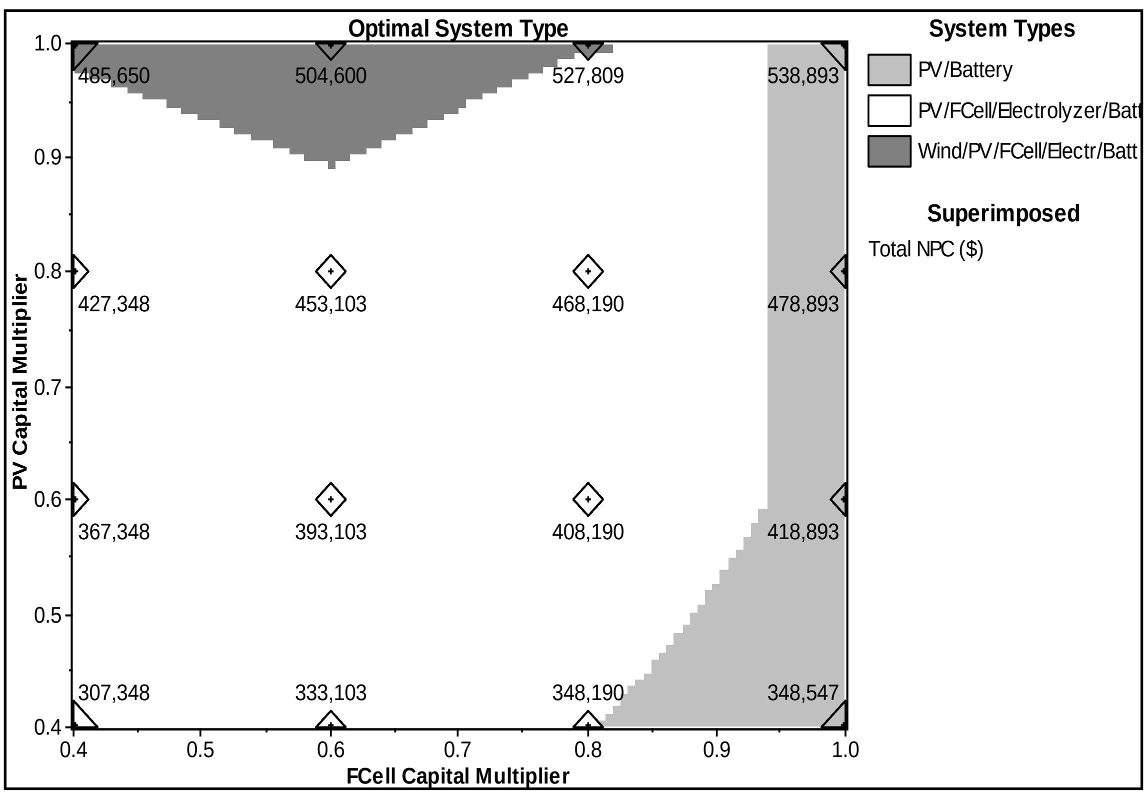

Figure 6-5 Sensitivity of the optimal system type for PV and FC capital multiplier variations

6.2 Dynamic Performance Simulation Results of the HPS

Figure 6-6 shows simulation of wind speed results at different heights above the surface of the earth. The first graph (the bottom one) is the wind speed of the site at 10 m above the ground. As the plot shows, the average value of this continuous signal is around 3 m/s and this is in line with the data obtained from NASA. Then, this result has to be estimated at the hub height of the selected wind turbine (in this case PGE 20/25). Hence, the graph which is in the middle shows the wind speed at 36 m (hub height of PGE 20/25). Finally, as the cut in wind speed of PGE 20/25 wind turbine is 4 m/s, wind speeds which are greater than and equal to 4 m/s have been filtered in order to estimate the power output of the wind turbine and the one which is in the top shows this.

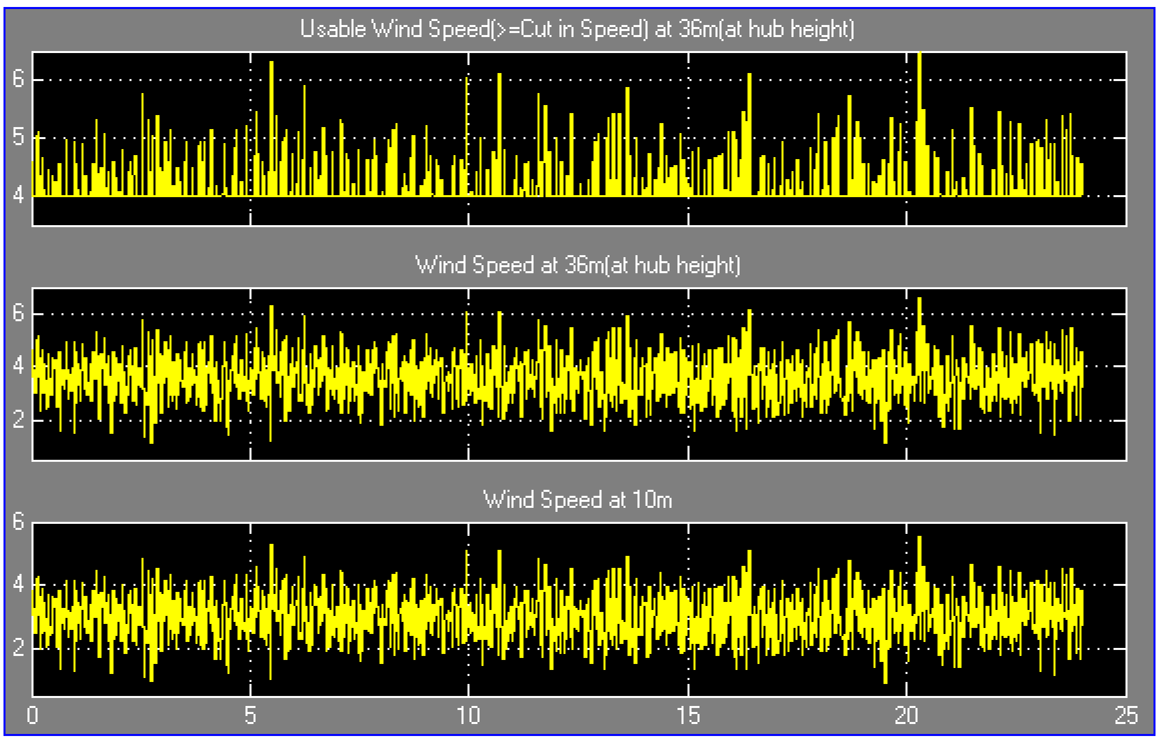

Figure 6-6 Wind speed simulation results of the study area at different heights

Figure 6-7 displays the power generated in a day by the PV and wind turbine. Moreover, it shows the comparison of power generated and power demand. When we come to the power production by the PV power unit, the peak power is generated at 12:00-noon (local 6:00). Then, it decreases in a resemblance of Gaussian trend curve to the afternoon and to the morning and finally becomes zero at the night. The power produced by the wind turbine is too intermittent and shows more dynamic nature compared to PV power output. The load curve has been imported from MATLAB workspace (see figure 4-1, pp. 49) for the comparison of power demand and supply (demand-supply). Accordingly, from 0:00 up to 5:00 and around 11:00 to 13:00 the net power is negative which indicates that supply is greater than demand and we expect the charging of the battery and/or turning ON of electrolyzer for hydrogen production. From 5:00 to 11:00 and 13:00 to 22:00 the net power is seen to be positive which implies that there is a shortage in this time and we expect the discharging of the battery and/or fuel cell operation.

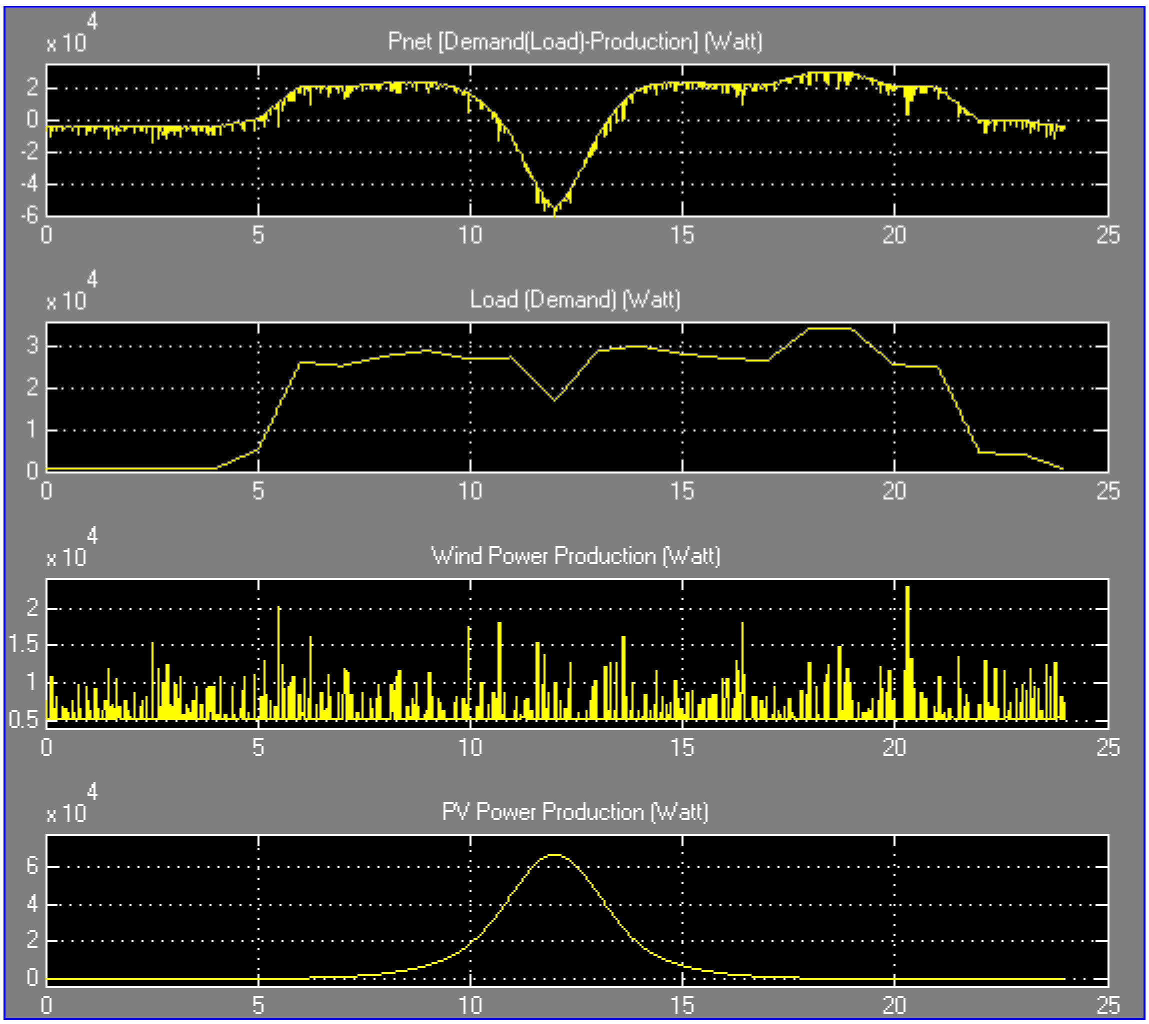

Figure 6-7 Power generated by the PV and wind turbine

Figure 6-8 contains plots of the battery dynamic responses over the 24 hour in a typical day. The battery terminal voltage is seen to be 120 V-DC. From time 0:00 to around 3:00

and from 11:00 to 13:00 the battery was charged as we expected before in fig. 6-7. During this time, the battery power and current are negative as we discussed so far while we are designing the overall control unit. From 5:00 to 11:00 and from 13:00 to 21:00 the battery was discharged. And during this time the battery power and current are positive (Recall the discussions presented in the overall control unit to answer "why?").

A reader can also relate the idea of battery charging and discharging process and passive sign convention. In simple words passive sign convention states that when power is absorbed by the system, power and current are negative and vice versa. Hence, if we consider the battery as a system, during charging process power is absorbed by the battery and the stored energy increases and that is why the current and power were seen to be negative. When the battery discharges, power is released from the battery and that is why the current and power were seen to be positive and the stored energy decreases.

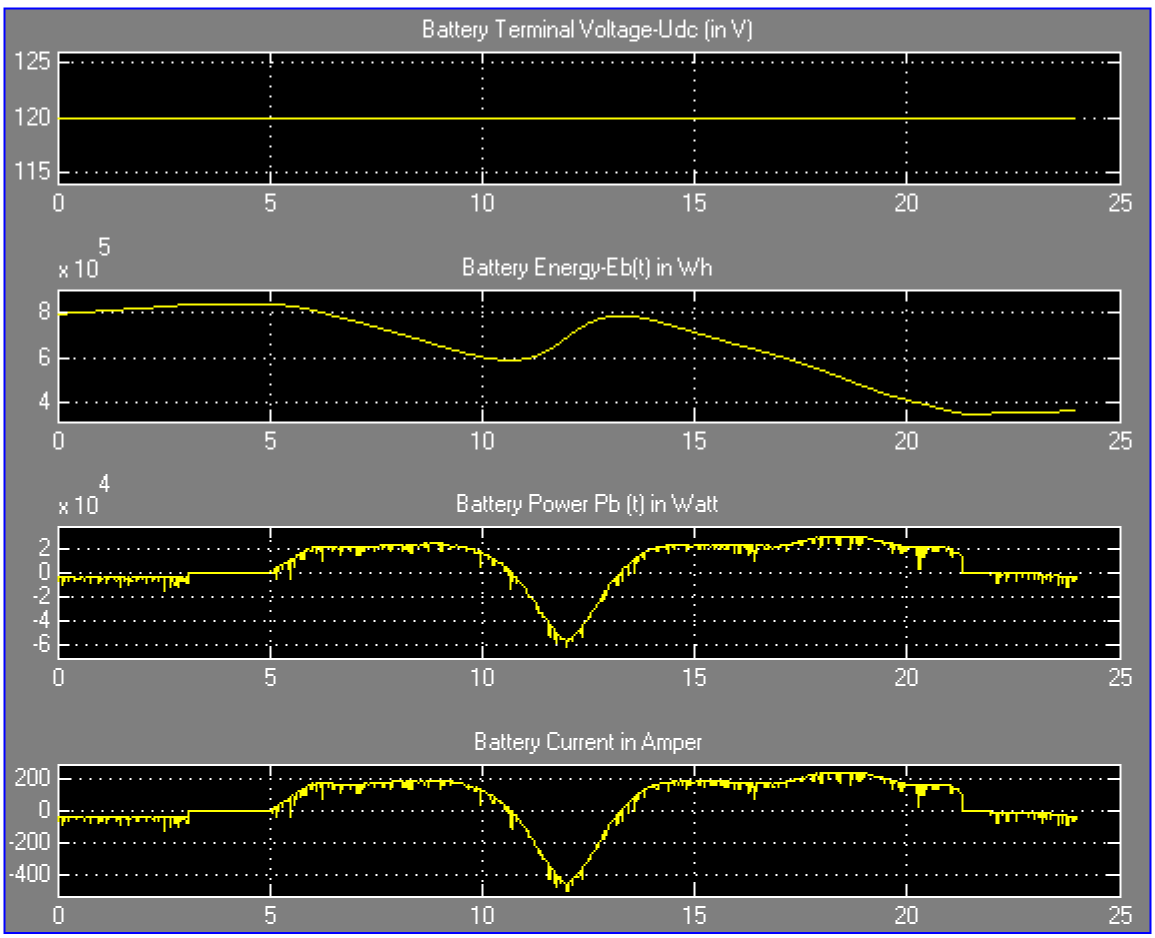

Figure 6-8 Battery dynamic responses over the 24 hour period

Figure 6-9 shows the hydrogen tank pressure variation, moles of hydrogen produced by the electrolyzer and electrolyzer input current over the 24 hour. The hydrogen gas is seen to be produced around 3:00 to 5:00. This is in agreement with the expectation that we have thought in fig. 6-7. Generally, the task of electrolyzer is to convert excess electricity in to hydrogen by the electrolysis of water and this will happen after the charging of the battery. That is, when there is excess electricity, battery charges first and if battery reaches to its peak energy storage and there is still excess electricity, battery will neither charges nor discharges (current and power becomes zero-see Figure 6-8) and hence, this excess electricity will be converted in to hydrogen gas and stored in to the tank for later use by the fuel cell. Therefore, the hydrogen tank pressure is also seen to increases which signifies that hydrogen gas is produced and interred in to the tank and get compressed!

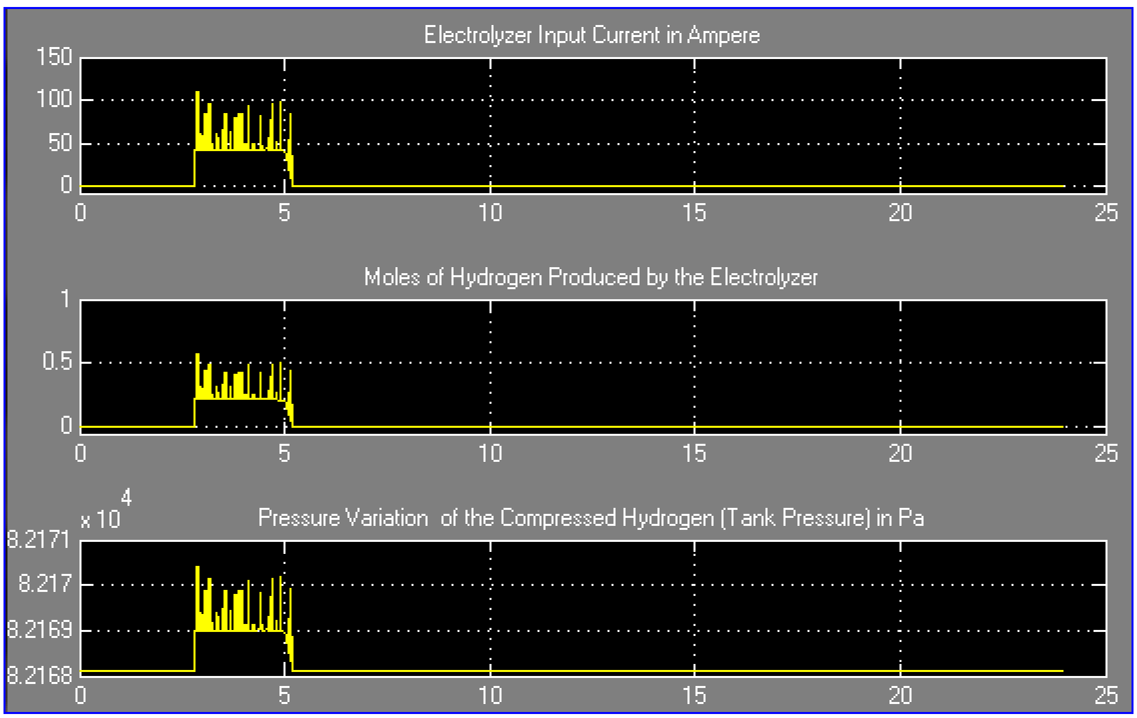

Figure 6-9 Tank pressure, hydrogen produced and electrolyzer input current

Figure 6-10 contains the graph plots of fuel cell power and its corresponding on/off signal. The fuel cell is seen to be operated around from 21:00 to 22:00 when the battery discharges to its minimum state of charge - 333120Wh is reached (energy is elapsed!). And during this time again the current and power of the battery is zero (see Figure 6-8) which indicates that the battery is neither charging nor discharging at this time.

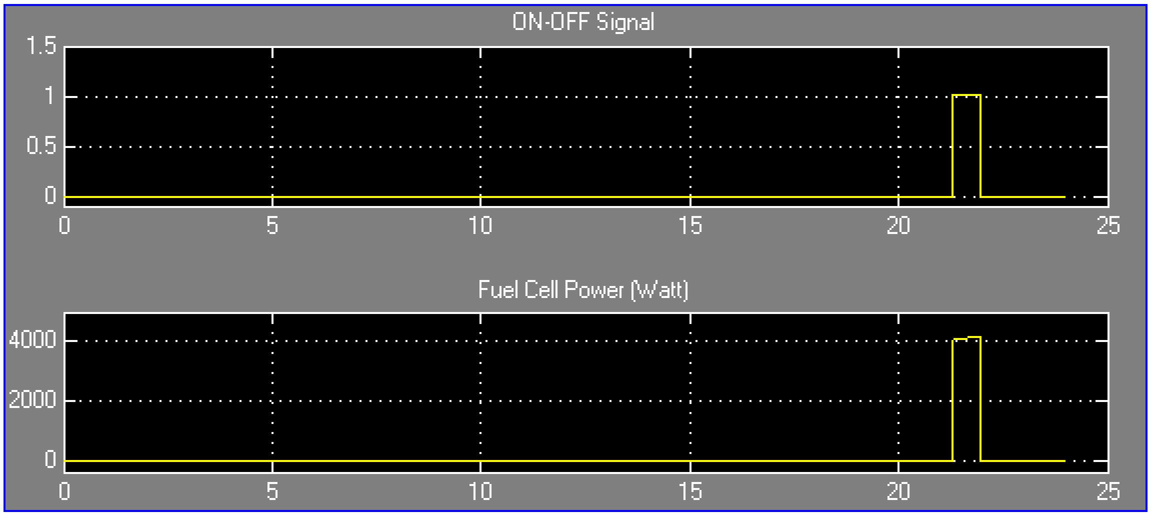

Figure 6-10 Fuel cell power and on/off signal

Figure 6-11 displays a sample on/off signals that were generated by the pulse generator used to control the solid state switching devices (IGBTs) of the inverter. From top to bottom the signals can be named as G_1, G_2, G_3, G_4, G_5 & G_6 that used to trigger/control/make on/off the IGBTs 1, 2, 3, 4, 5 & 6 respectively (Figure 4-33, pp. 76).

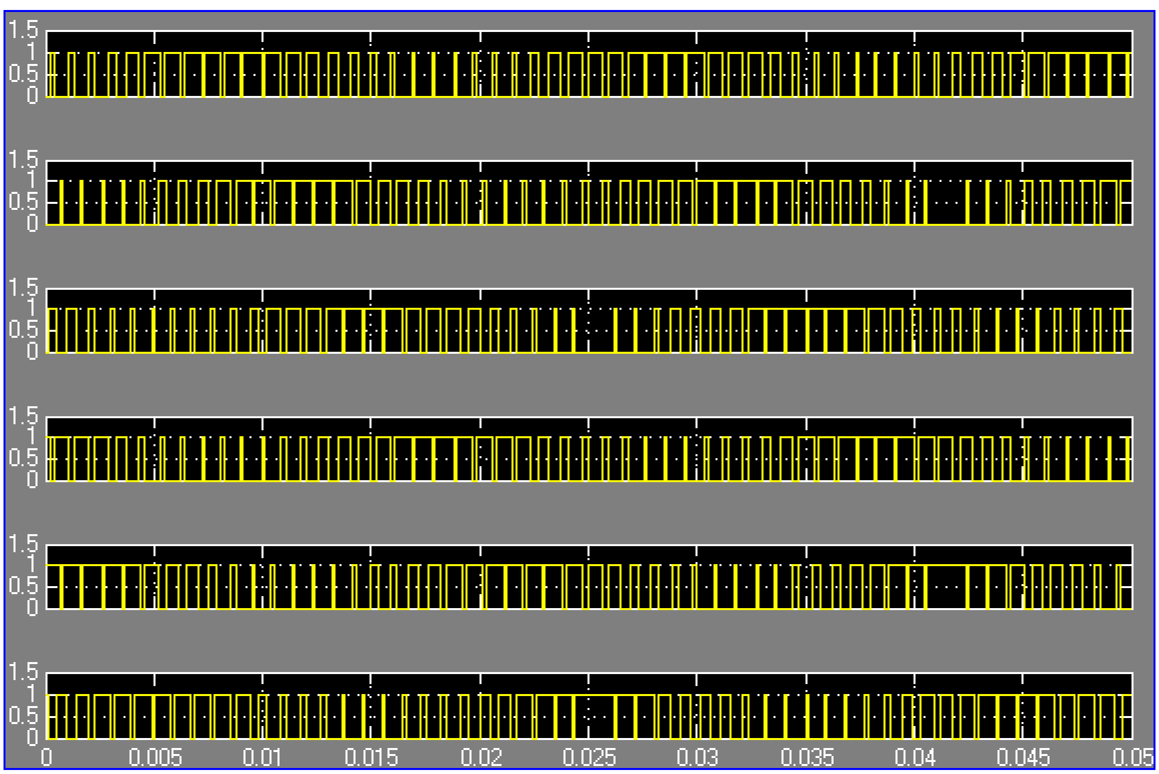

Figure 6-11 Sample on/off pulses to control solid state switching devices (IGBTs) of the inverter

Figure 6-12 displays the basic PWM output signals of the three phase inverter of the three phases. Clearly, phase a leads phase b and phase b in turn leads phase c.

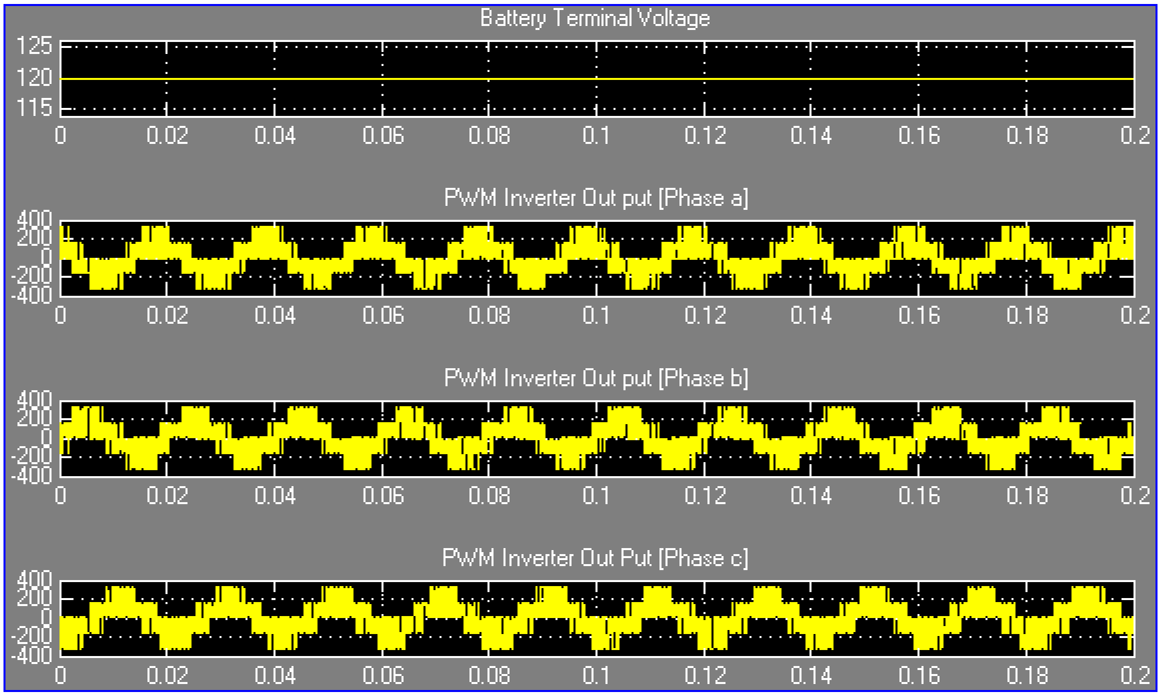

Figure 6-12 Inverter basic PWM output

Figure 6-13, figure 6-14 and figure 6-15 shows the fundamental component phase voltages of the three phase inverter outputs. Note that, the period (T) = 0.02 = 1/50 = 1/f.

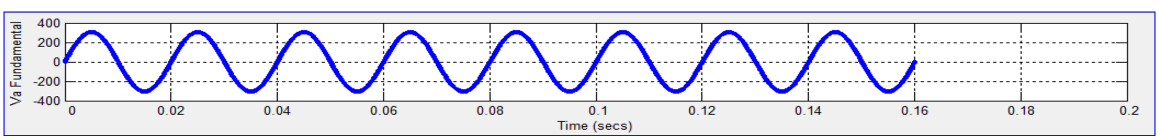

Figure 6-13 Phase a fundamental component of the inverter

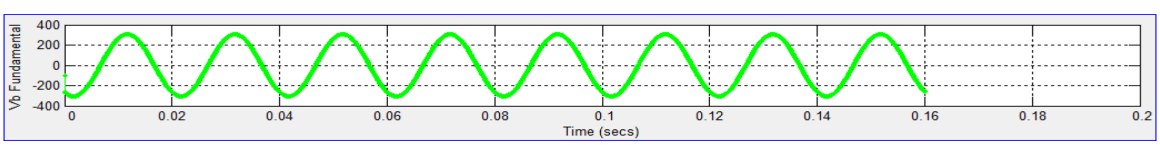

Figure 6-14 Phase b fundamental component of the inverter

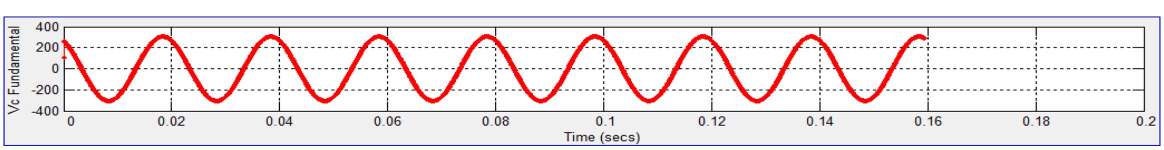

Figure 6-15 Phase c fundamental component of the inverter

Figure 6-16 is the three phase fundamental component voltage wave forms in one. Hence, one can clearly see that phase a (blue color) leads phase b (green color) and phase b intern leads phase c (red color).

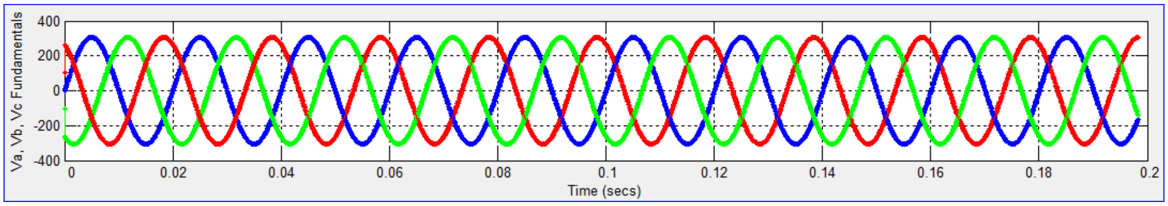

Figure 6-16 Fundamental components of phase a, b and c in one

6.3 Cost Comparison Result

Figure 6-17 displays the simulation result of cost comparison of the standalone system against grid extension. In the graph one can see the breakeven grid extension distance (the distance at which the cost of a standalone system and grid extension equates).

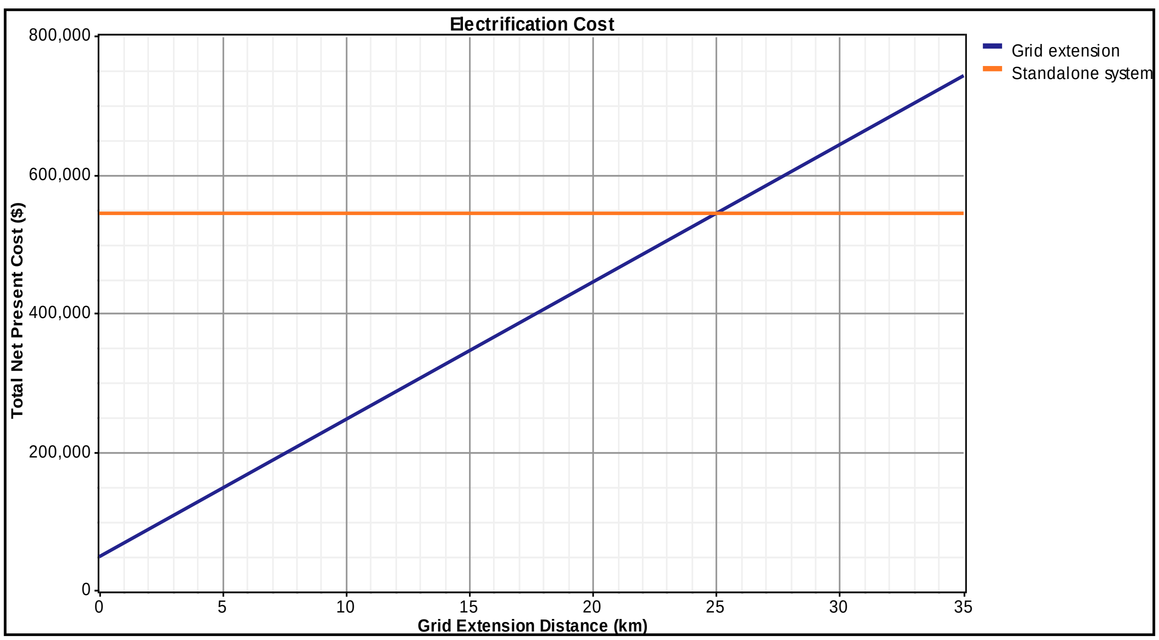

Figure 6-17 Cost comparison result of the hybrid system against grid extension

The simulation result shows that the breakeven grid extension distance to be 25.1 km. Figure 6-17 also shows this. Therefore, up to 25.1 kms extending the grid becomes cost effective and beyond 25.1 kms the standalone system is better.

CHAPTER SEVEN

7. CONCLUSIONS AND RECOMMENDATIONS

7.1 Conclusions

In this thesis work what has been done is first, after data collection and community load estimation, a techno-economic feasibility study (using HOMER) of a hybrid power system containing PV, wind and fuel cell power unit is studied. Then, with the optimized hybrid system, a MATLAB/Simulink model is developed to examine the dynamic responses of the designed power system over 24 hours of a typical day. Finally, grid extension from the closest substation has been designed for comparison of cost against the designed hybrid RES power system.

Regarding the potential of the resources, it is observed that, the wind energy potential of the site is of class 1 type according to the US Department of Energy (DOE) wind mapping. Such wind energy potential, although it may not be sufficient for a large independent wind farm; it is a viable preference if incorporated in to other energy conversion systems such as PV and others. The data sources for solar energy also confirmed the availability of huge potential of solar energy at the site.

The result of techno-economic feasibility study shows that there are numerous alternative feasible hybrid set-ups with 100 % contribution by the renewable resources and narrow range of COE (0.310 $/kWh to 0.328 $/kWh). Accordingly, the community electric demand can be satisfied by a hybrid system power source containing 110kW PV, one PGE 20/25 wind turbine, 40kW converter, 120 Surrette S6CS25P batteries, 5kW fuel cell, 25kW electrolyzer and 15kg hydrogen tank. This hybrid system needs $465,100 initial capital, $6,215 for operation & maintenance and $544,550 total NPC over the 25 life year horizon. With these economics, the COE of the selected hybrid system was found to be 0.313 $/kWh.

In terms of COE and renewable penetration, the result obtained in this study is comparable and even may be better than what previously studied PV-Wind-Genset hybrid set up showed. Moreover, due to Genset package, there is a considerably high level of emission to the atmosphere such as, CO_2, CO, unburned HC, SO_2, NO_X and particulate matter (smoke, soot, and liquid droplets) emitted per unit fuel consumed by the generator. Hence, hybrid PV-Wind-Fuel Cell power system can be considered as a good choice in this regard.

The result of the dynamic responses of the dynamic model that contains the optimal hybrid set-up shows that the overall power management strategy is effective and the load demand is balanced successfully. During shortage and surplus of electrical energy, the short-term primary back up (battery) and the long-term secondary back up (FC-Electrolyzer-Hydrogen Tank arrangement) were seen to operate with their proper sequence which is the indication of precise functioning of the designed controller algorism and its equivalent digital circuit model. Moreover, the perfect inverter output voltage waveforms obtained from the inversion of battery bank terminal DC bus voltage also authenticate that such a hybrid system can supply electric energy to the end users with the required voltage magnitude and frequency levels.

The grid extension design from the closest substation shows that the study area can be electrified by the investment cost of 8,681.22 $/km. This cost is shared in such a way that 65% goes to material cost, 20 % to construction, 5% to the transportation and 10 % to administration and control cost.

Hence, the attempt of electrifying Nifasso is determined by comparing the stand alone RES hybrid system against grid extension. Accordingly, the comparison result shows that the breakeven grid extension distance was found to be 25.1km.

Considering the fact that the study area is positioned below the breakeven grid extension distance (only 10km), current global electricity tariff and the tariff in the country (average 0.028 $/kWh) where the main source of electric energy is hydro-power supported by pilot geothermal plants and recently integrated wind farms of Adama and Ashegoda; the costs of the feasible set-ups obtained in this study are high, the COE is within the narrow range of 0.310 to 0.328 dollars per kilowatt hour and this is slightly worrisome. Therefore, in this regard, grid extension is preferable for the case study considered.

However, considering the shortage of power in the country in general and in rural areas in particular, rapid growth of gigantic industries in urban areas, its role in the protection of vegetation and forestry and therefore the prevention of soil degradation, the improvement to the quality of life of the many people residing in the countryside and the future situation regarding fossil fuel sources, the cost of the hybrid system should not be seen as a significant impairment. Besides, it should be emphasized that the cost of grid extension may have additional expenses, which are not considered in this study due to the immeasurability nature and the limitation of the scope of this research. As an example, it may be necessary to construct extensive civil works such as building bridges and gravel roads for concrete pole and transformer transportation which needs huge capital investment. However, the analysis result of installed capacity cost and O & M cost of grid extension can be applied to many similar areas in the country for far out from the reach of the grid system with a suitable road access.

7.2 Recommendations

The following recommendations can be considered based on this research work basic findings.

- ✍ Currently, in Ethiopia, the mandate of electrifying rural areas is in the shoulder of EEPCo under UEAP (**U**niversal **E**lectricity **A**ccess **P**rogram) department. And their work is focused on extending the national grid from closest substation and/or tapping from existing MV line. Hence, rather than simply extending the grid, the office has to conduct such a hybrid system techno-economic feasibility study first as an option of electrifying the rural areas. Then, if the hybrid system is optimal, grid extension has to be taken as a secondary option.

- ✍ A similar research work can be conducted for different rural villages in Ethiopia containing different renewable resources hybrid system in future. Moreover, the studies should have to contain not only a mere feasibility studies but also a dynamic modeling approaches of a hybrid system and grid extension comparison.

References

[1]. Abatcha H.G., Ahmad M.Y., Ladan M., 2011, Design and simulation of a hybrid PV/Fuel Cell Energy System, ISSN: 2141-4068.

[2]. Abd El-Aal A., 2005, Modeling and Simulation of a Photovoltaic-Fuel Cell Hybrid System, Ph.D. dissertation, Kassel, Germany.

[3]. Aldo V., 2005, *Fundamentals of Renewable Energy processes*, Elsevier Inc.

[4]. Amphlett J.C., 1996, A Model Predicting Transient Responses of Proton Exchange Membrane Fuel Cells, *Journal of Power Sources*, pp. 183-188.

[5]. Anthony J.P., 2005, *Guide to Electrical Power Distribution Systems*, 6th Edition.

[6]. Baalbergen J.F., 2007, System Design and Power Management of a Generator-set with Energy Storage for a 4Q Drive, M.Sc. Thesis in Electrical Power Engineering, Delft University of Technology.

[7]. Barbir F., Gomez T., 1997, Efficiency and Economics of Proton Exchange Membrane (PEM) Fuel Cells, *International Journal of Hydrogen Energy*, Vol. 22, No. 10/11, pp. 1027-1037.

[8]. Barry W., Williams D., 2006, *Power Electronic Devices, Drivers, Applications, and Passive Components.*

[9]. Becherif M., Paire D., Miraoui A., 2007, Energy Management of Solar Panel and Battery System with Passive Control, *International Conference on Clean Electrical Power*, pp. 14-19.

[10]. Bekele G., 2009, The Study In to the Potential and Feasibility of Standalone Solar-Wind Hybrid Electric Energy Supply System for Application in Ethiopia, KTH Royal Institute of Technology Doctoral Thesis, ISSN: 1102-0245, ISBN: 978-91-7415-329-3.

[11]. Boneya G.H., 2011, Design of a Photovoltaic-Wind Hybrid Power Generation System for Ethiopian Remote Area, Addis Ababa Institute of Technology Master Thesis.

[12]. Brouwer J., 1998, *Distributed Generation: The Power Paradigm for the New Millennium*.

[13]. Debnath D., Kumar A.C., Ray S., 2012, Optimization and Modeling of PV/ FC/Battery Hybrid Power Plant for Standalone Application, *International Journal of Engineering Research & Technology (IJERT)*, Vol. 1, Issue 3, ISSN : 2278-0181.

[14]. Duffie J.A., Beckman W.A., 1991, *Solar Engineering of Thermal Process*, 3rd edition, Wiley, New York.

[15]. EEPCo, Ethiopian Electric Power Corporation, 2013, *Supervision and commissioning manual for distribution network.*

[16]. Eroglu M., Kepoglu G., Sevencan S., Yazici S., 2009, A Stand-Alone Mobile House using PV/Wind/Fuel Cell Hybrid Power System, International Centre for

Hydrogen Energy Technologies (UNIDO-ICHET), *3rd world congress of young scientists on hydrogen energy systems.*

[17]. Esmaeili S., Shafiee M., 2012, Simulation of Dynamic Response of Small Wind Photovoltaic-Fuel Cell Hybrid Energy System, *Scientific research on Smart Grid and Renewable Energy*, pp. 194-203.

[18]. Forrai H.F., Yanagita Y., Kato Y., 2005, Fuel-Cell Parameter Estimation and Diagnostics, *IEEE Transactions on Energy Conversion*, ISSN: 668-675.

[19]. Fraile D., Latour M., Annett M., 2005, *Photovoltaic Energy*.

[20]. Gomatom P., Jewell W., 2003, Fuel Parameter and Quality Constraints for Fuel Cell Distributed Generators, *proceedings of the IEEE Transmission and Distribution Conference*, Wichita State University, Wichita. http://www.pserc.wisc.edu/ecow/get/publication/2003public/

[21]. Google, 2013, www.googleimage.com

[22]. Hirschenhofer J.H., Stauffer D.B., Engleman R.R., Klett M.G., 1999, *Fuel Cell Handbook*, 4th Edition, Federal Energy Technology Centre, P.O. Box 880,3610, Collins Ferry Road, Morgantown.

[23]. Hoogers G., 2003, *Fuel Cell Technology Handbook*, CRC presses LLC.http://www.lbst.de

[24]. Hottinen T., 2001, Technical Review and Economic Aspects of Hydrogen Storage Technologies, Helsinki University of Technology Master Thesis, Department of Engineering Physics and Mathematics, Espoo.

[25]. Hussein K.H., Muta I., Hoshino T., Osakada M., 2005, Maximum Photovoltaic Power Tracking: An Algorithm for Rapidly Changing Atmospheric Conditions, *IEEE Proceedings of Generation, Transmission and Distribution*, Vol. 142, No. 1, pp. 953-959.

[26]. IRENA, 2012, Renewable Power Generation Costs.

[27]. Krykunov O., 2007, Comparison of the DC/DC Converters for Fuel Cell Applications, *International Journal of Electrical, Computer, and Systems Engineering*, pp. 71-79.

[28]. Leake E.W., 2010, Genset-Solar-Wind Hybrid Power System of Off Grid Power Station for Rural Applications, Delft University of Technology Master Thesis, Delft-The Netherlands.

[29]. Linden D., Reddy T.B., 2002, *Handbook of Batteries*, 3rd edition, McGraw-Hill Education, New York, ISBN: 978-0-07-135978-8.

[30]. Mahalakshmi M., Latha S., 2012, Modeling, Simulation and Sizing of Photovoltaic/Wind/Fuel Cell Hybrid Generation System, *International Journal of Engineering Science and Technology (IJEST)*, Vol. 4, No. 05, ISSN: 0975-5462.

[31]. Mina T., Abu W.D., Wahab K., 2005, Performance Assessment of Fuel Cell Based Energy System, American University of Beirut.

[32]. Ming L., 2005, Dynamic Model of Proton Exchange Membrane Fuel Cell and Implementation.

[33]. Möller C., Lucks R., 2000, Seminar: Fuel Cells, Technology Faculty, University of Kiel, Germany. http://www.texnic.de/FC/

[34]. Mukund R.P., 1999, *Wind and Solar Power Systems*, Kings Point, CRC Press LLC, New York, ISBN: 0-8493-1605-7.

[35]. NASA,2012,http://eosweb.larc.nasa.gov/cgibin/sse/retscreen.cgi?email=rets%40nrcan.gc.ca&step=1&lat= 9.9777892&lon=39.8342339&submit=Submit

[36]. NREL, 2012, Cost and Performance Data for Power Generation Technologies, Black and Veatch Holding Company.

[37]. Outeiro M.T, Carvalho A., 2011, Matlab/Simulink as Design Tool of PEM Fuel Cells as Electrical Generation Systems, *European Fuel Cell Forum*, Lucerne, Switzerland.

[38]. Outeiro M.T., Chibante R., Carvalho A.S., Almeida A.T., 2008, A Parameter Optimized Model of a PEM Fuel Cell Including Temperature Effects, *Journal of Power Sources*.

[39]. Park S.J., Kang B.B., Yoon J.P., Cha I.S., Lim J.Y. , 2004, A Study on the Stand-Alone Operation of Photovoltaic-Wind Power Hybrid Generation System, *35^th^ Annual IEEE Power Electronics Specialists Conference*, Aachen, Germany, pp. 2095 - 2099, ISBN: 0-7803-8399-0.

[40]. Patil N., Mukind R., 1999, *Wind and Solar Power Systems*, CRC pres LLC, USA

[41]. Rani C., Sriganesh S., Muralikrishnan B., 2011, Dynamic Modeling and Control of a Wind Turbine Generator with Fuel Cell, Ultra Capacitor Stack as an Auxiliary Storage, *International Journal of Power System Operation and Energy Management (IJPSOEM)*, Vol. 1, Issue 1.

[42]. Rashid M., 2004, *Power Electronics Circuits, Devices and Applications*, 3rd edition, Pearson Prentice Hall, ISBN: 0-13-122815-3.

[43]. Recayi P., Salim M.D., Timmerman M., 2000, A Hybrid Solar-Wind Power Generation System as an Instructional Resource for Industrial Technology Students, *Electronic Publication of the National Association of Industrial Technology, Journal of Industrial Technology*, Vol. 16, No. 3.

[44]. Sen R., 2011, Off Grid Electricity Generation with Renewable Energy Technologies in India; An application of HOMER, M.Sc. Thesis in Renewable Energy & Environmental Modeling, University of Dundee, India.

[45]. Sobotka K., 2009, A Wind Power-Fuel Cell Hybrid System Study, Master Thesis at the School of Renewable Energy Science, University of Iceland.

[46]. SWERA, 2012, http://en.openei.org/apps/SWERA/

[47]. Tadesse G., 2011, Feasibility Study of Small Hydro/PV/Wind Hybrid System for Off-Grid Rural Electrification in Ethiopia, Addis Ababa Institute of Technology Master Thesis.

[48]. Tamrat B., 2007, Comparative Analysis of Feasibility of Solar PV, Wind and Micro Hydropower Generation for Rural Electrification in the Selected Sites of Ethiopia, Addis Ababa Institute of Technology Master Thesis.

[49]. The Micropower Optimization Software, Ver. 2.68 beta, http://homerenergy.com/

[50]. Tsai H.L., Tu C.S., and Su Y.J., 2008, Development of Generalized Photovoltaic Model Using Matlab/Simulink, *Proceedings of the World Congress on Engineering and Computer Science* (WCECS), San Francisco, USA.

[51]. Twidell J., Weir T., 2006, *Renewable Energy Resources*, 2nd edition, Taylor & Francis, London.

[52]. Ulleberg O., 1998, Standalone Power Systems for the Future: Optimal Design, Operation & Control of Solar-Hydrogen Energy Systems, Ph.D. dissertation, Norwegian University, Trondheim.

[53]. USAID, 2005, *Powering Health: Electrification Options for Rural Health Centers*.

[54]. Wang C., 2006, Modeling and Control of Hybrid Wind/Photovoltaic/Fuel Cell Distributed Generation Systems, Montana State University Doctoral Thesis, Bozeman, Montana.

[55]. Wang C., Hashem M., 2008, Power Management of a Stand-Alone Wind/Photovoltaic/Fuel Cell Energy System, *IEEE transactions on energy conversion*, Vol. 23, No. 3.

[56]. Wikipedia, Dec. 2013, http://en.wikipedia.org/wiki/Electricity_pricing

[57]. Wurster R., 1999, *PEM Fuel Cells in Stationary and Mobile Applications-Commercialization*, Ludwig Bölkow System Technique-GmbH, Daimlerstrasse 15, Ottobrunn.

Appendix A: Over All Optimization Results

PV (kW)	PGE25	FCell (kW)	S6CS25P	Conv. (kW)	Elec. (kW)	H2 Tank (kg)	Disp. Strgy	Initial Capital	Operating Cost ($/yr)	Total NPC	COE ($/kWh)	Ren. Frac.	Capacity Shortage	FCell (hrs)
150			160	40			CC	$ 464,800	5,796	$ 538,893	0.310	1.00	0.01	
150			160	40			LF	$ 464,800	5,796	$ 538,893	0.310	1.00	0.01	
150		10	100	40	30	10	LF	$ 486,500	4,436	$ 543,207	0.313	1.00	0.01	2,057
150		5	120	40	20	10	LF	$ 478,600	5,087	$ 543,624	0.312	1.00	0.01	2,939
110	1	5	120	40	25	15	LF	$ 465,100	6,215	$ 544,550	0.313	1.00	0.01	2,731
150		10	100	40	25	15	LF	$ 488,000	4,469	$ 545,128	0.314	1.00	0.01	2,072
150		5	120	40	15	15	LF	$ 480,100	5,091	$ 545,175	0.314	1.00	0.01	2,844
150			160	40		5	CC	$ 471,300	5,846	$ 546,032	0.314	1.00	0.01	
150			160	40		5	LF	$ 471,300	5,846	$ 546,032	0.314	1.00	0.01	
150		5	120	40	30	5	LF	$ 482,100	5,064	$ 546,832	0.315	1.00	0.01	2,836
150			160	50			CC	$ 471,800	5,982	$ 548,270	0.316	1.00	0.01	
150			160	50			LF	$ 471,800	5,982	$ 548,270	0.316	1.00	0.01	
150		5	140	40	10	5	LF	$ 479,200	5,462	$ 549,019	0.316	1.00	0.01	2,271
150		5	120	40	25	10	LF	$ 483,600	5,124	$ 549,097	0.315	1.00	0.01	2,994
110	1	5	120	40	30	15	LF	$ 470,100	6,246	$ 549,951	0.316	1.00	0.01	2,759
150		10	100	40	30	15	LF	$ 493,000	4,516	$ 550,727	0.316	1.00	0.01	2,114
150		5	120	40	20	15	LF	$ 485,100	5,148	$ 550,903	0.316	1.00	0.01	2,989
110	1	5	120	40	25	20	LF	$ 471,600	6,275	$ 551,814	0.317	1.00	0.01	2,774
150		5	120	40	15	20	LF	$ 486,600	5,146	$ 552,379	0.318	1.00	0.01	2,867
150		10	100	40	25	20	LF	$ 494,500	4,528	$ 552,380	0.318	1.00	0.01	2,089
150		10	100	50	30	10	LF	$ 493,500	4,622	$ 552,585	0.318	1.00	0.01	2,057
150		5	120	50	20	10	LF	$ 485,600	5,273	$ 553,001	0.318	1.00	0.01	2,939
110	1		180	40			CC	$ 456,900	7,528	$ 553,128	0.318	1.00	0.01	
110	1		180	40			LF	$ 456,900	7,528	$ 553,128	0.318	1.00	0.01	
150			160	40		10	CC	$ 477,800	5,896	$ 553,171	0.319	1.00	0.01	
150			160	40		10	LF	$ 477,800	5,896	$ 553,171	0.319	1.00	0.01	
150			160	40		10	CC	$ 477,800	5,896	$ 553,171	0.319	1.00	0.01	
150			160	40		10	LF	$ 477,800	5,896	$ 553,171	0.319	1.00	0.01	
110	1	5	120	40	20	25	LF	$ 473,100	6,284	$ 553,426	0.319	1.00	0.01	2,703
110	1	5	120	50	25	15	LF	$ 472,100	6,401	$ 553,927	0.319	1.00	0.01	2,731
150		5	120	40	30	10	LF	$ 488,600	5,151	$ 554,450	0.318	1.00	0.01	3,006
150		10	100	50	25	15	LF	$ 495,000	4,655	$ 554,505	0.319	1.00	0.01	2,072
110	1	5	140	40	25	5	LF	$ 469,200	6,674	$ 554,515	0.319	1.00	0.01	2,422
150		5	120	50	15	15	LF	$ 487,100	5,277	$ 554,552	0.319	1.00	0.01	2,844
150		10	120	40	25	5	LF	$ 492,100	4,886	$ 554,555	0.319	1.00	0.01	1,858
150			160	50		5	CC	$ 478,300	6,032	$ 555,409	0.320	1.00	0.01	
150			160	50		5	LF	$ 478,300	6,032	$ 555,409	0.320	1.00	0.01	
150		5	140	40	15	5	LF	$ 484,200	5,586	$ 555,612	0.319	1.00	0.01	2,686
150	1	5	80	40	15	10	LF	$ 494,400	4,826	$ 556,086	0.320	1.00	0.01	2,616
150		5	140	40	10	10	LF	$ 485,700	5,512	$ 556,158	0.320	1.00	0.01	2,271
150		5	120	40	25	10	CC	$ 483,600	5,678	$ 556,189	0.320	1.00	0.01	5,136
150		5	120	50	30	5	LF	$ 489,100	5,250	$ 556,209	0.320	1.00	0.01	2,836
150		5	120	40	25	15	LF	$ 490,100	5,181	$ 556,336	0.319	1.00	0.01	3,030
110	1	5	140	40	20	10	LF	$ 470,700	6,733	$ 556,766	0.320	1.00	0.01	2,563
150		10	120	40	20	10	LF	$ 493,600	4,948	$ 556,848	0.321	1.00	0.01	1,926
150		5	160	40	5		CC	$ 484,800	5,643	$ 556,941	0.321	1.00	0.01	0
150		5	160	40	5		LF	$ 484,800	5,643	$ 556,941	0.321	1.00	0.01	0
110	1	5	120	40	30	20	LF	$ 476,600	6,307	$ 557,225	0.320	1.00	0.01	2,806
150		5	140	40	15	5	CC	$ 484,200	5,717	$ 557,289	0.321	1.00	0.01	3,263
150		15	100	40	30	10	LF	$ 501,500	4,373	$ 557,404	0.321	1.00	0.01	1,804
150	1		120	40			CC	$ 485,600	5,633	$ 557,609	0.321	1.00	0.01	
150	1		120	40			LF	$ 485,600	5,633	$ 557,609	0.321	1.00	0.01	
150		10	120	40	25	5	CC	$ 492,100	5,141	$ 557,821	0.321	1.00	0.01	2,349
150		10	100	40	30	20	LF	$ 499,500	4,583	$ 558,084	0.320	1.00	0.01	2,147
150		5	120	40	20	20	LF	$ 491,600	5,203	$ 558,111	0.320	1.00	0.01	3,014
110	1	10	80	40	50	30	LF	$ 490,400	5,302	$ 558,174	0.321	1.00	0.01	2,246
150		5	140	50	10	5	LF	$ 486,200	5,648	$ 558,396	0.322	1.00	0.01	2,271
150		5	120	50	25	10	LF	$ 490,600	5,310	$ 558,474	0.321	1.00	0.01	2,994
110	1	5	120	40	25	25	LF	$ 478,100	6,330	$ 559,016	0.321	1.00	0.01	2,796
110	1	5	120	50	30	15	LF	$ 477,100	6,432	$ 559,328	0.321	1.00	0.01	2,759

150		10	100	40	25	25	LF	$ 501,000	4,583	$ 559,586	0.322	1.00	0.01	2,099
150		5	120	40	15	25	LF	$ 493,100	5,201	$ 559,587	0.322	1.00	0.01	2,891
110	1	5	140	40	30	5	LF	$ 474,200	6,703	$ 559,885	0.322	1.00	0.01	2,438
150		10	120	40	30	5	LF	$ 497,100	4,922	$ 560,015	0.322	1.00	0.01	1,878
150		10	100	50	30	15	LF	$ 500,000	4,702	$ 560,104	0.322	1.00	0.01	2,114
110	1		180	40		5	CC	$ 463,400	7,578	$ 560,267	0.322	1.00	0.01	
110	1		180	40		5	LF	$ 463,400	7,578	$ 560,267	0.322	1.00	0.01	
150		5	120	50	20	15	LF	$ 492,100	5,333	$ 560,280	0.322	1.00	0.01	2,989
150			160	40		15	CC	$ 484,300	5,946	$ 560,310	0.323	1.00	0.01	
150			160	40		15	LF	$ 484,300	5,946	$ 560,310	0.323	1.00	0.01	
150		10	140	40	10	5	LF	$ 494,200	5,181	$ 560,425	0.323	1.00	0.01	1,132
150		10	140	40	10	5	CC	$ 494,200	5,183	$ 560,459	0.323	1.00	0.01	1,143
110	1	5	120	40	20	30	LF	$ 479,600	6,340	$ 560,650	0.323	1.00	0.01	2,732
110	1	10	100	40	50	15	LF	$ 488,000	5,689	$ 560,720	0.323	1.00	0.01	2,062
150		5	140	40	20	5	LF	$ 489,200	5,630	$ 561,170	0.322	1.00	0.01	2,768
110	1	5	120	50	25	20	LF	$ 478,600	6,461	$ 561,191	0.323	1.00	0.01	2,774
150		5	100	40	50	10	CC	$ 491,500	5,461	$ 561,313	0.323	1.00	0.01	6,246
150	1	5	80	40	20	10	LF	$ 499,400	4,851	$ 561,406	0.323	1.00	0.01	2,616
150		5	120	40	30	15	LF	$ 495,100	5,206	$ 561,655	0.322	1.00	0.01	3,030
150		5	120	50	15	20	LF	$ 493,600	5,332	$ 561,756	0.323	1.00	0.01	2,867
150		10	100	50	25	20	LF	$ 501,500	4,714	$ 561,757	0.323	1.00	0.01	2,089
110	1	5	160	40	10	5	LF	$ 471,300	7,082	$ 561,830	0.323	1.00	0.01	1,847
110	1	5	160	40	10	5	CC	$ 471,300	7,083	$ 561,844	0.323	1.00	0.01	1,851
150		5	120	40	30	10	CC	$ 488,600	5,752	$ 562,128	0.323	1.00	0.01	5,313
100	2	10	80	40	30	15	LF	$ 485,900	5,965	$ 562,154	0.324	1.00	0.01	1,890
150		15	80	40	50	15	LF	$ 510,900	4,012	$ 562,190	0.323	1.00	0.01	1,951
150		5	160	40	10		CC	$ 489,800	5,668	$ 562,260	0.324	1.00	0.01	0
150		5	160	40	10		LF	$ 489,800	5,668	$ 562,260	0.324	1.00	0.01	0
110	1	5	140	40	25	10	LF	$ 475,700	6,772	$ 562,265	0.323	1.00	0.01	2,623
110	1		180	50			CC	$ 463,900	7,714	$ 562,505	0.324	1.00	0.01	
110	1		180	50			LF	$ 463,900	7,714	$ 562,505	0.324	1.00	0.01	
150			160	50		10	CC	$ 484,800	6,082	$ 562,548	0.324	1.00	0.01	
150			160	50		10	LF	$ 484,800	6,082	$ 562,548	0.324	1.00	0.01	
100	2	5	100	40	20	15	LF	$ 478,000	6,620	$ 562,624	0.324	1.00	0.01	2,564
150		10	120	40	25	10	LF	$ 498,600	5,013	$ 562,682	0.323	1.00	0.01	2,001
110	1	5	120	50	20	25	LF	$ 480,100	6,470	$ 562,804	0.324	1.00	0.01	2,703
150		5	140	40	15	10	LF	$ 490,700	5,657	$ 563,013	0.323	1.00	0.01	2,776
150		5	140	40	10	15	LF	$ 492,200	5,562	$ 563,297	0.324	1.00	0.01	2,271
150	1	5	80	40	15	15	LF	$ 500,900	4,882	$ 563,303	0.324	1.00	0.01	2,642
150		5	120	40	25	20	LF	$ 496,600	5,236	$ 563,533	0.323	1.00	0.01	3,051
150		10	120	40	30	5	CC	$ 497,100	5,202	$ 563,597	0.325	1.00	0.01	2,422
150		5	120	40	25	15	CC	$ 490,100	5,767	$ 563,826	0.324	1.00	0.01	5,278
150		5	120	50	30	10	LF	$ 495,600	5,337	$ 563,827	0.324	1.00	0.01	3,006
110	1	5	140	50	25	5	LF	$ 476,200	6,860	$ 563,893	0.325	1.00	0.01	2,422
150		10	120	50	25	5	LF	$ 499,100	5,072	$ 563,932	0.325	1.00	0.01	1,858
110	1	5	120	40	50	10	LF	$ 483,600	6,284	$ 563,932	0.325	1.00	0.01	2,705
110	1	5	140	40	20	15	LF	$ 477,200	6,792	$ 564,025	0.324	1.00	0.01	2,603
110	1	10	120	40	30	15	LF	$ 485,100	6,175	$ 564,032	0.324	1.00	0.01	1,976
150			180	40			CC	$ 481,900	6,428	$ 564,066	0.324	1.00	0.01	
150			180	40			LF	$ 481,900	6,428	$ 564,066	0.324	1.00	0.01	
100	2	10	80	40	25	20	LF	$ 487,400	6,006	$ 564,175	0.324	1.00	0.01	1,919
150		10	120	40	20	15	LF	$ 500,100	5,016	$ 564,215	0.325	1.00	0.01	1,959
110	1	5	140	40	25	10	CC	$ 475,700	6,929	$ 564,273	0.325	1.00	0.01	3,302
150		5	140	40	20	5	CC	$ 489,200	5,875	$ 564,306	0.324	1.00	0.01	3,739
100	2	5	100	40	15	20	LF	$ 479,500	6,636	$ 564,335	0.325	1.00	0.01	2,528
110	1	5	120	40	30	25	LF	$ 483,100	6,357	$ 564,367	0.324	1.00	0.01	2,807
150		10	100	40	50	10	LF	$ 506,500	4,550	$ 564,660	0.325	1.00	0.01	2,083
150	1		120	40		5	CC	$ 492,100	5,683	$ 564,748	0.325	1.00	0.01	
150	1		120	40		5	LF	$ 492,100	5,683	$ 564,748	0.325	1.00	0.01	
150		5	140	40	15	10	CC	$ 490,700	5,800	$ 564,839	0.325	1.00	0.01	3,375
150		15	100	40	30	15	LF	$ 508,000	4,456	$ 564,968	0.325	1.00	0.01	1,844
150		5	140	50	15	5	LF	$ 491,200	5,772	$ 564,989	0.325	1.00	0.01	2,686
150		10	100	40	30	25	LF	$ 506,000	4,640	$ 565,309	0.324	1.00	0.01	2,160
150		5	120	40	20	25	LF	$ 498,100	5,259	$ 565,328	0.324	1.00	0.01	3,042
150	1	5	80	50	15	10	LF	$ 501,400	5,011	$ 565,463	0.325	1.00	0.01	2,616

150		5	140	50	10	10	LF	$ 492,700	5,698	$ 565,535	0.326	1.00	0.01	2,271
150		5	120	50	25	10	CC	$ 490,600	5,864	$ 565,566	0.326	1.00	0.01	5,136
150		5	120	50	25	15	LF	$ 497,100	5,367	$ 565,713	0.325	1.00	0.01	3,030
150		5	160	40	5	5	LF	$ 491,300	5,827	$ 565,786	0.325	1.00	0.01	1,114
150		5	160	40	5	5	CC	$ 491,300	5,829	$ 565,809	0.325	1.00	0.01	1,128
110	1	5	140	50	20	10	LF	$ 477,700	6,919	$ 566,143	0.326	1.00	0.01	2,563
110	1	5	120	40	25	30	LF	$ 484,600	6,382	$ 566,187	0.325	1.00	0.01	2,807
150		10	120	50	20	10	LF	$ 500,600	5,134	$ 566,226	0.326	1.00	0.01	1,926
150		5	160	50	5		CC	$ 491,800	5,829	$ 566,318	0.326	1.00	0.01	0
150		5	160	50	5		LF	$ 491,800	5,829	$ 566,318	0.326	1.00	0.01	0
150		10	120	40	25	10	CC	$ 498,600	5,302	$ 566,381	0.326	1.00	0.01	2,580
150		5	140	40	25	5	LF	$ 494,200	5,661	$ 566,571	0.325	1.00	0.01	2,796
110	1	5	120	50	30	20	LF	$ 483,600	6,493	$ 566,603	0.325	1.00	0.01	2,806
150		5	140	50	15	5	CC	$ 491,200	5,903	$ 566,666	0.326	1.00	0.01	3,263
150	1	5	80	40	25	10	LF	$ 504,400	4,876	$ 566,725	0.326	1.00	0.01	2,616
150		15	100	50	30	10	LF	$ 508,500	4,559	$ 566,782	0.327	1.00	0.01	1,804
150		5	120	40	15	30	LF	$ 499,600	5,256	$ 566,791	0.326	1.00	0.01	2,914
150		10	100	40	25	30	LF	$ 507,500	4,639	$ 566,798	0.326	1.00	0.01	2,110
150	1		120	50			CC	$ 492,600	5,819	$ 566,986	0.326	1.00	0.01	
150	1		120	50			LF	$ 492,600	5,819	$ 566,986	0.326	1.00	0.01	
150		10	120	50	25	5	CC	$ 499,100	5,327	$ 567,198	0.327	1.00	0.01	2,349
110	1		180	40		10	CC	$ 469,900	7,628	$ 567,406	0.326	1.00	0.01	
110	1		180	40		10	LF	$ 469,900	7,628	$ 567,406	0.326	1.00	0.01	
150		10	140	40	15	5	LF	$ 499,200	5,339	$ 567,449	0.326	1.00	0.01	1,630
150			160	40		20	CC	$ 490,800	5,996	$ 567,450	0.327	1.00	0.01	
150			160	40		20	LF	$ 490,800	5,996	$ 567,450	0.327	1.00	0.01	
150		10	100	50	30	20	LF	$ 506,500	4,769	$ 567,461	0.326	1.00	0.01	2,147
150		5	120	50	20	20	LF	$ 498,600	5,389	$ 567,488	0.326	1.00	0.01	3,014
110	1	10	80	50	50	30	LF	$ 497,400	5,488	$ 567,551	0.326	1.00	0.01	2,246
150		10	140	40	10	10	LF	$ 500,700	5,231	$ 567,564	0.327	1.00	0.01	1,132
150		5	160	40	15		CC	$ 494,800	5,693	$ 567,580	0.327	1.00	0.01	0
150		5	160	40	15		LF	$ 494,800	5,693	$ 567,580	0.327	1.00	0.01	0
150		10	140	40	10	10	CC	$ 500,700	5,233	$ 567,599	0.327	1.00	0.01	1,143
110	1	5	140	40	30	10	LF	$ 480,700	6,802	$ 567,653	0.326	1.00	0.01	2,646
150		10	140	40	15	5	CC	$ 499,200	5,361	$ 567,727	0.327	1.00	0.01	1,668
150		15	120	40	25	5	LF	$ 507,100	4,746	$ 567,769	0.327	1.00	0.01	1,573
150	1	10	80	40	20	5	LF	$ 507,900	4,688	$ 567,825	0.327	1.00	0.01	1,840
100	2	5	100	40	25	15	LF	$ 483,000	6,647	$ 567,974	0.327	1.00	0.01	2,574
150		5	120	40	50	5	LF	$ 502,100	5,166	$ 568,142	0.327	1.00	0.01	2,847
150		15	120	40	25	5	CC	$ 507,100	4,776	$ 568,153	0.327	1.00	0.01	1,623
150	1	5	100	40	10	5	LF	$ 500,000	5,334	$ 568,189	0.326	1.00	0.01	2,415
110	1	10	100	40	50	20	LF	$ 494,500	5,765	$ 568,200	0.327	1.00	0.01	2,113
150		10	120	40	30	10	LF	$ 503,600	5,057	$ 568,239	0.326	1.00	0.01	2,036
110	1	5	120	50	25	25	LF	$ 485,100	6,516	$ 568,393	0.326	1.00	0.01	2,796
110	1	5	160	40	15	5	LF	$ 476,300	7,210	$ 568,470	0.327	1.00	0.01	2,239
150	1	5	80	40	20	15	LF	$ 505,900	4,907	$ 568,622	0.327	1.00	0.01	2,642
150		5	140	40	20	10	LF	$ 495,700	5,710	$ 568,696	0.326	1.00	0.01	2,903
110	1	5	160	40	15	5	CC	$ 476,300	7,228	$ 568,704	0.327	1.00	0.01	2,312
150		5	120	40	30	20	LF	$ 501,600	5,261	$ 568,852	0.326	1.00	0.01	3,051
150		10	100	50	25	25	LF	$ 508,000	4,769	$ 568,963	0.327	1.00	0.01	2,099
150		5	120	50	15	25	LF	$ 500,100	5,387	$ 568,964	0.327	1.00	0.01	2,891
110	1	5	160	40	10	10	LF	$ 477,800	7,140	$ 569,074	0.328	1.00	0.01	1,877
110	1	5	160	40	10	10	CC	$ 477,800	7,141	$ 569,088	0.328	1.00	0.01	1,881
110	2	10	80	40	25	10	LF	$ 494,400	5,843	$ 569,097	0.328	1.00	0.01	1,805
150	1	5	100	40	10	5	CC	$ 500,000	5,414	$ 569,212	0.328	1.00	0.01	2,756
150		5	100	40	50	15	CC	$ 498,000	5,572	$ 569,230	0.327	1.00	0.01	6,482
110	1	5	140	50	30	5	LF	$ 481,200	6,889	$ 569,262	0.328	1.00	0.01	2,438
150		10	120	50	30	5	LF	$ 504,100	5,108	$ 569,392	0.328	1.00	0.01	1,878
110	1	5	140	40	25	15	LF	$ 482,200	6,836	$ 569,582	0.327	1.00	0.01	2,683
110	2	5	80	40	25	15	CC	$ 485,900	6,549	$ 569,624	0.328	1.00	0.01	4,710
100	2	10	80	40	30	20	LF	$ 492,400	6,042	$ 569,640	0.327	1.00	0.01	1,940
110	1		180	50		5	CC	$ 470,400	7,764	$ 569,644	0.328	1.00	0.01	
110	1		180	50		5	LF	$ 470,400	7,764	$ 569,644	0.328	1.00	0.01	
150		10	160	40	5		CC	$ 499,800	5,466	$ 569,669	0.328	1.00	0.01	0
150		10	160	40	5		LF	$ 499,800	5,466	$ 569,669	0.328	1.00	0.01	0
150			160	50		15	CC	$ 491,300	6,132	$ 569,688	0.328	1.00	0.01	
150			160	50		15	LF	$ 491,300	6,132	$ 569,688	0.328	1.00	0.01	
150		5	120	40	30	15	CC	$ 495,100	5,837	$ 569,712	0.327	1.00	0.01	5,442
150	1	5	80	40	20	10	CC	$ 499,400	5,504	$ 569,754	0.328	1.00	0.01	5,184
150		10	140	50	10	5	LF	$ 501,200	5,366	$ 569,802	0.328	1.00	0.01	1,132
110	2	5	100	40	15	10	LF	$ 486,500	6,517	$ 569,815	0.327	1.00	0.01	2,449
150		15	80	40	50	20	LF	$ 517,400	4,101	$ 569,822	0.327	1.00	0.01	1,999
150		10	140	50	10	5	CC	$ 501,200	5,369	$ 569,837	0.328	1.00	0.01	1,143
100	2	5	100	40	20	20	LF	$ 484,500	6,678	$ 569,865	0.328	1.00	0.01	2,598
150	1	10	80	40	15	10	LF	$ 509,400	4,736	$ 569,939	0.328	1.00	0.01	1,882
110	1	5	140	40	30	10	CC	$ 480,700	6,984	$ 569,983	0.328	1.00	0.01	3,409
110	1	5	120	50	20	30	LF	$ 486,600	6,526	$ 570,028	0.328	1.00	0.01	2,732

Appendix B: Estimated Primary Load of the Community

Hour of the Day	Households (kW)	Clinic (kW)	Barber (kW)	Church (kW)	School (kW)	Milling (kW)	Shops (kW)	Weekday Total (kW)	Weekend Total (kW)
00 TO 1	0.214	0.162	0	0.073	0.073	0.03	0	0.552	0.423
1 TO 2	0.214	0.162	0	0.073	0.073	0.03	0	0.552	0.423
2 TO 3	0.214	0.162	0	0.073	0.073	0.03	0	0.552	0.423
3 TO 4	0.214	0.162	0	0.073	0.073	0.03	0	0.552	0.423
4 TO 5	0.214	0.162	0	0.073	0.073	0.03	0	0.552	0.423
5 TO 6	0.214	0.162	0	0.163	0.073	0.03	0	0.642	0.513
6 TO 7	20.35	0.136	0	0.092	0.002	0	0	20.58	20.442
7 TO 8	19.535	0.136	0	0.002	0.002	0	0	19.675	19.537
8 TO 9	0.35	0.136	0	0.002	2.167	25	0	27.655	0.352
9 TO 10	0.35	2.761	0.048	0.002	0.807	25	0.015	28.983	0.415
10 TO 11	0.35	0.761	0.048	0.002	0.807	25	0.015	26.983	0.415
11 TO 12	0.35	1.001	0.048	0.002	0.967	25	0.015	27.383	0.415
12 TO 13	12.035	0.211	0	0.002	0.002	0	0	12.25	12.037
13 TO 14	0.35	0.211	0.048	0.002	2.327	25	0.015	27.953	0.415
14 TO 15	0.35	2.761	0.048	0.002	0.967	25	0.015	29.143	0.415
15 TO 16	0.35	1.001	0.048	0.002	0.807	25	0.015	27.223	0.415
16 TO 17	0.35	0.761	0.048	0.002	0.002	25	0.015	26.178	0.415
17 TO 18	0.35	0.136	0.048	0.017	0.002	25	0.015	25.568	0.43
18 TO 19	31.303	0.162	0.078	0.222	1.405	0.09	0.06	33.32	31.799
19 TO 20	31.303	0.162	0.078	0.073	1.405	0.09	0.06	33.171	31.65
20 TO 21	23.803	0.162	0.03	0.073	1.403	0.03	0.06	25.561	24.102
21 TO 22	23.803	0.162	0	0.073	0.073	0.03	0	24.141	24.012
22 TO 23	4.004	0.162	0	0.073	0.073	0.03	0	4.342	4.213
23 TO 00	3.949	0.162	0	0.073	0.073	0.03	0	4.287	4.158

Appendix C: KC175GT Solar Module Specifications

THE NEW VALUE FRONTIER

KYOCERA

KC175GT

HIGH EFFICIENCY MULTICRYSTAL
PHOTOVOLTAIC MODULE

UL LISTED

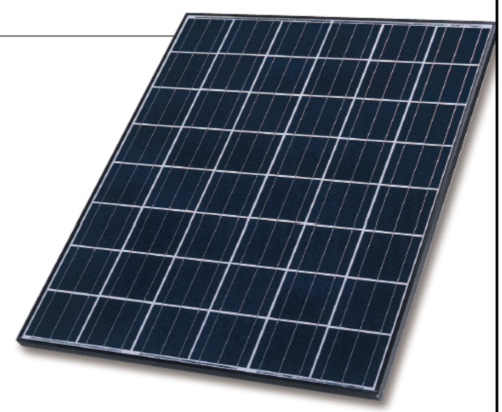

HIGHLIGHTS OF KYOCERA PHOTOVOLTAIC MODULES

Kyocera's advanced cell processing technology and automated production facilities produce a highly efficient multicrystal photovoltaic module.
The conversion efficiency of the Kyocera solar cell is over 16%.
These cells are encapsulated between a tempered glass cover and a pottant with PVF back sheet to provide efficient protection from the severest environmental conditions.
The entire laminate is installed in an anodized aluminum frame to provide structural strength and ease of installation.
Equipped with plug-in connectors.

APPLICATIONS

KC175GT is ideal for grid tie system applications.

- Residential roof top systems
- Large commercial grid tie systems
- Water Pumping systems
- High Voltage stand alone systems
- etc.

QUALIFICATIONS

- **MODULE** : UL1703 certified
- **FACTORY** : ISO9001 and ISO 14001

QUALITY ASSURANCE

Kyocera multicrystal photovoltaic modules have passed the following tests.

- Thermal cycling test
- Thermal shock test
- Thermal / Freezing and high humidity cycling test
- Electrical isolation test
- Hail impact test
- Mechanical, wind and twist loading test
- Salt mist test
- Light and water-exposure test
- Field exposure test

LIMITED WARRANTY

※1 year limited warranty on material and workmanship
※20 years limited warranty on power output: For detail, please refer to "category IV" in Warranty issued by Kyocera
(Long term output warranty shall warrant if PV Module(s) exhibits power output of less than 90% of the original minimum rated power specified at the time of sale within 10 years and less than 80% within 20 years after the date of sale to the Customer. The power output values shall be those measured under Kyocera's standard measurement conditions. Regarding the warranty conditions in detail, please refer to Warranty issued by Kyocera)

ELECTRICAL CHARACTERISTICS

Current-Voltage characteristics of Photovoltaic Module KC175GT at various cell temperatures

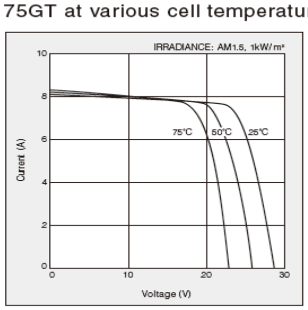

Current-Voltage characteristics of Photovoltaic Module KC175GT at various irradiance levels

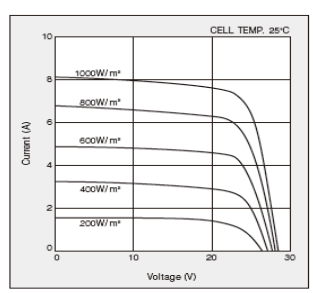

SPECIFICATIONS

KC175GT

Physical Specifications

Unit : mm (in.)

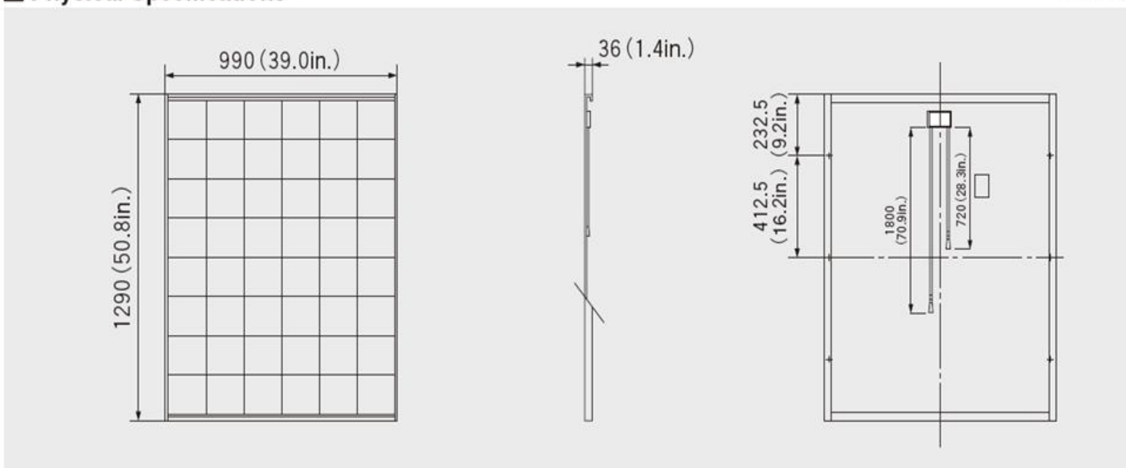

Specifications

Electrical Performance under Standard Test Conditions (*STC)	
Maximum Power (Pmax)	175W (+10%/−5%)
Maximum Power Voltage (Vmpp)	23.6V
Maximum Power Current (Impp)	7.42A
Open Circuit Voltage (Voc)	29.2V
Short Circuit Current (Isc)	8.09A
Max System Voltage	600V
Temperature Coefficient of Voc	-1.09×10^{-1} V/℃
Temperature Coefficient of Isc	3.18×10^{-3} A/℃

*STC : Irradiance 1000W/m², AM1.5 spectrum, module temperture 25℃

Electrical Performance at 800W/m², NOCT, AM1.5	
Maximum Power (Pmax)	125W
Maximum Power Voltage (Vmpp)	20.9V
Maximum Power Current (Impp)	5.99A
Open Circuit Voltage (Voc)	26.5V
Short Circuit Current (Isc)	6.53A

NOCT (Nominal Operating Cell Temperature) : 47℃

Cells	
Number per Module	48

Module Characteristics	
Length × Width × Depth	1290mm(50.8in)×990mm(39.0in)×36mm(1.4in)
Weight	16.0kg(35.3lbs.)
Cable	(+)720mm(28.3in),(-)1800mm(70.9in)

Junction Box Characteristics	
Length × Width × Depth	113.6mm(4.5in)×76mm(3.0in)×9mm(0.4in)
IP Code	IP65

Reduction of Efficiency under Low Irradiance	
Reduction	5.1%

Reduction of efficiency from an irrandiance of 1000W/m² to 200W/m² (module temperature 25℃)

Please contact our office for further information

KYOCERA

KYOCERA Corporation

■ **KYOCERA Corporation Headquarters**
CORPORATE SOLAR ENERGY DIVISION
6 Takeda Tobadono-cho
Fushimi-ku, Kyoto
612-8501, Japan
TEL:(81)75-604-3476 FAX:(81)75-604-3475
http://www.kyocera.com

● **KYOCERA Solar, Inc.**
7812 East Acoma Drive
Scottsdale, AZ 85260, USA
TEL:(1)480-948-8003 or (800)223-9580 FAX:(1)480-483-6431
http://www.kyocerasolar.com

● **KYOCERA Solar do Brasil Ltda.**
Av. Guignard 661, Loja A
22790-200, Recreio dos Bandeirantes, Rio de Janeiro, Brazil
TEL:(55)21-2437-8525 FAX:(55)21-2437-2338
http://www.kyocerasolar.com.br

● **KYOCERA Solar Pty Ltd.**
Level 3, 6-10 Talavera Road, North Ryde
N.S.W. 2113, Australia
TEL:(61)2-9870-3948 FAX:(61)2-9888-9588
http://www.kyocerasolar.com.au/

● **KYOCERA Fineceramics GmbH**
Fritz Muller strasse 107, D-73730 Esslingen, Germany
TEL:(49)711-93934-917 FAX:(49)711-93934-950
http://www.kyocerasolar.de/

● **KYOCERA Asia Pacific Pte. Ltd.**
298 Tiong Bahru Road, #13-03/05
Central Plaza, Singapore 168730
TEL:(65)6271-0500 FAX:(65)6271-0600

● **KYOCERA Asia Pacific Ltd.**
Room 801-802, Tower 1 South Seas Centre, 75 Mody Road,
Tsimshatsui East, Kowloon, Hong Kong
TEL:(852)2-7237183 FAX:(852)2-7244501

● **KYOCERA Asia Pacific Ltd. Taipei Office**
10 Fl., No.66, Nanking West Road, Taipei, Taiwan
TEL:(886)2-2555-3609 FAX:(886)2-2559-4131

● **KYOCERA(Tianjin) Sales & Trading Corporation**
19F, Tower C HeQiao Building 8A GuangHua Rd.,
Chao Yang District, Beijing 100026, China
TEL:(86)10-6583-2270 FAX:(86)10-6583-2250

LIE/I09J0703-SAGKM